

**DESIGN AND FABRICATION OF A HIGH-POWER
NITROGEN LASER AND ITS PARAMETRIC STUDIES
AND LASER-INDUCED FLUORESCENCE ANALYSIS
OF CERTAIN DOPED PHOSPHORS**

THOMAS BABY

**THESIS SUBMITTED TO
COCHIN UNIVERSITY OF SCIENCE AND TECHNOLOGY
FOR THE AWARD OF THE DEGREE OF
DOCTOR OF PHILOSOPHY**

**LASER DIVISION
DEPARTMENT OF PHYSICS
COCHIN UNIVERSITY OF SCIENCE AND TECHNOLOGY
COCHIN - 682 022**

1991

DECLARATION

Certified that the work presented in this thesis is based on the original work done by me under the guidance of Prof.V.P.N.Nampoory, at the Department of Physics, Cochin University of Science and Technology, and has not been included in any other thesis submitted previously for the award of any degree.




THOMAS BABY

Cochin- 682 022

December 20,1991

CERTIFICATE

Certified that the work presented in the present thesis is based on the bona fide work done by Shri.Thomas Baby, Research Scholar, under my guidance, in the Department of Physics, Cochin University of Science and Technology, and has not been included in any other thesis submitted previously for the award of any degree.



Dr.V.P.N.NAMPOORI

Professor of Physics

(Supervising Teacher)

Cochin- 682 022

December 20,1991

PREFACE

Since the laser was first demonstrated in 1960, it has played an increasingly important role in the progress of diverse fields like Chemical Physics, Material Science, Spectroscopy, Display Devices, Communication, Medicine etc. Right from the beginning, laser device with its highly directional, intense and monochromatic output beam offered the spectroscopist a tool which has the excitation capabilities that could not be achieved with any of the conventional light sources. Subsequent advances in laser technology have been instrumental in the development of a large number of new spectroscopic techniques and in the discovery of various phenomena relating to light-matter interactions.

Broadly, laser based research has two directions, viz., (1) development of laser sources with continuous and pulsed optical output, and (2) use of laser to study light induced phenomena. The former aspect stresses on various pumping mechanisms, selection of proper laser media, design of laser cavity, optimisation of laser efficiency etc.

while the latter direction of research deals with the study of phenomena like photochemical reactions, fluorescence and phosphorescence, non-linear optics, photoionisation etc.

Nitrogen laser is one of the laser sources which can be fabricated without much difficulty. N_2 laser finds important applications in Spectroscopy, Solid State Physics, Chemical Physics and Biomedical Engineering. As the levels of laser based research are raised in terms of quality and quantity, the demand on the laser characteristics such as power, pulse width, stability and repetition rate have become more precise. The present thesis reports the work carried out by the author on the design, fabrication and parametric studies of a high-power nitrogen laser system and its use to study the fluorescence characteristics of certain doped phosphor samples. Phosphors have direct applications in various optical devices and hence considerable importance is attached to a detailed study of phosphor materials. N_2 laser operating at 337.1 nm is an effective source of UV excitation to study fluorescence characteristics of phosphors. The investigations outlined above are presented in seven chapters and one appendix.

As a general introduction, the first chapter consists of two parts. In part A, a historical survey on the various designs of nitrogen lasers are briefly outlined followed by an overview of the theoretical analysis of laser action in nitrogen gas. It is known that very fast excitation of nitrogen molecules is a pre-requisite for population inversion. This is accomplished by a fast electrical discharge which dictates a very low impedance pulse circuit. A Blumlein circuit with transverse excitation is ideal for this, since with a moderate voltage it is possible to excite the gas at high pressures. Necessary theory of the Blumlein circuit which is incorporated with the nitrogen laser system is also presented in this chapter. Part B contains the general description of the phenomenon of luminescence. The different factors affecting the luminescence efficiency along with an outline of the necessary theory are also included in this section.

The second chapter contains the details of the design and fabrication of the nitrogen laser system. The laser constitutes mainly of plasma tube, spark gap, Blumlein

capacitors, high voltage power supply, trigger circuit and gas flow system. Calculations show that in order to have the inter electrode gap to be uniformly filled with plasma, it is advisable to use a cylindrical cathode and plane anode. Hence a cylindrical cathode and plane anode had been selected for electrode configuration to give uniform and reproducible discharge. A free-running type spark gap and a triggered spark gap with trigger circuits are developed for the laser. The system has low inductance, long life and high current carrying capacity. A 30 kV switched mode power supply is used as the pumping source and double side copper clad fibre glass epoxy laminates are used as high voltage capacitors. A modified gas flow system is designed so as to obtain a uniform gas flow throughout the discharge region.

The parametric studies of the laser system are given in the **third chapter**. At a charging voltage of 9.3 kV and an optimum pressure of 90 torr, the laser gives an output power of 700 kW with FWHM of 3 ns which is remarkably high for an N_2 laser system. The dependence of output power on parameters such as gas pressure, voltage and repetition rate

are studied on both the single and double-Blumlein circuits. This has been done for the laser with both free-running and triggered spark gap. It is found that the laser with free-running type spark gap has higher efficiency while the stability in repetition rate as well as pulse intensity is found to be better for the triggered mode. The laser with free-running type spark gap at a charging voltage of 6.18 kV gave maximum efficiency of 0.51%, which is the second highest value reported so far. The dependence of the pulse width on spark gap distance and pressure are also described. Variation of efficiency with voltage and E/P ratios are also included in this chapter. Studies on the divergence of the beam as well as the variation of the power density distribution over the cross section of the discharge cell are also included in this chapter.

It has been shown that higher output power and conversion efficiency can be achieved by mixing certain other gases to the nitrogen gas in the discharge tube. It is important to investigate the role played by these impurity gases in enhancing the power output efficiency of the N_2 laser

because there are at present a number of conflicting theories which try to explain the function of these gases. The additives used for the present study are 1,2-dichloroethane, carbon tetrachloride and thionyl chloride. A proposed model of the effect of these additives on the efficiency of N_2 laser is given in the fourth chapter.

The fifth chapter deals with the studies on fluorescence emission of SrS phosphor doped with cerium and europium under N_2 laser excitation. The method of preparation of the phosphor samples are also discussed in this chapter. For SrS:Ce, two bands at 408 nm and 450 nm are observed. A band with line structure in the region 350-430 nm and a new broad band at 460 nm are observed for SrS:Eu phosphors. The probable energy level diagrams are also given.

Crystal field splitting analysis is adopted for explaining the observed emission in SrS:Sm, SrS:Dy and SrS:Er phosphors, results of which are included in chapter six. The proposed model and the energy level scheme of luminescence centres are also discussed in this chapter.

General conclusions are given in **chapter seven**.
Future scope of work in this field of research is also
discussed in this chapter.

An **appendix** is given as an addendum to the
present work. This chapter deals with the application of rare
earths in optical devices especially for TV. The preparation
of the primary colour phosphors and their fluorescence spectra
using N_2 laser as an excitation source are briefly given in
this chapter.

A list of references is cited at the end of each chapter.

Most of the work presented in this thesis has been
published/accepted for publication in the form of the following
research papers.

- [1] "High power N_2 laser with a modified gas flow system and
discharge geometry",
Rev.of Sci.Instrum,(US).., **62(9)**, 2076 (1991).

- [2] "A low inductance, long life, triggered spark gap switch for Blumlein-driven lasers".
Measur.Sci.and Tech, (UK)., 2, 873 (1991).
- [3] "Some considerations on the design of a high-power N_2 laser", (communicated).
- [4] "Triggered and free-running type spark gap switches-A comparative study on N_2 laser performance".
Proc. of National Symp. on Instrum.(NSI-16), Cochin, C-39, P.22 (1991).
- [5] "Fluorescence emission of SrS:Ce and BaS:Ce phosphors under N_2 laser excitation".
Proc.of Symp.on Quant.Electron, BARC, Bombay., P.180(1985).
- [6] "On the analysis of fluorescence emission in SrS:(Cu,Ce) phosphors under laser excitation".
Proc. of the International Conf.on Laser Applns.in Spectroscopy and Optics (LASO), IIT Madras, P.17(1987).
- [7] "Fluorescence emission of SrS:Eu²⁺ phosphor-Energy level splitting of Eu²⁺", Solid State Commun. (UK) (in press).
- [8] "On luminescent properties of SrS:Sm and SrS:Eu phosphors using nitrogen laser excitation".
Proc.of 18th Optical Soc.of India Symp; Indian Institute of Astrophysics, Bangalore, OI-6, P.6(1990). (to appear

in Kodaikanal Observatory Bulletin).

- [9] "Laser-induced fluorescence studies of SrS:Er and SrS:Dy phosphors".

Proc. of the Second Indo-USSR Symp. on Rare-earth Materials Research, Trivandrum, p.34 (1990). (to appear in Bulletin of Materials Science).

- [10] "Fluorescence spectrum, term assignments and crystal field splittings of SrS:Sm phosphor".(communicated).

- [11] "Energy level splitting of rare earth doped SrS phosphors".

Proc. of the Seminar on Photochemistry, Laser Chemistry, and Photobiology, University of Madras (1991).

CONTENTS

		<u>Page</u>
CHAPTER 1	GENERAL INTRODUCTION	
	Abstract	1
	 PART A: NITROGEN LASER	
1.01	Basic concept of gas lasers	2
1.02	Spectroscopic description of N_2 laser	6
1.02.1	Introduction	6
1.02.2	Spectroscopy of nitrogen molecule	7
1.02.3	Ultraviolet laser transition in nitrogen	10
1.02.4	Infrared laser transition in nitrogen	12
1.02.5	Laser action in N_2^+	17
1.03	Theory of nitrogen laser	18
1.03.1	Electrical characteristics of nitrogen laser	22
1.03.2	Blumlein circuit	24
1.04	Longitudinally excited N_2 lasers	32
1.05	Transversely excited N_2 lasers	33
1.06	Travelling wave excitation in N_2 lasers	34
1.07	Electron beam and proton beam excitation techniques	35
1.08	Some applications of N_2 laser	36
	 PART B: LUMINESCENCE IN PHOSPHORS	
1.09	Basic concept of luminescence	39
1.10	Types of luminescence	40
1.11	Fluorescence and emission processes	43
1.12	Models of luminescence	44
1.12.1	Configuration co-ordinate model	44
1.12.2	Band theory model	47
1.13	Kinetics of luminescence	47
1.13.1	First order kinetics	48
1.13.2	Second order kinetics	48
1.14	Quantum efficiency	49
1.15	Life time of the excited state	51

1.16	Relation between fluorescence and concentration	52
1.17	Action of temperature	53
1.18	Phosphors	54
1.18.1	Classes of phosphors	55
1.18.2	Activators	56
1.18.3	Rare earth activated phosphors	57
1.19	Energy level diagram of rare earth ions	59
1.20	Energy transfer	63
	References	66
CHAPTER 2	DESIGN AND FABRICATION OF A HIGH POWER NITROGEN LASER	
	Abstract	86
2.10	Introduction	87
2.20	Details of the laser fabrication	90
2.21	Laser cavity	93
2.22	Gas flow	99
2.23	Spark gap	101
2.23.1	Free-running type spark gap	104
2.23.2	Triggered spark gap switch	105
2.24	Energy storage capacitor	110
2.25	High voltage power supply	114
2.26	Electromagnetic shielding of the laser	115
2.27	Operation of the laser	115
	References	118
CHAPTER 3	PARAMETRIC STUDIES OF NITROGEN LASER	
	Abstract	121
3.1	Introduction	122
3.1.1	Blumlein circuit and E/P requirements	123
3.1.2	The pulse forming net works	125
3.2	Methods of measurement	129
3.2.1	Pulse width	129
3.2.2	Pulse energy and peak power output	133
3.2.3	Divergence and beam size	135
3.2.4	Efficiency	136
3.3	Experimental observations	137
3.3.1	Dependence of laser pulse energy on the spark gap pressure	137
3.3.2	Variation of pulse width with spark gap distance	137

3.3.3	Variation of pulse width with cavity pressure	140
3.3.4	Variation of laser power with spark gap distance	140
3.3.5	Variation of output peak power with the pressure	140
3.3.6	Variation of output power with voltage	145
3.3.7	Variation of power with repetition rate	150
3.3.8	Variation of overall efficiency with the voltage and E/P ratios	153
3.3.9	Variation of the power density over the cross section of the laser electrodes	157
	References	163
CHAPTER 4	EFFECT OF ADDITIVES ON NITROGEN LASER PERFORMANCE	
	Abstract	166
4.1	Introduction	167
4.2	Experimental set up	172
4.3	Variation of power on adding additives	174
4.3.1	Power variation with O ₂ and Ar	174
4.3.2	Power variation with 1,2-Dichloroethane	174
4.3.3	Power variation with carbon tetrachloride	177
4.3.4	Power variation with thionyl chloride	177
	References	179
CHAPTER 5	FLUORESCENCE IN SrS:Ce AND SrS:Eu PHOSPHORS	
	Abstract	183
5.1	Introduction	184
5.2	Sample preparation	184
5.3	Sample cell	186
5.4	Experimental set up	188
5.5	SrS:Ce phosphors	188
5.6	SrS:Eu phosphors	196
	References	205

CHAPTER 6	CRYSTAL FIELD ANALYSIS OF SrS:Sm, SrS:Dy AND SrS:Er PHOSPHORS	
	Abstract	208
6.1	Effect of crystal field on the spectra of ions	209
6.2	Theoretical calculation	210
6.3	Fluorescence in SrS:Sm, SrS:Dy and SrS:Er phosphors	216
6.3.1	Introduction	216
6.3.2	Phosphor preparation and experimental set up	216
6.3.3	SrS:Sm phosphors	217
6.3.4	SrS:Dy phosphors	225
6.3.5	SrS:Er phosphors	231
	References	239
CHAPTER 7	GENERAL CONCLUSIONS	242
APPENDIX	APPLICATION OF PHOSPHORS IN OPTICAL DEVICES	246

CHAPTER 1

GENERAL INTRODUCTION

Abstract

PART A: In order to make the thesis self contained, the basic theory of gas lasers are briefly described with special reference to N_2 laser. It is concluded that a fast excitation of the nitrogen molecule is a prerequisite for population inversion which requires a fast electrical discharge. IR N_2 and N_2^+ laser transitions are also mentioned. A review on the advances in the fabrication of N_2 lasers, since 1963, with special emphasis on laser transition at 337.1 nm is also included in this chapter along with some of the important applications.

PART B: The field of luminescence is so vast and old making it difficult to give an exhaustive review, but a general introduction to the subject is presented, which gives a brief description of the basic phenomenon, the mechanism involved and energy transfer which help one to understand the Physics behind the fluorescence emission is given. This is followed by a comprehensive report on luminescence in phosphors.

PART A: NITROGEN LASER

Nitrogen laser technology is growing very rapidly even after three decades since the discovery of the first laser. This is one of the laser sources which can be fabricated without much difficulty and efforts are still going on to improve its efficiency, power and stability. This chapter surveys the basic concept of gas lasers and the nitrogen laser technology in detail.

1.01. Basic concept of gas lasers

The number of gas laser systems in use today, differing in active media and methods of pumping, runs into hundreds. They range from the powerful industrial carbon dioxide units to the helium-neon lasers of modest powers. They can be operated continuously or on a pulsed basis with output frequencies ranging from the ultraviolet to the infrared. The various types of gas lasers will fall into the following categories : (1) neutral atom gas lasers, (2) ion gas

lasers, (3) molecular lasers, and (4) pulsed lasers.

Normally, the active medium of a gas laser is a mixture of more than one type of gases, one of which contains atoms or molecules forming the active centres while other gaseous components serve to produce population inversion between the lasing levels of the active centres. One such possible mixture, for instance, is helium and neon (with neon atoms as active centres) at proper pressure as in the case of He-Ne laser.

Although different excitation mechanisms have been employed for pumping, most gas lasers are excited by means of an electric discharge inside the laser cavity. Electrons in the discharge are accelerated by the electric field between a pair of electrodes. As the electrons collide with the atoms, ions or molecules of the active medium, they induce transitions to higher energy states. With sufficient pumping power, a population inversion is created between the upper and lower levels. Characteristics of electrical discharges are influenced by a variety of parameters like type of the gas, gas pressure, discharge current etc. The maximum supply voltage should be

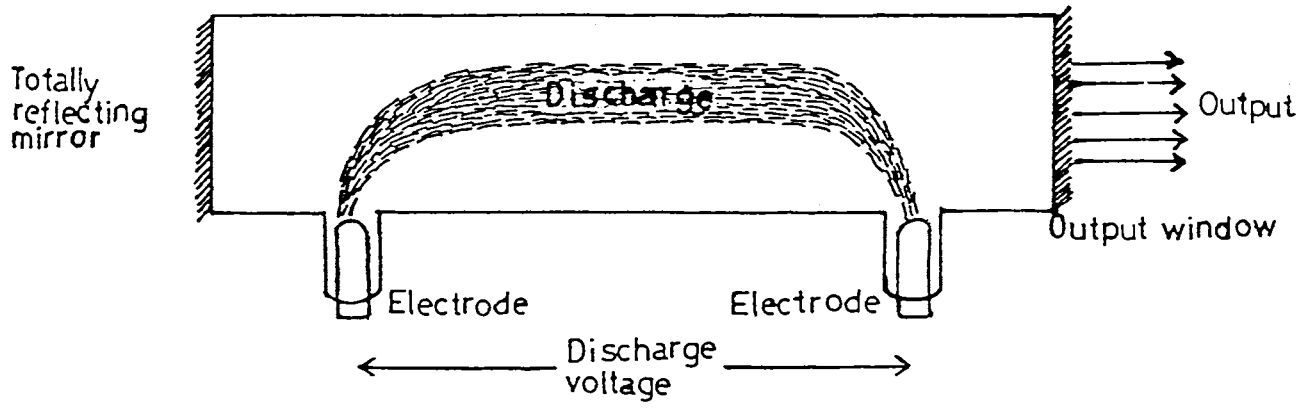


Fig.1.1. Longitudinally discharged gas laser.

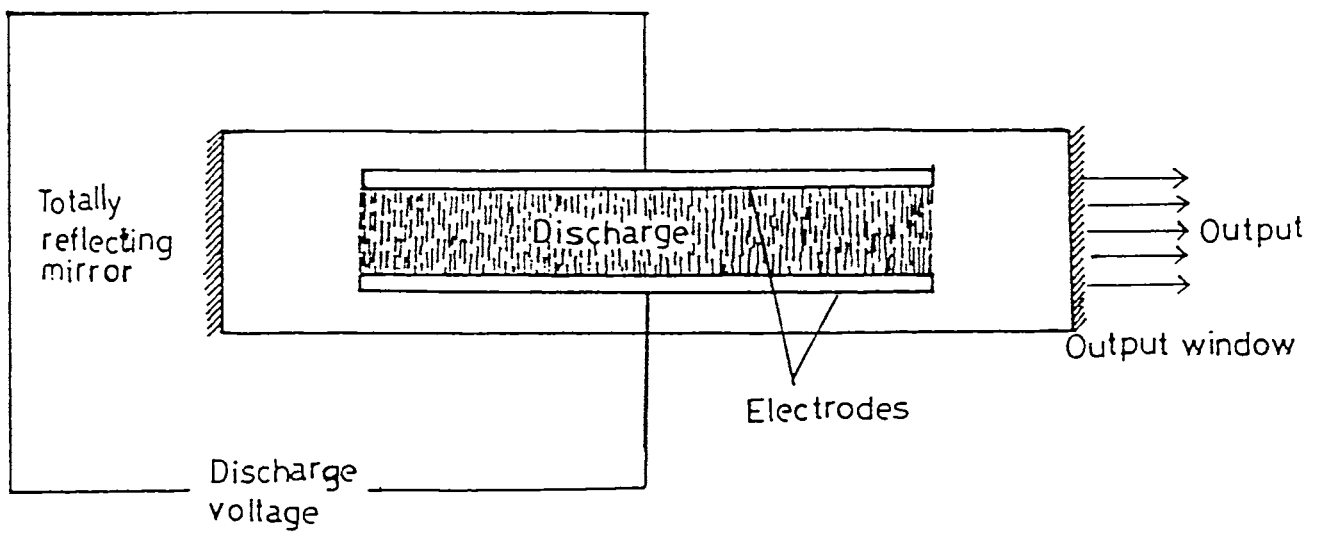


Fig.1.2. Transversely discharged gas laser.

sufficient to cause initial breakdown of the medium between the electrodes in the laser cavity. For stable operation, the voltage across the discharge is usually about half the open-circuit voltage. Alternatively, a separate high voltage surge injection source may be used to initiate the discharge.

The principal gas lasers available are the helium-neon, argon ion, carbon-dioxide and nitrogen lasers, all of which have been extensively studied and are being widely used for various applications.

A typical gas laser cavity is shown in Fig.1.1. The pumping source is normally an electric discharge. The discharge is along the axis of the cavity. Uniform excitation of a larger volume of gas enabling higher powers to be obtained is possible with a discharge transverse to the optic axis of the laser (Fig.1.2). The transverse discharge configuration is best suited for pulsed lasers.

The end windows of the laser cavity can be mounted at the Brewster angle at either end of the tube so that external mirrors may be used for optical feed back. Spherical

mirrors are generally used rather than plane mirrors since the former provide more stability to the resonator. The cavity walls of atomic and molecular lasers are normally borosilicate glass which at high powers may be water cooled.

Even though Nitrogen lasers (UV) with high intensity pulsed outputs at 337.1 nm have been studied by several workers, the design has not yet been optimised in terms of efficiency. The design and fabrication of a discharge-excited N_2 laser [peak powers in excess of 700 kW and duration of 3 ns (FWHM)] are described in the second chapter.

1.02. Spectroscopic description of N_2 laser

1.02.1. Introduction

The N_2 laser operating at 337.1 nm is a typical UV light source, which can easily produce short optical pulses with high peak power and therefore is suitable to pump dye lasers and can be used for photo-chemistry applications. Lasing in the N_2 first positive bands (503-1042 nm) was first reported by Mathias and Parker [1] in 1963 and later that year

Heard [2] observed lasing in the second positive bands (281.4-497.6 nm). Since then considerable research and developmental activity have been reported on N_2 lasers. Different aspects of N_2 lasers have been investigated. viz; power output, pulse width, dependence on power input and gas flow conditions, lasing frequencies and their spectral examination under different experimental conditions, mechanisms for population inversion etc. Excitation of the gas medium is achieved either using electrical discharge or intense electron beams. At present, mega watt pulsed pulsed N_2 lasers [3,4] are available. N_2 lasers operating at atmospheric pressures (TEA lasers) [5,6] have also been made.

It has been noted that addition of a small quantity of other gases like SF_6 , BF_3 etc. increases the power output [7,8] to a very great extent.

1.02.2. Spectroscopy of nitrogen molecule

Molecular nitrogen has been observed to lase on the following identified transitions : ($C^3\Pi_u \longrightarrow B^3\Pi_g$), ($B^3\Pi_g \longrightarrow A^3\Sigma_u^+$), ($a^1\Pi_g \longrightarrow a'^1\Sigma_u^-$), ($W^1\Delta_u \longrightarrow a^1\Pi_g$),

($a^1\Pi_g \longrightarrow X^1\Sigma_g^+$) [9-11] and ($W^3\Delta_u \longrightarrow B^3\Pi_g$) [12,13] and oscillations observed between 540 and 807 nm are not yet assigned [12,14]. Though lasing has been reported in the above systems for a number of bands, the (0,0) band of (C \longrightarrow B) transition has been found to lase much efficiently. Therefore in normal parlance an N_2 laser means lasing at 337.1 nm.

The three lowest lying triplet electronic states of molecular nitrogen are $A^3\Sigma_u^+$, $B^3\Pi_g$ and $C^3\Pi_u$. The first positive system lies in the region 503-1042 nm and results from the $B^3\Pi_g \longrightarrow A^3\Sigma_u^+$ transition, where as the second positive system lies in the region 281.4 - 497.6 nm and results from the $C^3\Pi_u \longrightarrow B^3\Pi_g$ transition. $A^3\Sigma_u^+$ is a metastable state having a life time of about 2 seconds while the life times of the $B^3\Pi_g$ and $C^3\Pi_u$ states are of the order of 10 μ s and 40 ns respectively [15,16]. Potential energy diagram of N_2 (Fig.1.3) is helpful in describing the various laser transitions. It is now a fairly well known fact that the excitation of the upper laser level in N_2 can be brought about easily by electron impact.

The equilibrium internuclear separations in the three electronic states are in the order :

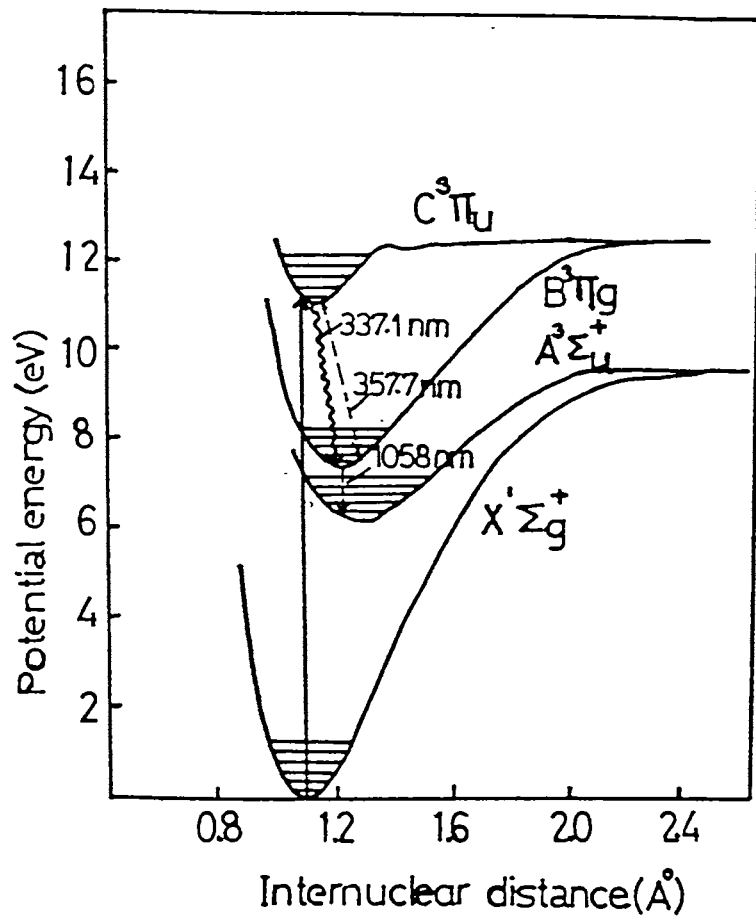


Fig.1.3. Potential energy diagram of the nitrogen molecule.

$$r_e (A^3\Sigma_u^+) > r_e (B^3\Pi_g) > r_e (C^3\Pi_u) > r_e (X^3\Sigma_g^+);$$

In accordance with the Frank-Condon principle, the vertical transitions from the ground state to the excited electronic states would be more probable and could be brought about easily by electron impact [17,18]. The electron impact excitation cross-sections to the different vibrational levels of the three low lying triplet excited states corresponding to the incident electron energy of 16 eV are given in Table 1 [ref:19].

A comparison of the relative excitation cross sections of $B^3\Pi_g$ and $C^3\Pi_u$ states at incident electron energy of 35 eV has been made by Willett [20]. Calculations of Cartwright [19] indicate that the total excitation cross-sections for the three triplet states are maximum near incident electron energy of 16 eV. It is evident from Table 1.1 that the excitation rates of levels with $v' = 0,1$ in $C^3\Pi_u$ state with $v' = 2,3,4$ in $B^3\Pi_g$ state and with $v' > 4$ in $A^3\Sigma_u^+$ state would be significantly larger in comparison to the rates of other vibronic levels.

1.02.3. Ultraviolet laser transition in nitrogen

Laser action in nitrogen at pressures of the

Table. 1.1. Electron excitation cross-sections ($Q_{v'0}$ in units of Πa_0^2 where a_0 is the Bohr radius) at incident electron energy of 16 eV from the $v'' = 0$ level of the $X^1\Sigma_g^+$ state of N_2 molecule to different vibrational levels (v') of the excited triplet states [Ref.19].

v'	$Q_{v'0} A^3 \Sigma_u^+$	$Q_{v'0} B^3 \Pi_g$	$Q_{v'0} C^3 \Pi_u$
0	0.003	0.033	0.450
1	0.014	0.085	0.332
2	0.039	0.122	0.139
3	0.079	0.133	0.126
4	0.128	0.133	0.013
5	0.175	0.090	---

order of 40 torr was first observed by Heard [2] at 337.1 nm, which corresponding to the (0,0) band of the second positive system ($C^3\Pi_u \longrightarrow B^3\Pi_g$). Lasing action also occurs at 357.7nm (0,1 band) and at 315.9 nm (1,0 band) with less intensities as compared to that at 337.1 nm. The laser band width of these transitions is typically of the order of 0.1 nm and involves many rotational transitions.

The life time of the upper laser level being smaller (40 ns) than that of the lower level (10 μ s), the lasing stops automatically in a duration less than or equal to the life time of the upper level. This type of lasers are known as 'self-terminating lasers' and the population inversion can be achieved by applying a short rise-time, high voltage pulse excitation, in which the rise-time of the current pulse is less than the life time of the upper level. Although the electron excitation cross-section of the $B^3\Pi_g$ state is five times higher than that of $C^3\Pi_u$ state, the excitation cross-section of $v = 0$ in $C^3\Pi_u$ state is ten times that of $v = 0$ in $B^3\Pi_g$ state; and a population inversion is possible between the two states during the rise time of the discharge current pulse. The relative emission probabilities (estimated from the electron excitation cross-sections and Frank-Condon factors for the second positive band system) for the three laser transitions have been found to be considerably large in comparison with other bands (Table.1.2). It has been observed that the gain is so high that the lasing has been observed even without cavity mirrors.

1.02.4. Infrared laser transition in nitrogen

Information on the infrared (IR) laser is

Table 1.2. Electron excitation cross-sections ($Q_{v'0}$) for $C^3\Pi_u$ state, Frank-Condon factors ($q_{v',v''}$) and relative emission probabilities for vibronic bands of the $C^3\Pi_u \longrightarrow B^3\Pi_g$ system [Ref.15].

Band	$Q_{v'0}$	$q_{v',v''}$	Relative emission probabilities		Observed laser transitions (nm)
			$Q_{v'0}$	$q_{v'v''}$	
0,0	0.450	0.449	0.202		337.1
0,1		0.329	0.148		357.7
0,2		0.147	0.066		---
1,0	0.332	0.390	0.129		315.9
1,1		0.019	0.006		---
1,2		0.204	0.068		---
2,0	0.139	0.135	0.019		---
2,1		0.332	0.046		---
2,2		0.033	0.005		---

limited as compared to the ultraviolet (UV) laser. Lasing in the IR region has been obtained in the axial [1,21-24] and transverse [25-27] mode of excitation. Pulsed laser emission of IR (750 nm - 1230 nm) bands due to the $B^3\Pi_g \longrightarrow A^3\Sigma_u^+$

transition was first reported by Mathias and Parker [1] in 1963. Willett [20] lists laser oscillations in 11 bands arising from the first four levels ($v' = 0-4$) of $B^3\Pi_g$ to the first four levels ($V'' = 0-4$) of $A^3\Sigma_u^+$. The laser action is pulsed with a pulse width between 10 and 100 ns with the bandwidth of the laser transition varying from 2 to 10 nm for different vibronic bands. The peak laser power output of these transitions is less than that of the UV transitions and the mirrors are required for laser cavity in order to increase the gain. The optimum operating conditions for IR and UV lasers are also different.

A semiquantitative explanation for IR laser transitions can be given on the same lines as that for the UV transitions. However, there is one significant difference between the excitation mechanism of the upper laser levels in the two cases. It is possible to neglect the population build up in the $C^3\Pi_u$ state due to the downward transitions from the various excited electronic states in comparison to that from the electron excitation of molecules from the ground state; while this is not the case with the population build up in the $B^3\Pi_g$ state. For the sake of simplicity, it is assumed here that

Table.1.3. Electron excitation cross-sections ($Q_{v'o}$) for $B^3\Pi_g$ state, Frank-Condon factors ($q_{v'v''}$) and relative emission probabilities for vibronic bands of the $B^3\Pi_g \rightarrow A^3\Sigma_u^+$ system [ref.15].

$v'v''$	$Q_{v'o}$	$q_{v'v''}$	Relative emission probabilities $Q_{v'o} q_{v'v''}$	Observed laser transitions (nm)
0,0	0.033	0.338	0.011	1043.9-1053.8
0,1		0.325	0.011	1230.6-1235
0,2		0.190	0.006	1498.3
1,0	0.085	0.406	0.035	883.6-891.1
1,1		0.002	0.0002	----
1,2		0.103	0.009	1193.3
2,0	0.122	0.197	0.024	771.4-775.5
2,1		0.212	0.026	865.6-872.5
2,2		0.113	0.014	----
3,0	0.133	0.050	0.007	----
3,1		0.299	0.040	757.4-762.7
3,2		0.039	0.005	----
3,3		0.162	0.022	959.9
4,0	0.133	0.007	0.001	----
4,1		0.132	0.018	----
4,2		0.274	0.036	748.5-750.4

the population inversion between the $B^3\Pi_g$ and $A^3\Sigma_u^+$ vibrational levels is brought about mainly due to the electron impact excitation from the ground state. A perusal of Table.1.1 shows that under this assumption, the condition of population inversion will exist only between a number of pairs of vibrational levels involving $v = 0,1,2,3,4$ in the two electronic states. Table 1.3 lists relative emission probabilities involving $v = 0,1,2,3,4$ in $B^3\Pi_g$ state and $v = 0,1,2$ in $A^3\Sigma_u^+$ state.

In the observed laser transitions (Table 1.3) it can be seen that (0,2) and (1,2) transitions do occur though their emission probability is low, whereas (2,2) and (4,1) transitions have not been observed, though they are predicted to be more probable. One should however, bear in mind the assumption of neglecting the population increase of the upper laser level due to the radiative transitions from the $C^3\Pi_u$ state while making the above semiquantitative comparison.

Kaslin et al.[28] observed that the efficiency of IR N_2 laser also increases considerably on cooling the laser tube to liquid nitrogen temperature. Gleason et al.[25]

reported the peak laser output as 0.5 kW, whereas Hocker [29] was able to extend this limit to 4 kW. In the latter work, laser action was observed at six vibronic bands in the wavelength region 750-1054 nm, with maximum intensity in the range 871-894 nm. This laser has also been used to pump tunable dye lasers in 915-1040 nm range.

1.02.5. Laser action in N_2^+

The negative group of bands during a discharge through nitrogen gas arises due to the electronic transitions of singly ionized nitrogen molecule ($B^2\Sigma_u^+ \rightarrow X^2\Sigma_g^+$) with the most intense band (0,1) at 427.8 nm. Laser action at this wavelength has been observed under both electron beam excitation and electric discharge excitation. These excitations are, however, not caused directly by electron impact. The electron energy is taken up by a rare gas molecule which gets ionized and transfers its energy to the nitrogen molecule; which gets ionized subsequently leading to laser emission. The mechanism of excitation is known as energy through charge transfer and its successful operation requires high pressures, so that collisional transfer rates may be fast

enough to compete with spontaneous de-excitation rates. These laser systems are important because of their efficiency and potential use of giant pulse.

Collins et al. [30,31] were the first to report laser action at 427.8 nm having a line-width less than 0.3 nm. They used a mixture of He and N_2 at a pressure of 7 atm. which was excited by electron beam from a fast pulsed electron gun. Ishchenko et al.[32] and Laudenslager et al.[33] reported lasing in self-sustained discharges where the high pressure gas mixture is preionized by a high voltage pulse passed through the glass walls. This design is, however, not suitable for high pulse repetition frequencies (PRF). Rothe and Tan [34] described the UV preionization technique using an array of spark along each side of the electrode gap to achieve a PRF of 2 Hz. They reported a power output of 0.5 MW at 427.8 nm with a pulse width of 6 ns in a gas mixture of He and N_2 at 3 atm. Laser emission from N_2^+ was obtained with a nitrogen concentration of 0.05%, but at higher concentrations (2-10%), strong lasing was observed at 337.1 nm due to N_2 .

1.03. Theory of nitrogen laser

For laser action, one usually requires a

metastable upper level and a fast decaying lower level. The radiative life time of the C-state is 40 ns, that of B-state is $10\mu\text{s}$ and that of A-state is 2 sec.[35-37]. Hence a continuous laser action between C and B states is impossible in a nitrogen molecule. But if we can pump the C-level in a time less than that its life time, due to a transient population inversion pulsed laser action is possible.

A simple theory based on the assumption of direct electron impact excitation of N_2 was first proposed by Gerry [38] to understand the characteristics of N_2 lasers. The rate equations involving the population densities of the upper and lower levels were established and solved with the approximation that the laser power density was saturated. The solutions were quantitatively in agreement with the observed results of Leonard [39]. This theory was later extended by Ali et al.[40] to include the effect of the collisional mixing of the laser levels by electron impact and collisional ionization from the upper laser level, whose contributions are significant at electron densities greater than $6 \times 10^{14} / \text{cm}^3$ and an electron temperature of 4 eV.

For the above formulations, an ultraviolet N_2

laser is considered as a three level laser :

$$\begin{aligned}
 X^1\Sigma_g^+ & \quad (\text{ground state level 1}) \\
 B^3\Pi_g & \quad (\text{lower laser level 2}) \\
 \text{and } C^3\Pi_u & \quad (\text{upper laser level 3})
 \end{aligned}$$

Let N_1 , N_2 and N_3 denotes the population densities of the ground state, the lower (i) and the upper (j) laser levels respectively. X_{ij} be the rate of collisional excitation by electron impact from level i to j where $i < j$, Y_{ji} the rate of collisional de-excitation from j to i, τ_{ji}^{-1} the rate of the radiative decay and R_{ji}^i denotes the rate of induced emission. Then the rate equations governing the population densities of these levels can be written as:

$$\begin{aligned}
 \frac{dN_3}{dt} = & X_{13} N_1 + X_{23} N_2 - (Y_{31} + Y_{32} + \tau_{31}^{-1} + \tau_{32}^{-1}) N_3 \\
 & - R_{32}^i [N_3 - N_2 (g_3/g_2)] \quad \dots\dots\dots(1.1)
 \end{aligned}$$

$$\begin{aligned}
 \frac{dN_2}{dt} = & X_{12} N_1 + (\tau_{32}^{-1} + Y_{32}) N_3 - (\tau_{21}^{-1} + Y_{21} + X_{23}) N_2 \\
 & + R_{32}^i [N_3 - N_2 (g_3/g_2)] \quad \dots\dots\dots(1.2)
 \end{aligned}$$

$$\begin{aligned}
 \frac{dN_1}{dt} = & - (X_{12} + X_{13}) N_1 + (\tau_{21}^{-1} + Y_{21}) N_2 \\
 & + (\tau_{31}^{-1} + Y_{31}) N_3 \quad \dots\dots\dots(1.3)
 \end{aligned}$$

where g_2 and g_3 are the statistical weights. The induced emission and absorption rates are neglected along with the rate of the collisional de-excitation from the laser levels to the ground state. Remembering that $\tau_{31} \gg \tau_{32}$ ($3 \rightarrow 1$ is a spin forbidden transition) and $\tau_{21} \gg \tau_{32}$ ($\tau_{32} = 40$ ns while $\tau_{21} = 10$ μ s), the sum of equations (1.1) and (1.2) is expressed as

$$d/dt (N_3 + N_2) = X_{13} N_1 \dots\dots\dots(1.4)$$

($X_{13} > X_{12}$ being taken as proportional to F.C.factors), which on integration yields

$$N_3 + N_2 = X_{13} N_1 t \dots\dots\dots(1.5)$$

Using equations (1.4) and (1.5), equation (1.1) is rewritten as

$$dN_3 / dt = X_{13} N_1 + (X_{13} N_1 t - N_3) X_{23} - \beta N_3 \dots\dots(1.6)$$

$$\text{where } \beta = (\tau_{32}^{-1} + Y_{32})$$

The solution of equation (1.6) is

$$N_3 = (N_1 X_{13} / \alpha^2) (Y_{32} + \tau_{32}^{-1}) (N_1 X_{13} / \alpha^2) (Y_{32} + \tau_{32}^{-1}) e^{-\alpha t} + (N_1 X_{13} X_{23} t / \alpha) \dots\dots\dots(1.7)$$

$$\text{where } \alpha = \beta + X_{23}$$

For small time intervals one can write equation (1.7) by expanding $e^{-\alpha t}$ upto terms in t^2 , as

$$N_3 = N_1 X_{13} t - \frac{1}{2} N_1 X_{13} (Y_{32} + \tau_{32}^{-1}) t^2 \dots\dots(1.8)$$

Equations (1.5) and (1.8) yield

$$N_2 = \frac{1}{2} N_1 X_{13} (Y_{32} + \tau_{32}^{-1}) t^2 \quad \dots\dots(1.9)$$

Thus to obtain a population inversion (ie. $N_3 > N_2$),

$$t < \frac{1}{(Y_{32} + \tau_{32}^{-1})} \quad \dots\dots\dots(1.10)$$

This means that the population inversion can only take place during a time of the order shorter than the radiative life time of the $C^3\Pi_u$ state as long as $Y_{32} < \tau_{32}^{-1}$. When the electron density N_e is greater than $6 \times 10^{14} \text{ cm}^{-3}$, Y_{32} will be greater than τ_{32}^{-1} , as a result of which the inversion duration becomes still less. Therefore, it is necessary to have a fast excitation of nitrogen molecules because inversion will cease to exist after 10-20 ns.

1.03.1. Electrical characteristics of nitrogen laser

The engineering of high peak power nitrogen lasers center principally on the problem of achieving excitation of the gas in a few nano seconds. This can be achieved by using very low impedance pulse circuits. Usually, nitrogen gas flowing through the laser cavity is excited by a

Blumlein circuit. The pulse-forming network consists of two parallel-plate transmission lines located at both sides of the laser cavity. A spark gap is used to short circuit the end of one line. Both sides are charged to a high voltage by a D.C. power supply. When one of the transmission lines is short circuited at its end, by the spark gap, a transient voltage occurs across the laser cavity, creating a powerful discharge between the electrodes. It is generally assumed that after the spark gap is fired, a travelling wave occurs in one of the transmission lines initiating the gas discharge and generating a second travelling wave in the other line. The superposition of these two travelling waves causes a complex voltage wave form across the electrodes that sustains the discharge.

If the electric field in the laser cavity at the time when the discharge is fully developed is E (in other words, E is approximately the peak electric field in the cavity), and P is the laser cavity pressure in torr. The mean free path (λ) of the electrons at 16 eV in N_2 as a function of the pressure is $\lambda = (\sigma N)^{-1}$, where σ is the total cross section and N is the number of molecules per unit volume and per torr. Godard [41] found the value of $\lambda = 0.064$ cm for one

torr. The maximum field E , required for an electron to acquire an energy of 16 eV in one mean free path at a pressure of one torr is $E = 16/\lambda$. This gives E/P (electric field per unit pressure of gas), a value of 250 V/cm.torr approximately. As the rise time of the voltage across the laser cavity is increased one must lower the pressure in the cavity to achieve the optimum condition. It may be noted that most of the cross-sections given by Cartwright [19] are a bit higher than the observed values. Therefore we can expect that the actual (E/P) values may be slightly higher.

In order to obtain a higher output and small power variation from pulse to pulse it is advantageous that the discharge starts reproducibly at one end of the cavity. This goal can be achieved more efficiently by a tapered electrode gap [15].

1.03.2. Blumlein circuit

The lack of knowledge of the electrical behaviour of the system leads to the construction of low-efficiency systems. The main problem of the constructors

is the putting of sufficiently large electrical energy into the laser tube for a short time duration. Theoretical analysis and experimental data published up to date show that there is a complete dependence between the pulse laser performance and the electrical and geometrical characteristics of the circuit.

Fig.1.4 represent the basic circuits for a Blumlein circuit. The equivalent electrical circuit of a Blumlein type N_2 laser is shown in Fig.1.5. A spark gap is used as the ignition system, while the capacitors are usually flat-plate ones also playing the role of the transmission lines. R_1, L_1 and R_2, L_2 are the resistance and inductance of the spark gap switch and laser discharge channel, respectively. These quantities are strongly time dependent only for a short time before the breakdown, while they remain nearly constant during the main discharge where the laser output occurs. Just before the ignition system breaks down, the full charging voltage U_0 is applied across it, while at the same time the voltage across the laser cavity is nearly zero.

When the laser cavity is ineffective (in practice, this can be achieved by setting the gas pressure high

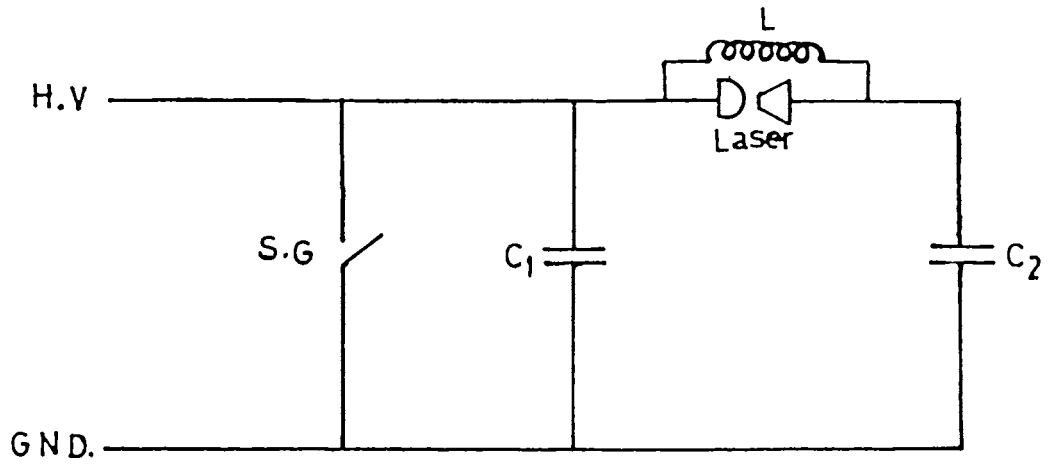


Fig.1.4. Blumlein discharge circuit.

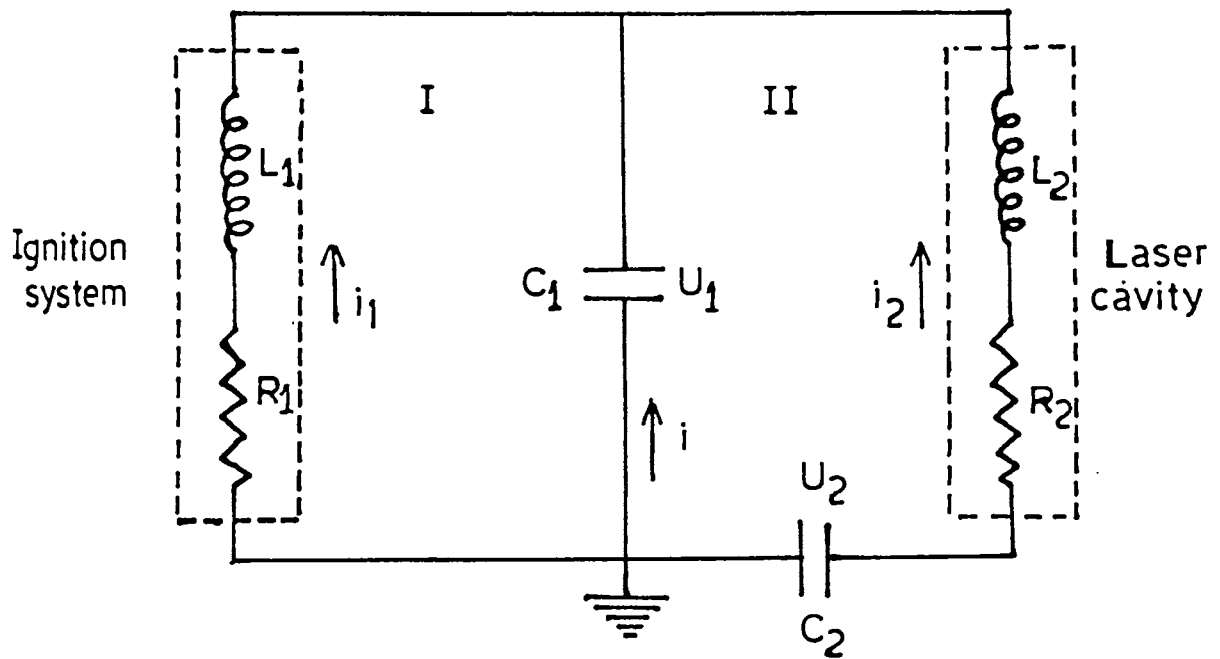


Fig.1.5. Equivalent electrical circuit of a Blumlein N_2 laser.

enough), so that no breakdown occurs, then only a part of the circuit oscillates (part I of the circuit in fig 1.5). After the firing in the ignition system, the equation governing the performance of this circuit are governed by the relationships:

$$U_1 = L_1 \frac{di_1}{dt} + i_1 R_1 \dots\dots\dots(1.11)$$

$$i_1 = -C_1 \frac{dU_1}{dt} \dots\dots\dots(1.12)$$

By combining these equations, we have

$$L_1 C_1 \frac{d^2 U_1}{dt^2} + R_1 C_1 \frac{dU_1}{dt} + U_1 = 0 \dots\dots(1.13)$$

The general solution for this differential equation is

$$U_1(t) = K_1 e^{-at} \cos \omega t + K_2 e^{-at} \sin \omega t \dots\dots(1.14)$$

The initial conditions [$U(0) = U_0$ and $U'(0) = 0$] reduce this relationship so that final form is given by,

$$U_1(t) = U_0 e^{-at} \cos \omega t \dots\dots\dots(1.15)$$

Part I of the circuit of fig.1.4 oscillates with angular frequency ω and damping constant a , where

$$a = R_1 / 2L_1 \dots\dots\dots(1.16)$$

$$\omega = \sqrt{1/L_1 C_1 - R_1^2 / 4L_1^2} \dots\dots\dots(1.17)$$

From the above relationships R_1 and L_1 can be estimated if we know the measured quantities ω and a from the experimental

data. Similarly, the voltage across the laser cavity oscillates and is given by the form,

$$U_L(t) = U_0 (1 - e^{-\alpha t} \cos \omega t) \dots\dots (1.18)$$

On the other hand, when the laser cavity is effective (by adjusting the gas pressure), the performance of the entire electrical circuit is more complex and is realized in two stages: (a) the stage before the breakdown in the laser cavity and (b) the stage after the breakdown in the cavity.

During the first stage, the laser channel is ineffective, so that after the firing in the ignition system, only part I of the circuit shown in Fig.1.5 begins to oscillate according to the above description. Thus the voltage across the laser electrodes increases following the rise of the waveform of relation (1.18). Then, as the discharge in the tube develops, producing a highly conducting plasma, the voltage stops increasing, reaching a peak value V_p (actual starting voltage) and falling rapidly while the optical output occurs.

During the second stage, the laser cavity becomes effective, and so the entire laser system as shown in Fig.1.5 oscillates. The equations governing the performance of all the system are given by the relationships:

$$U_1 = U_2 + L_2 \frac{di_2}{dt} + R_2 i_2 \quad \dots\dots\dots(1.19)$$

$$U_1 = L_1 \frac{di_1}{dt} + R_1 i_1 \quad \dots\dots\dots(1.20)$$

$$i_1 = - (i_1 + i_2) \quad \dots\dots\dots(1.21)$$

By combining these equations we have the differential equation for the voltage across the capacitor C_1 :

$$\alpha U_1^{(4)} + \beta U_1^{(3)} + \gamma U_1^{(2)} + \delta U_1^{(1)} + U_1 = 0 \quad (1.22)$$

where,

$$\alpha = L_1 L_2 C_1 C_2$$

$$\beta = L_1 C_1 R_2 C_2 + L_2 C_2 R_1 C_1 \quad \dots (1.23)..$$

$$\gamma = L_1 C_1 + (L_1 + L_2) C_2 + R_1 C_1 R_2 C_2$$

$$\delta = R_1 C_1 + (R_1 + R_2) C_2$$

Similarly, the differential equation of the voltage across the capacitor C_2 has the same form as eqn.(1.22) with the same coefficients, and so we have;

$$\alpha U_2^{(4)} + \beta U_2^{(3)} + \gamma U_2^{(2)} + \delta U_2^{(1)} + U_2 = 0 \quad .(1.24)$$

The solution of the similar eqns. (1.22) and (1.24), bearing in mind the initial conditions, has the form:

$$U(t) = A e^{-a_1 t} \cos v_1 t + B e^{-a_2 t} \cos \omega_2 t \quad \dots\dots(1.25)$$

where $A + B = U_0$.

Equation (1.25) describes a superposition of two oscillations. Conclusively, we can say that the two voltages U_1 and U_2 oscillate according to relationship (1.25) as a

superposition of two oscillations. The angular frequencies ω_1 and ω_2 as well as damping constants a_1 and a_2 are the same for the voltages U_1 and U_2 because these quantities depend on the coefficients of differential equations (1.22) and (1.24), which are the same for both equations. Thus we can say that the entire system oscillates with these angular frequencies and damping constants too. After an adequate time this complex oscillation decays fully, and the system is ready to repeat the performance for the next pulse.

The stability or instability of the laser pulses depends on the conditions of pressure and pulse repetition rate [42,43]. These conditions have been depicted in the area defined by the pressure - versus - time interval between two successive pulses, namely, the inverse of the repetition rate. In this area, three regions are distinguished as: Region I, where the pulses are stable; region II, where the pulses are unstable with high energy; and region III, where no breakdown occurs in the laser tube. The boundaries of these three regions are not distinct. Persephonis [43] reported these three regions as depicted in Fig. 1.6 for the double-Blumlein circuit (applied voltage: 10 kV).

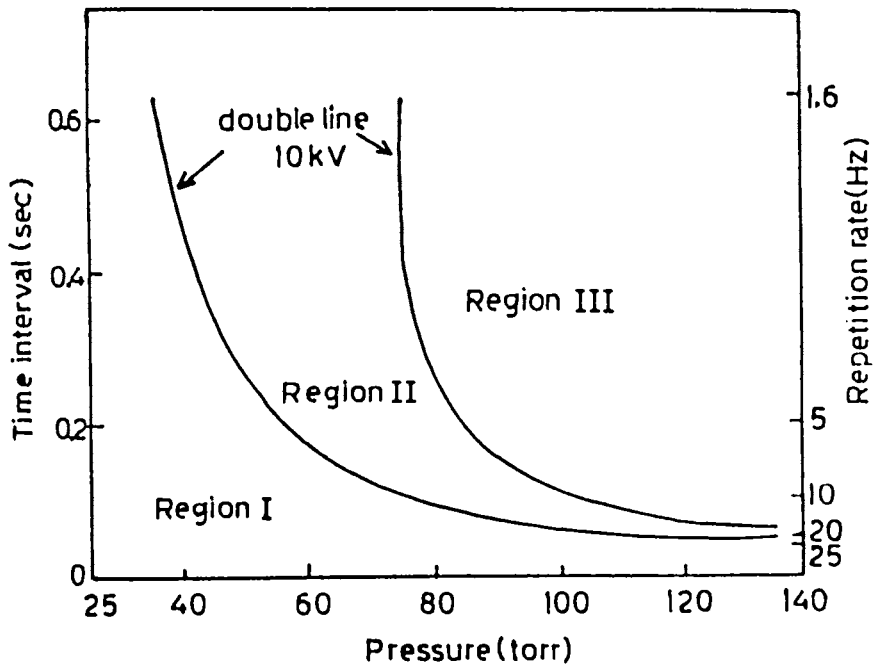


Fig.1.6 Regions where the N_2 laser operates into stable or unstable mode or yet no breakdown occurs for the double-Blumlein circuit. (applied voltage: 10 kV).

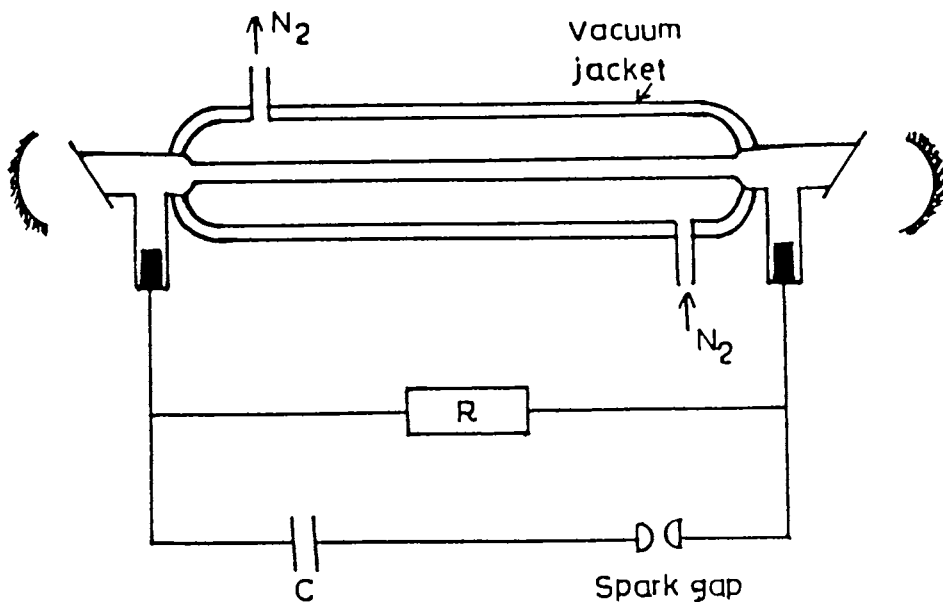


Fig.1.7 Longitudinally excited N_2 laser.

1.04. Longitudinally excited N_2 lasers

In longitudinally excited N_2 lasers, the laser emission is in the direction of the electric field. There are several versions of axial excitation of low pressure type (~ pressure less than 760 torr) and high pressure type lasers (~ high pressure at and above 760 torr) which , although differing in the details of design and electrical circuitary, works in the following basic principle : Generally, a capacitor is charged to a high voltage and then discharged via a spark gap (switch) through the flowing N_2 gas in a glass/quartz tube. The excited molecules emit radiation at different frequencies corresponding to differnt bands, some of which lase under appropriate conditions [2,33-59]. A typical experimental set up is shown in Fig.1.7. It has been found that cooling axially excited N_2 lasers to liquid - air temperature, gave a substantial increase in laser output in comparison with that obtained at room temperature. Usually, very high voltages are required to operate this type of lasers. The efficiencies of an axially excited N_2 laser is low (0.06%) [59], with energy conversion efficiency of 0.35% [56]. For high output power, one needs long discharge tubes which in turn require

enormously high voltages for excitation, which makes the design difficult and uneconomical. More over, uniform distribution of discharge in the cavity may not be possible by axial excitation.

1.05. Transversely excited N_2 lasers

In the majority of TE N_2 lasers [68-152], a Blumlein circuit is employed as an efficient discharge circuit for providing fast rising discharge. The required current rise is of the order of 10^{12} A/s and places severe restrictions on the inductance and resistance (impedance) of the entire discharge circuit. The rate of rise of voltage on the pulse forming line is a function of the switch inductance and the effective capacitances of the energy storage and pulse forming line . To achieve this, the inductance of these elements is minimised [63,71]. Decreasing the impedance of the pulse forming line increases the current and electron density for a fixed electric field. This results in an increase in the excitation rate and a larger population density of the upper laser level leading to higher power. Fig.1.4 represent basic circuits for a Blumlein circuit. The overall maximum

efficiency [41] as determined by dividing the average optical power by the electrical input was 1% and the efficiency defined in terms of the optical energy per pulse divided by the stored electrical energy [72] was about 0.085%. Uniformity in the discharge region can be maintained in the case of TE lasers.

1.06. Travelling wave excitation in N_2 lasers

In order to make the discharge uniform and the high extraction efficiency, a method has been developed in which the electrical discharge starts at one end of the laser tube and moves towards other end with a velocity nearly equal to the velocity of light [83]. This makes it possible for the stimulated light intensity from different segments of the laser tube to be added in only one direction along the cavity axis, leading to a significant difference in the laser output. This method of excitation is known as the travelling wave excitation and Shipman [83] was able to obtain a 2.5 MW peak laser power output with a pulse width of 4 ns. The most elegant and easy way to achieve this is by making a slight wedge between the electrodes where by the electrical discharge starts from the end where the electrodes are closer [86]. For effective

travelling wave excitation, the discharge rise time should be smaller than the light propagation time.

1.07. Electron beam and proton beam excitation techniques

In electron beam excitation, larger volumes can be excited by using high energy electron beam generators and the efficiency of laser systems can also be improved. When the electron beam is propagating in the same direction as the laser beam, the excitation is called longitudinal beam excitation, While the electron beam propagates perpendicular to the axis of the laser tube, the latter called transverse electron beam excitation. Dreyfus and Hodgson [155,156] were the first to report a nitrogen laser excited by a 4 GW longitudinal electron beam. The efficiency of electron-beam power to laser power and energy conversion efficiency were 0.15% and 0.03% respectively.

Golden et al.[157,158] were the first to demonstrate laser action in Ar-N₂ mixtures using a current and space charge-neutralized proton beam as a pump source. The proton beam produced from a reflex tetrode (energy 0.5 J and 450 KeV) was incident transversely on the mylar window gas cell

containing the Ar-N₂ (95% : 5%) mixture at a total pressure ranging from 1 to 1.5 atm.

1.08. Some applications of N₂ laser

A number of N₂ lasers are now commercially available with a range of power, energy and pulse width. Some of the commercial models in use are : Molelectron UV 100 [159], Photochemical Research Associates (PRA) LN 103 [160], EG & G [161], Lambda Physik M 1000 [162], and Central Electronic Ltd.(CEL) NL 103 [163]. It is possible to choose a specific model that will meet the requirements of the desired application. However, some workers still prefer to build their own N₂ laser.

Due to the high peak power and short pulse duration, N₂ laser has been found to be an ideal pump source for dye lasers [164-170], dye laser oscillator-amplifiers [171] and distributed feed back dye lasers (DFDL) [172]. N₂ lasers are useful in the study of laser-induced fluorescence [173], time resolved fluorescence [174,136] and life time studies [175-179] of excited states of a number of molecules in vapour and liquid phase. In addition to these , N₂ lasers have been

employed in various fields like chemical reactions [180] , plasma diagnostics [181-183], remote sensing [184,185], ultra high speed cinematography [146], optical ranging, optical fiber measurements [186], sub-nanosecond interferometry and holography [187-190], fluorescence [191], medical treatment for dermatomycosis [190], laser triggering of spark gaps (LTSG) [124] excitation of rare earth ions in single crystals [193] etc.

A dual channel N_2 laser giving two pulses separated by 15 ns has been used in studying the excited states of molecules [194]. The first pulse excites the molecules (sample under study) and the second pumps a dye laser which is used to probe the excited state of the sample. Microplasma has been generated by high power N_2 lasers [181] and plasma density fluctuations have been investigated by obtaining interference patterns with a sub-nanosecond TEA N_2 laser. Interferometric studies of plasma of dimension less than 1 mm [182] have been carried out.

The nitrogen laser is also used as a frequency mixing component in parametric experiments [101]. The high power density of N_2 laser is well suited for Raman scattering

from gases and vapours [195] and for the study of atmospheric pollutants by remote sensing [185,196,197].

PART B: LUMINESCENCE IN PHOSPHORS

Luminescence is exhibited by almost all substances possessing selective absorption, and under the proper choice of chemical and physical conditions it can be excited in all forms of matter.

1.09. Basic concept of luminescence

In solids and liquids, the excited molecules are apt to lose a part of the absorbed energy in the form of heat to the surrounding molecules and hence the frequency of the emitted light will be less than that of the exciting light. In fact, Stoke's law states that the fluorescent light always has a greater wavelength than the exciting light. If it is recalled that the light absorption occurs when molecules are excited from the ground to excited states, we may well enquire into the fate of the energy so absorbed. Then it leads to an insight into an entirely different realm of spectroscopic phenomena. viz., the fluorescence and phosphorescence emission.

The theory of fluorescence analysis uses the concepts of the light absorption and fluorescence spectra of the substances studied.

1.10. Types of luminescence

Depending on the duration of emission, one can distinguish two types of luminescence phenomena: (i) fluorescence, which ceases abruptly when the excitation source is removed, and (ii) phosphorescence, which persists for a certain time after the removal of the excitation source. A typical pattern of these spectra are shown in Fig.1.8.[198].

At room temperature, virtually all molecules remain in the ground (non-excited) state (level S_0). After the absorption of a light quantum, a molecule get excited (levels S_1^* and S_2^*). This state of a molecule, when the spin of two non-paired electrons are antiparallel, is called the singlet state. Fluorescence is the emission of light during $S_1^* \longrightarrow S_0$ electron transition, in a very short time of the order of 10^{-9} sec. If the spin of the electrons within the excited molecules are parallel, then these molecules are said to be in

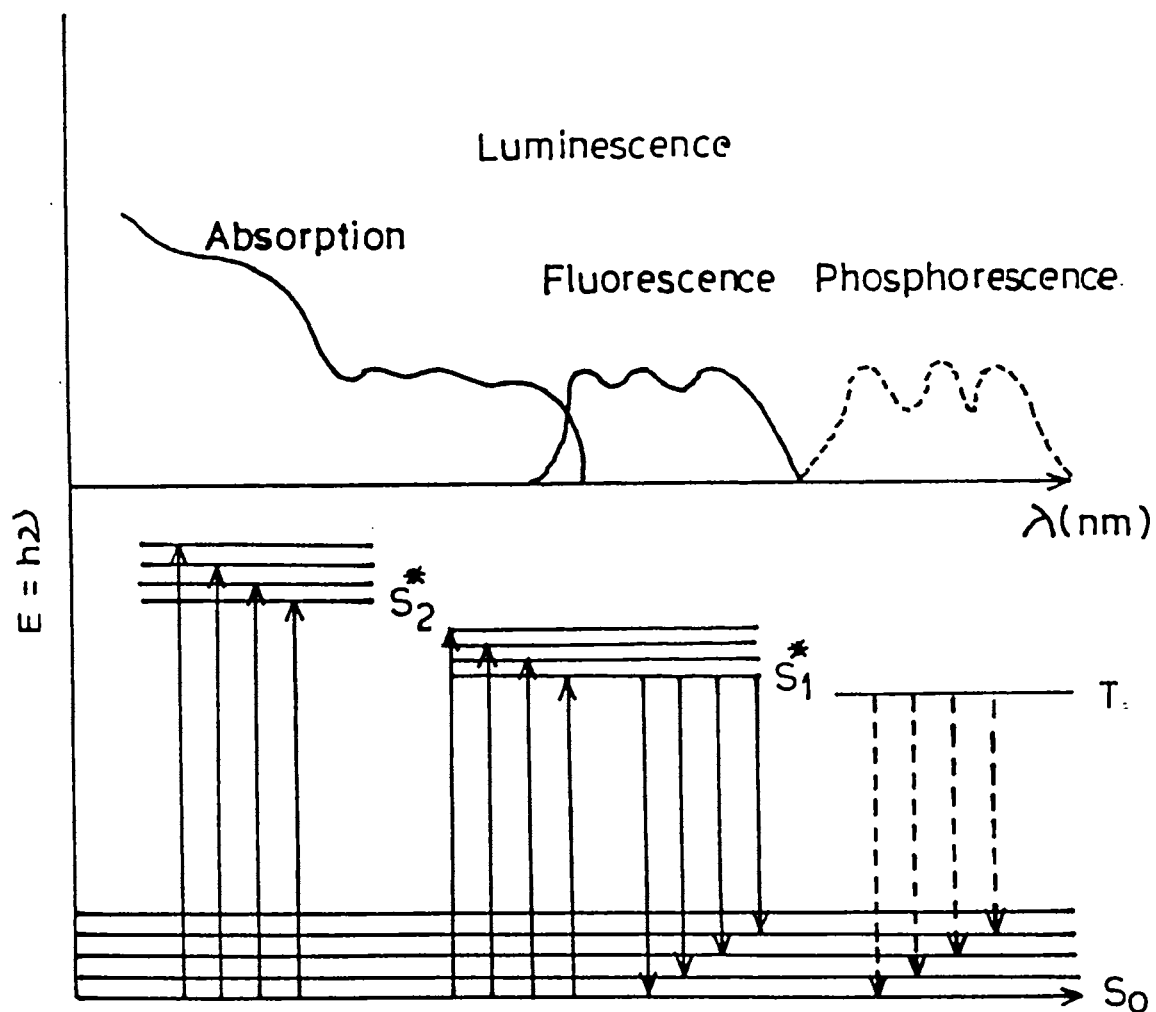


Fig.1.8. Energy levels and the spectra of absorption, fluorescence and phosphorescence of organic molecule.

the triplet state (T level). Phosphorescence is the light emission during $T \longrightarrow S_0$ transition, the life time of the excited state is being fairly long ($\sim 10^{-3}$ sec).

Delayed fluorescence is observed when a molecule in the state T is thermally excited to the upper state before reverting to the ground state S_0 . Thus results from two inter system crossings, first from the singlet to the triplet, then from the triplet to singlet.

The various types of luminescence can be classified according to the means by which energy is supplied to excite the luminescent molecule.

(a) Photoluminescence - the form of luminescence when molecules are excited by interaction with photons of electromagnetic radiation.

(b) Chemiluminescence - the process in which the excitation energy is obtained from the chemical energy of reaction.

(c) Bioluminescence - the electromagnetic energy is released by organisms.

(d) Triboluminescence (in Greek tribo = to rub) - produced as a

release of energy when certain crystals, such as sugar, are broken. The energy stored on crystal formation is released in the breaking of the crystal.

(e) Cathodoluminescence- resulting from a release of energy produced by exposure to cathode rays.

(f) Thermoluminescence - occurs when a material existing in high vibrational energy levels emits energy at a temperature below red heat, after being exposed to small amounts of thermal energy.

(g) Radioluminescence - excitation by means of high energy particles like protons, α and β particles and fission fragments.

(h) Electroluminescence - the excitation produced by the application of an electric field.

(i) Roentgenoluminescence - the process of excitation with the help of ordinary X - rays and its intensity increases with rising voltage.

1.11. Fluorescence and emission processes

The fluorescence normally observed in solutions is called Stoke's fluorescence. This is the reemission of less

energetic photons, which have a longer wavelength (lower frequency) than the absorbed photons.

Anti Stoke's fluorescence, has also been observed in dilute gases at high temperatures. If thermal energy is added to an excited state or a compound has many highly populated vibrational energy levels, emission at shorter wavelengths than those of absorption occurs.

Resonance fluorescence is the reemission of photons possessing the same energy as the absorbed photon. It occurs in gases and crystals. Any fluorescent molecule has two characteristic spectra: (i) the excitation spectrum (the relative efficiency of different wavelengths of exciting radiation to cause fluorescence), and (ii) the emission spectrum (the relative intensity of radiation emitted at various wavelengths).

1.12. Models of luminescence

1.12.1. Configuration co-ordinate model

This is a scheme introduced by Von Hippel in 1936 to give qualitative description of optical processes in

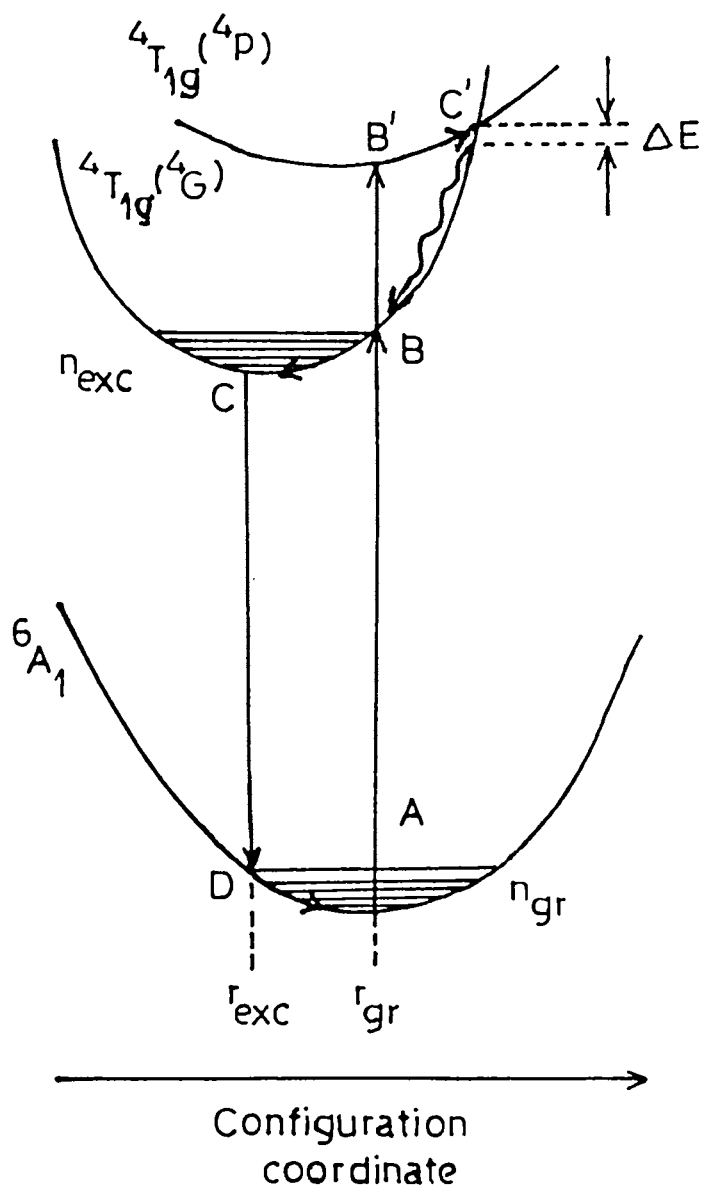


Fig.1.9. Absorption and emission in a configuration curve model depending upon distance between ions in the ground and excited states.

luminescent centres. Later this scheme was applied to many problems of luminescence. The configuration coordinate model is illustrated in Fig.1.9.[199]. The ordinate is the total energy of the system for ground and excited states of the centre including both ionic and electronic terms. The abscissa is a configuration co-ordinate which specifies the configuration of the ions around the centre. The equilibrium position of the ground state occurs at A. When the centre absorbs light, it is raised to the excited state at B obeying Franck Condon principle. After the centre has reached the excited state, the ions of the system adjust to a new equilibrium C. The energy difference between B and C is given off as lattice vibrations. Having reached the new equilibrium position C, the center may return to the ground state at D by emission of a quantum of luminescent light. Relaxation from D to A is by means of energy dissipation through lattice vibrations. Obviously the energy of the emitted photon is smaller than that of the absorbed photon. The amount of this shift in energy of photon (Stoke's shift) arising in a given system depends on the interaction of the centre with the neighbouring ions. In addition to the Stoke's shift, these curves account for the sudden decrease in luminescence

efficiency at very high temperatures.

1.12.2. Band theory model

The application of quantum mechanics to the luminescent phenomena resulted in the development of the band theory model for electrons in a periodic potential and theoretical basis for excitation in crystals. When atoms are arranged in an orderly way and in close proximity to each other to form a crystal, the energy states for the electron in atoms are disturbed by mutual interaction. As a result, the discrete electronic states are broadened into bands of allowed energy, separated by forbidden bands. The upper most completely filled band is called the valence band and the next allowed band is called the conduction band.

1.13. Kinetics of luminescence

We usually distinguish two kinds of luminescence processes, that with kinetics of the first order (monomolecular mechanism) and that having second order kinetics (bio-molecular mechanism).

1.13.1. First order kinetics

The number of excited electrons 'n' decreases according to a constant probability law:

$$\frac{dn}{n} = -\alpha dt \quad \dots\dots\dots(1.26)$$

which gives $n = n_0 e^{-\alpha t}$ and since the luminescence intensity

$$I = \frac{dn}{dt}$$

So,

$$I = I_0 e^{-\alpha t} \quad \dots\dots\dots(1.27)$$

One of the major characteristics of excited states is their life time, ie; the average stay of ion in a given excited state.

1.13.2. Second order kinetics

The probability for recombination is proportional to the number of available centres

$$\frac{dn}{n} = -\alpha n dt \quad \dots\dots\dots(1.28)$$

and so 'n' decreases hyperbolically with time,

$$n = \frac{n_0}{(1+n_0 \alpha t)} \dots\dots\dots(1.29)$$

the luminescence decay then being given by

$$I = \frac{dn}{dt} = \alpha n^2 \dots\dots\dots(1.30)$$

thus,

$$I = \frac{I_0}{(1 + at)^2} \dots\dots\dots(1.31)$$

where $a = (I_0 \alpha)^{1/2}$

The decay thus becomes more rapid as the excitation intensity is increased.

1.14. Quantum efficiency

Every molecule possesses a characteristic property that is described by a number called the quantum yield, or quantum efficiency, ϕ . This is the ratio of the total energy per quantum of energy absorbed.

$$\phi = \frac{\text{number of quanta emitted}}{\text{number of quanta absorbed}}$$

The higher the value of ϕ , the greater the fluorescence of a compound. Normally, the fluorescence quantum yield ϕ , is considerably less than 1.

The radiant energy efficiency (η) is defined as the ratio of the emitted fluorescent power to the power absorbed by the phosphor from the exciting radiation (expressed in watts). The luminous efficiency is the ratio of the emitted luminous flux in lumens to the absorbed power in watts.

Let us assume that the phosphor is excited by monochromatic radiation of wavelength λ_0 and that the absorbed power P_a . If the fluorescence is emitted over a wide range of wavelengths,

$$\text{the total power involved } P = \int P_\lambda \, d\lambda \quad \dots\dots\dots(1.32)$$

where,

P_λ - the emitted power of wavelength λ

The integration being taken over the whole range of wavelengths.

The radiant efficiency is then given by,

$$\eta = \frac{P}{P_a} = \frac{\int P_{\lambda} d\lambda}{P_a} \dots\dots(1.33)$$

The energy of one quantum is $h\nu = hc/\lambda$, where h is the Planck's constant and C is the velocity of light. So the quantum efficiency is,

$$q = \frac{\int \lambda P_{\lambda} d\lambda}{\lambda_o P_a} \dots\dots\dots(1.34)$$

The lumen efficiency L can be of great practical importance ,

$$L = \frac{K_m \int P_{\lambda} \bar{Y}_{\lambda} d\lambda}{P_a} \dots\dots\dots(1.35)$$

where, \bar{Y}_{λ} denotes the sensitivity of the eye as a function of wavelength and K_m is the maximum value of the luminous flux per watt of radiant power.

ie; 673 lm/W (at 555 nm).

1.15. Life time of the excited state

The fluorescence life time of most organic molecule is in the nanosecond region. The fluorescence life time τ refers to the mean life time of the excited state. The

probability of finding a given molecule that has been excited still in the excited state after time t is $e^{-t/\tau}$. The general equation relating the fluorescence intensity I and the life time τ is,

$$I = I_0 e^{-t/\tau} \dots\dots\dots(1.36)$$

where, I - the fluorescence intensity at time t

I_0 - the maximum fluorescence intensity during the excitation

t - the time after removing source of excitation,

and, τ - the average life time of the excited state.

1.16. Relation between fluorescence and concentration

The basic equation defining the relationship of fluorescence to concentration is,

$$F = \phi I_0 (1 - e^{-\epsilon bc}) \dots\dots\dots(1.36)$$

where, ϕ - the quantum efficiency

I_0 - the incident radiant power

ϵ - the molar absorptivity

b - the path length of the cell

c - the molar concentration

There are three major factors other than concentration that affect the fluorescence intensity. They are the quantum efficiency ϕ , the intensity of incident radiation I_0 and the molar absorptivity of the compound ϵ .

As per Beer's law in spectrophotometry,

$$F = K \phi I_0 \epsilon b c \quad \dots\dots\dots(1.37)$$

Thus a plot of fluorescence versus concentration is linear at low concentrations and reach a maximum at higher concentrations. At higher concentration, quenching becomes so great that the fluorescence intensity decreases. The quenching is due to enhancement in nonradiative de-excitation as concentration is increased.

1.17. Action of temperature

Fluorescence spectra undergo drastic changes with change of temperature. When the temperature is raised, vibrational and rotational energies increase on account of thermal agitation and a general broadening of the emission spectrum takes place. But the effect of large decreases in temperature approximating that of liquified gases is to break

up the broad bands into individual vibrational bands due to the reduction of thermal agitation and the simplification of the modes of vibration and rotation of the molecules. The emission lines at these low temperatures, therefore, arise from one or at most a few low-lying levels. The spectra arising from higher levels vanish because of the disappearance of the population of the atom in these levels and hence low-temperature conditions become favourable for the existence of metastable states.

1.18. Phosphors

The word 'phosphor' is a Greek word meaning 'light bearer' and is usually applied to inorganic luminescence solids which are prepared by a suitable heat treatment. Luminescence of oxygen-dominated lattices has been observed for many years in naturally occurring phosphates, silicates, carbonates and other minerals. It was not until the advent of the fluorescent lamp in the middle of 1930's that any significant amount of technical effort was expended in studying and developing these phosphors. The basis of the fluorescent lamp is the efficient conversion of electrical energy into

ultraviolet radiation in the low pressure mercury vapour discharge, followed by the efficient conversion of ultraviolet to visible radiation by a phosphor. Most of the early classical work on phosphors was concerned with sulphides. These had been developed to a high state of perfection before serious attempts were made to synthesize the oxygen containing materials which now form the basis of the fluorescent lamp industry.

Phosphors have achieved ever increasing importance in optical technology since 1938. Mercury discharge lamps are well known for the excellent light yield (30-75 lumens/watt). Low pressure mercury discharge lamps produce a large amount of short wave ultraviolet radiation. It is an obvious step to transform the spectrum of these lamps by phosphors from uv to light of a colour of emission that would both be transmitted by glass envelopes and suit the peak sensitivity of the human eye (540 nm).

1.18.1. Classes of phosphors

Phosphors may be divided broadly into two classes, according to the distinction between the types of

chemical bonding of the matrix lattice: sulphide phosphors with mainly covalent bonding, and oxygen-dominated phosphors of a more ionic in character. Although the distinction between the two classes is by no means rigid, there are differences in behaviour which can be theoretically explained. Sulphide phosphors behave as photoconductors under the influence of an electric field and suitable source of radiation, whereas oxygen dominated phosphors are more nearly insulators under these conditions. The mechanism of the process in sulphide phosphors is based on the familiar energy band model and applied successfully to modern semiconductor materials.

Phosphors containing oxygen, such as silicates, phosphates and borates are mainly ionic in character and have properties more closely associated with the activator centre than with the host lattice. In these phosphors, it is assumed that excited electrons remain within the field of the activator centre and consequently little or no photoconduction is observed.

1.18.2. Activators

Phosphors as mentioned earlier are generally

inorganic solids which are able to convert absorbed energy into visible light. Most phosphors require the presence of a small quantity of a specific activator which is incorporated in the crystal matrix during heat treatment to induce luminescence when suitably excited. The emission spectra of most phosphors consists of broad structureless bands, the position of which may vary with a given activator over a range of wavelengths. For example, manganese in divalent state gives green colour in Zinc Silicate while red in Cadmium Borate. This variation indicates that the radiative processes in the activator centre are affected by the matrix environment. The valency state of the activator is also an important factor in determining both excitation and emission characteristics of phosphors.

1.18.3. Rare earth activated phosphors

Rare earth elements are widely used as activators in sulphide phosphors. Let us consider the possible optical process that may occur in a crystal containing rare earth ions. Fig.1.10. [200] shows part of a crystal M in which two kinds of foreign ions or ionic groups (centres) are incorporated. One centre of each type is shown, marked A (as

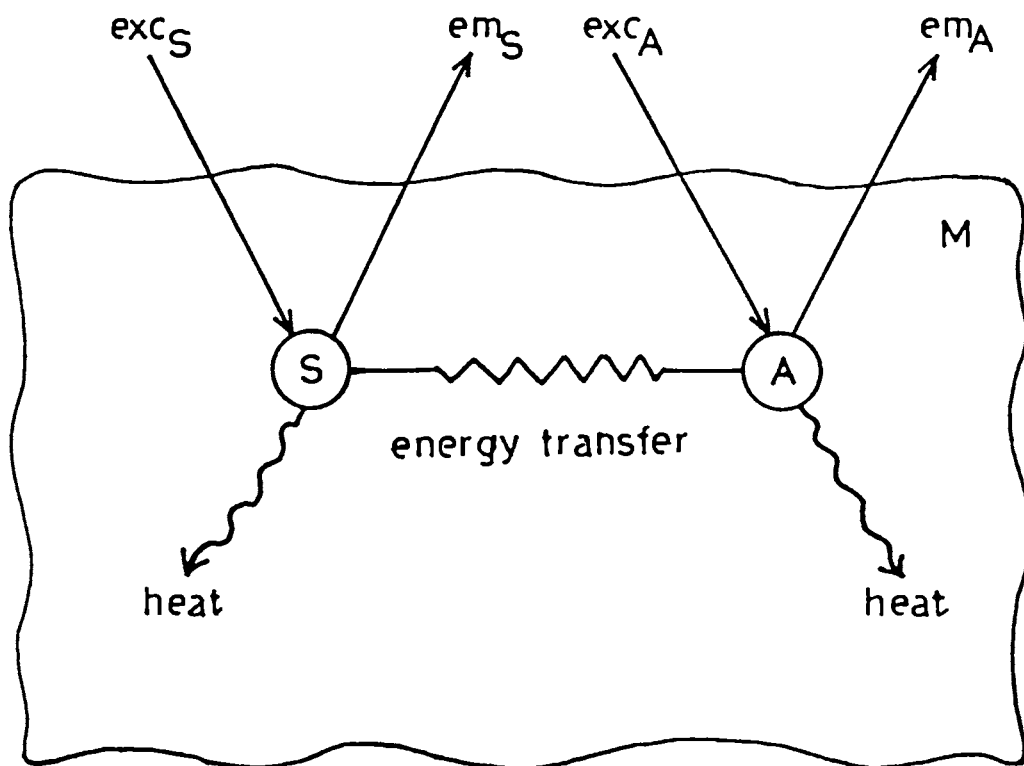


Fig.1.10. Diagrammatic representation of luminescence.
exc: excitation (absorption or radiation)
em : emission.

activator) and S (as sensitizer). The host lattice does not absorb incident radiation. The activator A can absorb radiation (exc_A). This excitation is followed by emission (em_A) and or by the dissipation of heat. The activator can also be excited via the sensitizer S. In this case S absorbs the radiation (exc_S) and then transfers excitation energy to A. Emission and/or heat dissipation from S are also possible.

Research on the phosphors has considerably advanced so as to help us in understanding luminescence phenomenon. The properties of phosphors can be studied on simple model compounds [201]. The host lattice may be, for instance, a compound of the ions La^{3+} , Y^{3+} or Lu^{3+} . The latter ions do not absorb ultraviolet radiation. Rare earth ions, for example Eu^{3+} or Tb^{3+} , are now substituted for a small proportion of the host lattice ions. These rare earth ions occupy in the host lattice at the crystallographic sites of La^{3+} , Y^{3+} or Lu^{3+} in a virtually random distribution. It is possible in this way to make phosphors whose chemical constitution is well defined.

1.19. Energy level diagram of rare earth ions

The characteristic properties of the rare earth

ions are attributable to the presence of the ion of a deep-lying 4f shell which is not entirely filled. The electrons of this shell are screened by the outer electron

Table 1.4. Rare earth elements and some of their spectroscopic properties.

Atomic number	Element	Electron configuration RE ³⁺	Ground term RE ³⁺
57	Lanthanum	4f ⁰ (5s ² 5p ⁶)	¹ S ₀
58	Cerium	4f ¹ (5s ² 5p ⁶)	² F _{5/2}
59	Praseodymium	4f ² (5s ² 5p ⁶)	³ H ₄
60	Neodymium	4f ³ (5s ² 5p ⁶)	⁴ I _{9/2}
61	Promethium	4f ⁴ (5s ² 5p ⁶)	⁵ I ₄
62	Samarium	4f ⁵ (5s ² 5p ⁶)	⁶ H _{5/2}
63	Europium	4f ⁶ (5s ² 5p ⁶)	⁷ F ₀
64	Gadolinium	4f ⁷ (5s ² 5p ⁶)	⁸ S _{7/2}
65	Terbium	4f ⁸ (5s ² 5p ⁶)	⁷ F ₆
66	Dysprosium	4f ⁹ (5s ² 5p ⁶)	⁶ H _{15/2}
67	Holmium	4f ¹⁰ (5s ² 5p ⁶)	⁵ I ₈
68	Erbium	4f ¹¹ (5s ² 5p ⁶)	⁴ I _{15/2}
69	Thulium	4f ¹² (5s ² 5p ⁶)	³ H ₆
70	Ytterbium	4f ¹³ (5s ² 5p ⁶)	² F _{7/2}
71	Lutecium	4f ¹⁴ (5s ² 5p ⁶)	¹ S ₀

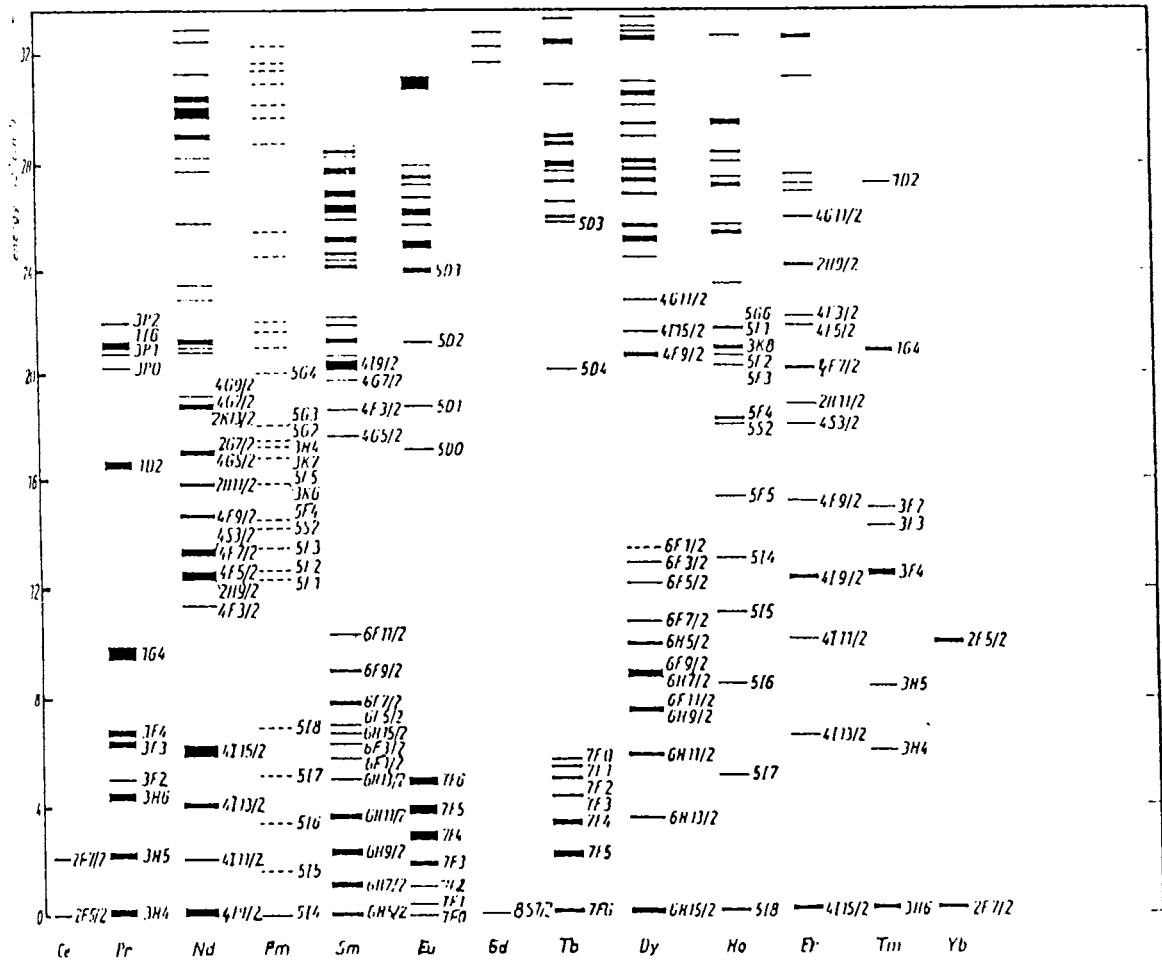


Fig.1.11 Energy level diagram for RE³⁺ ions.

shells, and as a result they give rise to a number of discrete energy levels. Since the presence of the crystal lattice scarcely affects the positions of these levels, there is a close resemblance between the energy level diagram of the free ion and that of the incorporated ion.

Table 1.4 shows the rare earth elements and some of their spectroscopic properties. The energy level diagram for RE^{3+} ions is shown in fig. 1.11. [199]. The Ce^{3+} ion has only one 4f electron which gives rise to two levels (${}^2F_{7/2}$ and ${}^2F_{5/2}$). As the number of electrons increases, there is in general a rapid increase in the number of possible states.

In addition to the discrete 4f levels, there are other levels present. These levels depend strongly on the lattice in which the RE ion is incorporated. They fall into two groups. In the first group, one of the 4f electrons is raised to the higher 5d level: $4f^n \longrightarrow 4f^{n-1} 5d$. The 5d orbit lies at the surface of the ion and is therefore strongly influenced by the lattice. In the second group one of the electrons of the surrounding anion of the lattice jumps into the 4f orbit of the central RE ion. This is called a charge transfer transition.

1.20. Energy transfer

The first requirement for a luminescent material is that it emits radiation. It is trivial that this leads to the requirement that exciting radiation must be absorbed. It is seen that 4f-4f transitions of RE are not very stable for absorption or radiation, because they are strongly forbidden. Excitation may occur efficiently in either the charge transfer state or the $4f^{n-1} 5d$ state. An example of the first case is $GdO_2 : Eu^{3+}$ [202]. Short wave uv radiation is strongly absorbed by the Eu^{3+} ion exciting it into its charge-transfer state. The ion then relaxes to the 5D_0 level from which luminescence occurs. An example of the second case is $YTbO_4 : Tb^{3+}$ which can be excited efficiently by UV radiation into the $4f^7 5d$ state [203].

Fig. 1.12 shows the mechanism by which the energy transfer occurs [200]. We start with the system S (excited) + A (ground state) and end up with the system S (ground state) + A (excited). This is only possible, if one of the levels of A lies at the same height as the luminescent level of S

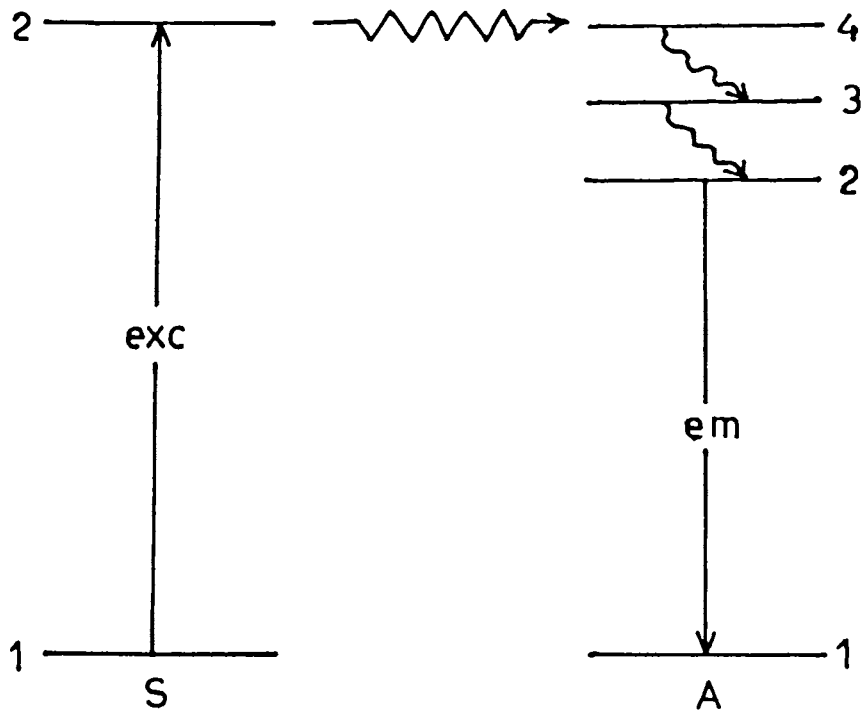


Fig.1.12. Energy transfer from S to A. Transfer occurs to level 4, followed by radiationless decay to level 2 from which emission occurs.

(resonance condition). Further we need an interaction between S and A.

Transfer can be brought about in the first place by the Coulomb interaction between all charged particles of S and A. If S and A are so far apart that their charge clouds do not overlap, this form of energy transfer is the only one possible. If these do overlap, however another process is possible by exchange interaction between the electrons of S and A. In this process, electrons are exchanged between S and A, in the former the electrons remain with their respective ions.

As described earlier RE^{3+} ions retain their characteristic free ion levels in a crystal lattice due to screening of f electrons by those in outer shells. However, their spectra are rich in fine structure due to ion-lattice interaction. The nature of this interaction depends on the ions and the symmetry of crystal field. Splitting of free ion terms in crystal fields are some times called Stark splitting [199]. Details of Stark splitting are given chapter 6.

REFERENCES

- [1] L.E.S.Mathias and J.T.Parker, Appl.Phys.Lett.,
3, 16 (1963).

- [2] H.G.Heard, Nature., 200, 667 (1963).

- [3] J.W.Keto, T.D.Raymond, S.T.Walsh, Rev.Sci.Instrum.,
51, 42 (1980).

- [4] V.F.Papakin and A.Yu.Sonin, Sov.J.Quant.Electron.,
8, 901 (1978).

- [5] H.Schmidt , H.Salzmann, H.Strohwal, Appl.Opt.,
14, 2250 (1975).

- [6] W.R.Bittle, E.E.Bergmann, N.Eberhardt, Bull.Am.Phys.Soc.,
21, 86 (1976).

- [7] S.N.Suchard, L.Galvan and D.G.Sutton, Appl.Phys.Lett.,
26, 521 (1975).

- [8] S.C.Mehendale and D.D.Bhawalkar, J.Appl.Phys.,
53(9), 6444 (1982).

- [9] R.A.McFarlane, Phys.Rev., **A 140**, 1070 (1965).
- [10] R.A.McFarlane, Phys.Rev., **146**, 37 (1966).
- [11] A.A.Tagliaferri, M.Gallardo, C.A.Massone and M.Garavaglia, Phys.Lett., **45A**, 211 (1973).
- [12] R.A.McFarlane, In : Physics of Quantum Electronics, P.655 (Proc. Int.Conf.San Juan, Puerto Rico 1965), Mc Graw-Hill, New York (1966).
- [13] S.N.Suchard, D.G.Sutton and R.F.Heidner, III, IEEE J.Quant.Electron., **QE-11**, 908 (1975).
- [14] R.Beck, W.English and K.Gurs, Table of Laser Lines in Gases and Vapours, P.36, Springer, Berlin (1976).
- [15] J.P.Singh and S.N.Thakur, J.Scient. and Ind.Res., **39**, 613 (1980).
- [16] R.S.Kunabenchi, M.R.Gorbal and M.I.Savadatti, Prog.Quant. Electron., **9**, 259 (1984).
- [17] J.R.Howorth, J.Phys.Atom.Molec.Phys., **5B**, 402 (1972).
- [18] J.C.Georges, J.Phys.Atom.Molec.Phys., **9B**, 2153 (1976)

- [19] D.C.Cartwright, *Phys.Rev.*, **2A**, 1331 (1970).
- [20] C.S.Willett, *An Introduction to Gas Lasers : Population Inversion Mechanisms* (Pergamon Press Ltd; Oxford), 342-362, (1974).
- [21] L.Allen, D.G.C.Jones and B.M.Sivaram, *Phys.Lett.*, **25A**, 280 (1967).
- [22] V.M.Kaslin and G.G.Petrash, *Proc.lebedev.Phys.Inst.*, **81**, 135 (1976).
- [23] T.Kasuya and D.R.Lide Jr. *Appl.Opt.*, **6**, 69 (1967).
- [24] C.A.Massone, M.Garavaglia, M.Gallrado, J.A.E.Calatroni and A.A.Tagaliaferri, *Appl.Opt.*, **11**, 1317 (1972).
- [25] T.J.Gleason, C.S.Willett, R.M.Curnutt and J.S.Kruger, *Appl.Phys.lett.*, **21**, 276 (1972).
- [26] M.A.Pollock, *Molecular Gas Lasers*, In: *Hand Book of Lasers*, P.298, Ed. R.J.Pressley, Chemical Rubber Co; Cleveland, Ohio (1971).
- [27] V.F.Tarsenko and Yu.I.Bychkov, *Sov.Phys-Tech.Phys.*, **19**, 693 (1974).

- [28] V.M.Kaslin, I.N.Knyazev and G.G.Petrash, *Kratk. Soobshch.Fiz.*, **1**, 51 (1971).
- [29] L.O.Hocker, *IEEE J.Quant.Electron.*, **QE-13**, 548 (1977).
- [30] C.B.Collins, A.J.Cunningham, S.M.Curry, B.M.Johnson and M.Stockton, *Appl.Phys.Lett.*, **24**, 477 (1977).
- [31] C.B.Collins, A.J.Cunningham and M.Stockton, *Appl.Phys. Lett.*, **25**, 344 (1974).
- [32] V.N.Ishchenko, V.N.Lisitsin, A.M.Razhev, V.N.Starinsky and P.L.Chapovsky, *Opt.Commun.*, **13**, 231 (1975).
- [33] J.B.Laudenslager, T.J.Pacala, C.Wittig, *Appl.Phys.Lett.*, **29**, 580 (1976).
- [34] D.E.Rothe and K.O.Tan, *Appl.Phys.Lett.*, **30**, 152 (1977).
- [35] M.Jeunhomme, *J.Chem.Phys.*, **44**, 2672 (1966).
- [36] M.Jeunhomme, *J.Chem.Phys.*, **45**, 1805 (1966).
- [37] M.Jeunhomme, *J.Chem.Phys.*, **41**, 1692 (1969).
- [38] E.T.Gerry, *Appl.Phys.Lett.*, **7**, 6 (1965).
- [39] D.A.Leonard, *Appl.Phys.Lett.*, **7**, 4 (1965).

- [40] A.W.Ali, A.C.Kolb and A.D.Anderson, Appl.Opt.,
6, 2115 (1967).
- [41] B.Godard, IEEE J.Quant.Electron., QE-10, 147 (1974).
- [42] P.Persephonis, Optics Commun., 62, 265 (1987).
- [43] P.Persephonis, J.Appl.Phys., 62(7), 2651 (1987).
- [44] V.M.Kaslin and G.G.Petrash, Proc.Lebedev Phys.Inst.,
81, 110 (1976); Pulse Gas-Discharge Atomic and Molecular
Lasers, Ed.by N.G.Basov.
- [45] K.E.Ericsson and L.R.Lidholt, Appl.Opt.,7, 211 (1968).
- [46] H.Gundel and W.Ross, Ann.Phys., 31, 263 (1974).
- [47] J.S.Kruger, IEEE J.Quant.Electron., QE-11, 801 (1975).
- [48] V.F.Tarassenko and Yu.A.Kurbatov, Instrum.Exp.Tech.,
16, 219 (1973).
- [49] W.W.Wladimiroff and H.E.B.Andersson, J.Phys.E : Sci.
Instrum., 10, 361 (1977).
- [50] M.Geller, D.E.Altman and T.A.DeTemple, J.Appl.Phys.,
37, 3639 (1966).

- [51] O.Steinvall and A.Anvari, J.Phys.E: Sci.Instrum.,
6, 1125 (1973).
- [52] A.V.Sviridov and Yu.D.Tropiklin, Sov.J.Quant.Electron.,
6, 1333 (1976).
- [53] A.V.Sviridov and Yu.D.Tropiklin, Sov.J.Quant.Electron.,
8, 1177 (1978).
- [54] W.Ross, J.Irmer and K.Seliger, 2nd int.Conf.on Gas
Discharges, P.115, London, England (1972).
- [55] H.Fisher, J.Opt.Soc.Am., 51, 543 (1961).
- [56] H.Fischer, R.Girnus and F.Ruhl, Appl.Opt., 13,1759 (1974).
- [57] H.Boersch and F.J.Theiss, Z.Naturforsch.A . ,
27 a, 236 (1974).
- [58] M.Garavagha, M.Gallardo and C.A.Massone, Phys.Lett.,
28A, 787 (1969).
- [59] Yu.I.Bychkov, M.N.Kostin, V.F.Losey and V.F.Tarasenko,
Instrum. Exp.Tech., 21, 1093 (1979).
- [60] F.J.Theiss, Opt.Comm., 9, 22 (1973).
- [61] G.Herziger and F.J.Theiss, Z.Angew Phys.,29, 157 (1970).

- [62] N.R.Nilsson, O.Steinvall, C.K.Subramanian and L.Hogberg,
Phys.Scripta., 1, 153 (1970).
- [63] F.Ruhl, F.W.Linder and H.Fischer, Appl.Phys., 3,245(1974).
- [64] H.E.B.Andersson and R.C.Tobin, Phys.Scripta., 9,215(1971).
- [65] H.E.B.Andersson and R.C.Tobin, Phys.Scripta., 9,7 (1974).
- [66] H.E.B.Andersson and R.C.Tobin, Phys.Scripta., 11,5 (1975).
- [67] A.G.Abramov, E.I..Asinovskii and L.M.Vasilyak,
Sov.J.Quant.Electron., 13, 1203 (1983).
- [68] Yu.M.Tokunov, E.I.Asinovskii and L.M.Vasilyk, High Temp.,
19, 347 (1981).
- [69] A.Svedberg, L.Hogberg and R.Nilsson, Appl.Phys.Lett.,
12, 1202 (1968).
- [70] T.Kobayashi, K.Sugimura and H.Inaba, Opt. Quantum.
Electron., 11, 373 (1979).
- [71] A.Nomura, N.Takgishi, Y.Saito and T.Kano, Trans.Inst.
Electr. Comm.Eng.Jpn., J66C, 102 (1983).
- [72] W.A.Fitzsimmons, L.W.Anderson, C.E.Riedhauser and

- J.M.Vrtilek, IEEE.J.Quant.Electron., QE-12, 624 (1976).
- [73] M.Geller, D.E.Altman and T.A.De Temple, Appl.Opt.,
7, 2232 (1968).
- [74] M.L.Pascu, A.Pascu, G.Dubraveanu and A.Constantinescu,
Rev.Roum.Phys., 23, 1041 (1978).
- [75] P.Schenck and H.Metcalf, Appl.Opt., 12, 183 (1973).
- [76] M.Feldman, P.Lebow, F.Raab and H.Metcalf, Appl.Opt.,
17, 774 (1978).
- [77] R.C.Hilborn, Am.J.Phys., 44, 1172 (1976).
- [78] P.Glowczewski, J.Goehowski, J.Krasinski and A.Sieradzan,
Opt.Appl., 10, 145 (1980).
- [79] T.Baer, Appl.Opt., 15, 2953 (1976).
- [80] G.J.Harvilla, R.B.Green and Trask, Appl.Opt.,
17, 3525 (1978).
- [81] R.Cubeddu and S.M.Curry, IEEE J.Quant.Electron.,
QE-9, 499 (1973).
- [82] I.Nagata and Y.Kimura, J.Phys.E : Sci.Instrum.,

| 6, 1193 (1973).

[83] D.Shipman, Jr. and A.C.Kolb, IEEE J.Quant.Electron.,
QE-2, 298 (1966).

[84] J.D.Shipman Jr, Appl.Phys.Lett., 10, 3 (1967).

[85] T.Mitani and T.Nakaya, J.Phys.D. Appl.Phys., 11, 2071 (1978).

[86] T.Mitani, H.Ninomiya, S.Horiguchi and T.Nakaya, Mem.Konan.
Univ.Sci.Ser., 19, 267 (1976).

[87] Tac-Soo Kim, Chut-Kew Hwang, Eun-Ka Kim, Doo-Hwan Suh and
Dae-Yoon Park, New Phys., 17, 197 (1977).

[88] D.Basting, F.P.Schaffer and B.Steyer, Opto-Electron.,
4, 43 (1972).

[89] J.I.Levatter and Shao-Chi Lin, Appl.Phys.Lett.,
25, 703 (1974).

[90] H.E.B.Andersson and S.A.Borgstrom, Opto-Electron.,
6, 225 (1974).

[91] R.S.Kunabenchi, M.R.Gorbal and M.I.Savadatti, Am.J.Phys.,
50, 568 (1982).

- [92] M.M.F.Sabry, A.Hasson and M. Ewaaida, J.Phys.E:Sci. Instrum., 17, 103 (1984).
- [93] J.G.Small, Laser Photochemistry, Tunable Lasers and other Topics, P.343, Santa Fe, New Mexico, U.S.A. 23 June-3 July 1975, Addison-Wesley, Reading, MA (1976).
- [94] J.G.Small and R.Ashari, Rev.Sci.Instrum., 43, 1205 (1972).
- [95] V.V.Itagi, B.H.Pawar and Sharada Itagi, Ind.J.Phys., 54B, 337 (1980).
- [96] C.S.Willett and D.M.Litynski, Appl.Phys.Lett., 26, 118 (1975).
- [97] R.Cubeddu and S.M.Curry, IEEE J.Quant.Electron., QE-9, 499 (1973).
- [98] M.Maeda, T.Ydmashita and Y.Miyazoe, Jap.J.Appl.Phys., 17, 239 (1978).
- [99] H.M.Bastiaens, T.Gerber and P.J.M.Peters, Opt.Lett., 9, 113 (1984).
- [100] W.Ross and K.Seligler, Beitr.Plasma Phys., 16,111 (1976).
- [101] C.L.Sam and M.M.Choy, Appl.Phys.Lett., 30, 199 (1977).

- [102] J.P.Singh and S.N.Thakur, Ind.J.Phys., 55B, 422 (1981).
- [103] V.F.Tarasenko, Yu.I.Bychkov, Sov.Phys-Tech.Phys.,
19, 693 (1974).
- [104] C.Lal and S.N.Thakur, Appl.Opt., 21, 2317 (1982).
- [105] L.B.Loeb, Science., 148, 1417 (1965).
- [106] V.Rebhan, J.Hildebrandt and G.Skopp, Appl.Phys.,
23, 341 (1980).
- [107] K.H.Krahn, J.Appl.Phys., 50, 6656 (1979).
- [108] K.H.Krahn, Appl.Phys., 21, 319 (1980).
- [109] I.Baltog and C.B.Collins, Opt.Comm., 18, 282 (1976).
- [110] N.A.Kurnit, S.J.Tubbs, K.Bidhichand, L.W.Ryan,Jr. and
J.Javan, IEEE J.Quant.Electron., QE-11, 174 (1975).
- [111] T.Arai,M.Obara and T.Fujioka,J.Appl.Phys.,51,3556(1980).
- [112] P.Persephonis, G.Giannetas and R.Rigopoulos, Rev.Phys.
Appl., 18, 731 (1983).
- [113] B.W.Woodward, V.J.Ehlers and W.C.Lineberger,
Rev.Sci.Instrum.,10, 361 (1977).

- [114] P.Persephonis, G.Giannetas and R.Rigopoulos,
Rev.Phys.Appl., 18, 295 (1983).
- [115] C.P.Wang, Rev.Sci.Instrum., 49,92 (1976).
- [116] V.S.Arakebyan, A.A.Avetisyan, V.G.Atakbkyan, V.M.
Mkhitaryan and V.V.Pakhlavuni, Instrum.Exp.Tech.,
24, 486 (1981).
- [117] A.J.Schwab and F.W.Hollinger, IEEE J.Quant.Electron.,
QE-12, 183 (1976).
- [118] J.Lawson, R.Coon and E.E.Bergmann, Bull.Am.Phys.Soc.,
18, 65 (1973).
- [119] C.Stanciulescu, R.C.Robulescu, D.Popescu, N.Ceausescu
and I.Popescu, Rev.Roum.Phys., 24, 301 (1979).
- [120] V.F.Papakin and A.Yu.Somin, Instrum.Exp.Tech.,
22, 210 (1979).
- [121] E.E.Bergmann and N.Eberhardt, IEEE J.Quantum.Electron.,
QE-9, 853 (1973).
- [122] M.L.Pascu, A.Constantinescu, A.Pascu and G.Dumbraveanu,
Rev.Roum.Phys., 23, 569 (1978).

- [123] S.Saikan and F.Shimizu, Rev.Sci.Instrum., 46, 1700(1975).
- [124] E.G.Jones, S.Afr.J.Phys. 3, 49 (1980).
- [125] V.F.Tarsenko, Instrum.Exp.Tech., 17, 197 (1974).
- [126] R.Targ, IEEE J.Quantum.Electron., QE-8, 726 (1972).
- [127] K.Schildback and D.Basting, Rev.Sci.Instrum.,
45, 1015 (1974).
- [128] M.I.Savadatti, R.S.Kunabenchi and M.R.Gorbal,
Ind.J.Phys., 54B, 204 (1980).
- [129] A.J.Schmidt, J.Phys.E: Sci.Instrum., 10, 453 (1977).
- [130] A.V.Armichev, V.S.Aleinko and T.B.Fogelson,
Sov.J.Quant.Electron., 10, 592 (1980).
- [131] R.T.Brown and D.C.Smith, Appl.Phys.Lett., 24, 236 (1974).
- [132] P.Richter, J.D.Kimel and G.C.Moulton, Appl.Opt.,
15, 756 (1976).
- [133] A.Rothem and S.rosenwaks, Opt.Comm., 30,227 (1979).
- [134] H.Salzmann and H.Strohwal, Opt.Comm., 12, 370 (1974).

- [135] A.W.Ali, *Appl.Opt.*, **8**, 993 (1969).
- [136] A.Saikan, *Jap.J.Appl.Phys.*, **15**, 187 (1976).
- [137] H.Strohwald and H.Salzmann, *Appl.Phys.Lett.*, **28**, 272 (1976).
- [138] C.L.Sam, *Appl.Phys.Lett.*, **29**, 505 (1976).
- [139] B.Godard and M.Vannier, *Opt.Commun.*, **16**, 37 (1976).
- [140] V.Hasson and H.M.von Bergmann, *Rev.Sci.Instrum.*,
50, 59 (1979).
- [141] H.M.von Bergmann, *J.Phys.E:Sci.Instrum.*, **10**, 1210 (1977).
- [142] H.M.von Bergmann, V.Hasson and D.Preussler, *Appl.Phys.*
Lett., **27**, 553 (1975).
- [143] E.E.Bergmann, *Appl.Phys.Lett.*, **28**, 84 (1976).
- [144] M.Hugenschmidt and J.Wey, *Opt.Commun.*, **29**, 191 (1979).
- [145] T.Jitsuno, T.Mitani and T.Nakaya, *J.Phys.D:Appl.Phys.*,
12, 1503 (1979).
- [146] E.E.Bergmann, *Rev.Sci.Instrum.*, **48**, 545 (1977).
- [147] H.M.von Bergmann, V.Hasson and J.Brink, *Opt.Commun.*,

18, 180 (1976).

[148] H.M.von Bergmann and V.Hasson, J.Phys.E:Sci.Instrum.,
9, 982 (1976).

[149] H.M.von Bergmann and A.J.Penderis, J.Phys.E:Sci.Instrum.,
10, 602 (1977).

[150] W.Herden, Phys.Lett., 54A, 96 (1975).

[151] V.Hasson, D.Preussler, J.Klimek and H.M.von Bergmann,
Appl. Phys.Lett., 25, 654 (1974).

[152] C.Iwasaki and T.Jitsuno, IEEE J.Quantum Electron.,
QE-18, 423 (1982).

[153] I.N.Knyazev, V.S.Letokhov and V.G.Movshev, Opt.Comm.,
6, 250 (1972).

[154] V.S.Antonov, I.N.Knyazev and V.G.Movshev, Sov.J.Quant.
Electron., 4, 246 (1974).

[155] R.W.Dreyfus and R.T.Hodgson, Appl.Phys.Lett.,
20, 195 (1972).

[156] R.W.Dreyfus and R.T.Hodgson, IEEE J.Quantum Electron.,
QE-8, 537 (1972).

- [157] J.G.Eden, J.Golden, R.A.Mahaffey, J.A.Pasour and R.W.Waynant, *Appl.Phys.Lett.*, **35**, 133 (1979).
- [158] J.Golden, J.G.Eden, R.A.Mahaffey, J.A.Pasour, A.W.Ali and C.A.Kapetanakos, *Appl.Phys.Lett.*, **33**, 143 (1978).
- [159] Molelectron Corporation, 177 north Wolfe Road, Sunnyvale, C A 94086, U.S.A.
- [160] Photochemical Research Associates Inc., 45 Meg Drive, London, Ontario, Canada, N6E 2V2.
- [161] EG & G Princeton Applied Research, Princeton, NJ 08540, U.S.A.
- [162] LAMBDA Physik, D-3400 Gottingen Postfach 204, Germany.
- [163] Central Electronics Ltd; 4 Industrial Area, Sahidabad-201 005, India.
- [164] G.Capelle and D.Phillips, *Appl. Opt.*, **9**, 2742 (1970).
- [165] F.B.Dunning and E.D.Stokes, *Opt.Commun.*, **6**, 160 (1972).
- [166] T.W.Hansch, *Appl.Opt.*, **11**, 865 (1972).
- [167] R.C.Hilborn, *Am.J.Phys.*, **46**, 565 (1978).

- [168] J.E.Lawler, W.A.Fitzsimmons and L.W.Anderson, Appl.Opt.,
15, 1083 (1976).
- [169] F.P.Schafer (Ed.) Topics in Applied Physics, Vol.1, Dye
lasers, Springer-Verlag, Berlin (1977).
- [170] Yu.V.Zvenevich, P.I.Myshalov and N.A.Nemkovich, J.Appl.
Spectrosc., 38, 499 (1983).
- [171] G.Veith and A.J.Schmidt, J.Phys.E: Sci.Instrum.,
11,833 (1978).
- [172] Z.Bor, A.Muller, B.Racz and F.P.Schafer, Appl.Phys.,
B.27, 9 (1982).
- [173] R.J.Cody, M.J.S.Dzvonik and W.M.Jackson, J.Chem.Phys.,
66, 2145 (1977).
- [174] A.Andereoni, R.Cubeddu, S.De Silvestri and P.Laporta,
Opt.Commun., 33, 277 (1980).
- [175] T.Imasaka and Ishibashi, Analyt.Chem., 52, 2083 (1979).
- [176] W.M.Jackson, J.Chem.Phys., 61 , 4177 (1974).
- [177] S.R.Leone and K.G.Kosnik, Appl.Phys.Lett.,30, 346(1977).

- [178] K.Saurai, G.Capelle and H.D.Brioda, J.Chem. Phys.,
54, 1412 (1971).
- [179] I.Suzuka, N.Mikami and M.Ito, J.Mol.Spectrosc.,
52, 21 (1974).
- [180] R.J.Galagali and S.D.Khattari, Ind.J.Phys., 54B, 332(1980).
- [181] W.Herden and W.H.Bloss, Appl.Phys.Lett., 31, 66 (1977).
- [182] W.Nawrot and L.Pokora, Sov.J.Quant.Electron.,
12, 960 (1982).
- [183] G.Roy, M.Blanchard and R.Tremblay, Opt.Comm.,
33, 65(1980).
- [184] K.Kagawa, H.Kobayashi and M.I.Shikane, Jap.J.Appl.Phys.,
18, 2187 (1979).
- [185] T.Kobayashi, M.Takemura, H.Shinizu and H.Inaba, IEEE J.
Quant.Electron., QE-8, 579 (1972).
- [186] D.L.Franzen, B.L.Danielson and G.W.Day, IEEE J.Quantum
Electron. QE-14, 402 (1978).
- [187] H.Schmidt, H.Salzmann and H.Strohwal, Appl.Opt.,
14, 2250 (1975).

- [188] M.V.Udrea and V.I.Vlad, Rev.Roum.Phys., 26, 51 (1981).
- [189] M.V.Udrea, Rev.Roum.Phys., 27, 607 (1982).
- [190] V.I.Vlad, M.V.Udrea and D.Popa, Rev.Roum,Phys.,
26, 565 (1981).
- [191] K.Sakurai, G.Capelle and H.P.Broida, J.Chem.Phys.,
54, 1220 (1971).
- [192] M.Maeda, K.Kagawa, T.Tachi, K.Miyazaki and M.Ueda, IEEE
Trans.Biomed. Eng. BME-28, 549 (1981).
- [193] C.Sudha Kartha, T.Ramachandran, V.P.N.Nampoori and
K.Sathianandan, Spectrochimica Acta, 43A, 911 (1987).
- [194] P.B.Stephenson and V.P.McDowell, Rev.Sci.Instrum.,
45, 427 (1972).
- [195] K.Kaya, N.Mikani, Y.Udagawa and M.Ito, Chem.Phys.Lett.,
13, 221 (1972).
- [196] H.Kiddal, Proc.IEEE., 59, 1644 (1971).
- [197] D.A.Leonard, Nature., 216, 142 (1967).
- [198] Luminescence in Public Health, By N.N.Barashkov, MIR

Publications, Moscow (1988).

[199] Spectroscopy, Luminescence and Radiation Centres in Minerals by A.S.Marfunin, Springer-Verlag, New York (1979).

[200] Theoretical basis for the use of rare earths in optical and luminescent materials by G.Blasse edtd. by Odd.B.Michleson (1973).

[201] Chemistry and Physics of R-activated phosphors by G.Blasse in Hand Book on the Physics and Chemistry of Rare earths, edtd. by K.A.Gschneidner, Jr. and L.Eyring, North Holland Publishing Co; (1979).

[202] A.Brill and W.L.Warnmaker, J.Electrochem.Soc., 111, 1363 (1964).

[203] G.Blasse and A.Brill, J.of Lumin., 3, 109 (1970).

CHAPTER 2

DESIGN AND FABRICATION OF A HIGH-POWER NITROGEN LASER

Abstract

The design and fabrication of a high-power N_2 laser with a modified electrode structure and gas flow arrangement are described in this chapter. Several novel features are introduced in the design of both the plasma tube and the spark gap. A cylindrical cathode and plane anode has been used as electrodes for the plasma tube in order to obtain uniform and reproducible discharge. The gas supply in the plasma tube is designed so as to obtain a uniform gas flow throughout the discharge region. Two types of spark gaps (free-running and triggered) with associated electronic circuits are also described in this chapter.

1.0 Introduction

An outline of several designs for attaining high output power from nitrogen lasers has been given in the previous chapter. Many important applications of nitrogen laser require a reliable and compact laser unit that could be used in the laboratory. Most of the systems described in the previous chapter are bulky and their commercial production with guarantee on their reliable performance is too expensive to be within the reach of the user. A number of investigators have, therefore, directed their attention towards the fabrication of low cost, compact and reliable laser units operating at 337.1 nm.

In this chapter, results obtained from the present study of a low-inductance pulsed nitrogen laser are reported. The nitrogen laser fabricated is of transverse discharge type, similar to those described by Basting et al [1], and Godard [2], however it differs in several important respects. The laser cavity [3,4] and spark gap switch [5] are designed in such a way that their physical sizes were kept minimum to lower the

inductance. The salient features of the present design of the laser are :

- (1) modified electrode configuration so as to give uniform and reproducible discharge,
- (2) tapered structure of the discharge tube suitable to produce stable laser pulses of short duration,
- (3) gas flow arrangement to obtain uniform pressure in the discharge tube, and
- (4) low inductance triggered-pressurised spark gap switch suitable for high current and fast discharge.

We observed significantly improved discharge uniformity and suppression of arcs over a wide pressure range, good reproducibility of both spatial profile and intensity of the laser output and increase in the range of permissible operating pressures.

The performance of a nitrogen laser depends on several parameters like applied voltage, length of active medium, storage capacity of the transmission lines, the inductance of the cavity and spark gap during discharge,

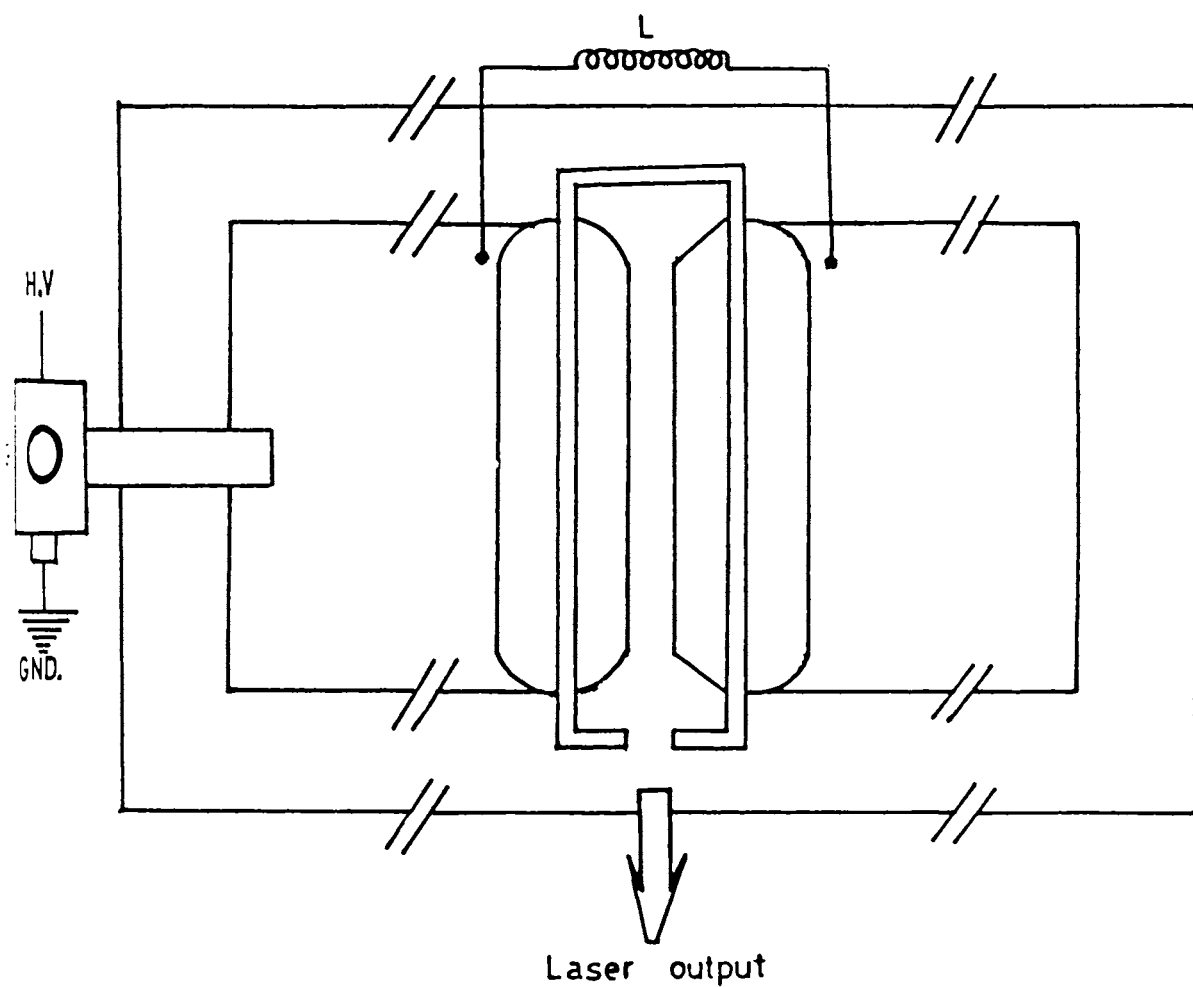


Fig.2.1. Schematic diagram of the experimental set up.

optimum electrode spacing, uniformity in the electrical discharge and gas flow, cooling of the laser cavity and spark gap, gas flow rate, electric field to pressure (E/P) ratios in the cavity and density of pre-ionization.

For maximum power output, the applied voltage should be maximum, but there is an optimum value for the length of the cavity and capacity of the transmission lines. The cavity and spark gap switch are designed in such a way that there is minimum mechanical joints, soldering points, and bends in order to minimize the inductance. Care is also taken to use thick sheets as conducting leads.

2.20 Details of the laser fabrication

The discharge circuit followed in the present design is a conventional flat-plate Blumlein. It consists of a combination of a laser discharge channel, a spark gap, and a flat plate transmission line. Fig.2.1. shows a schematic diagram of the experimental set up used in this work. The laser cavity is located at the centre. The spark gap is soldered on to one side of the transmission lines. Fig. 2.2

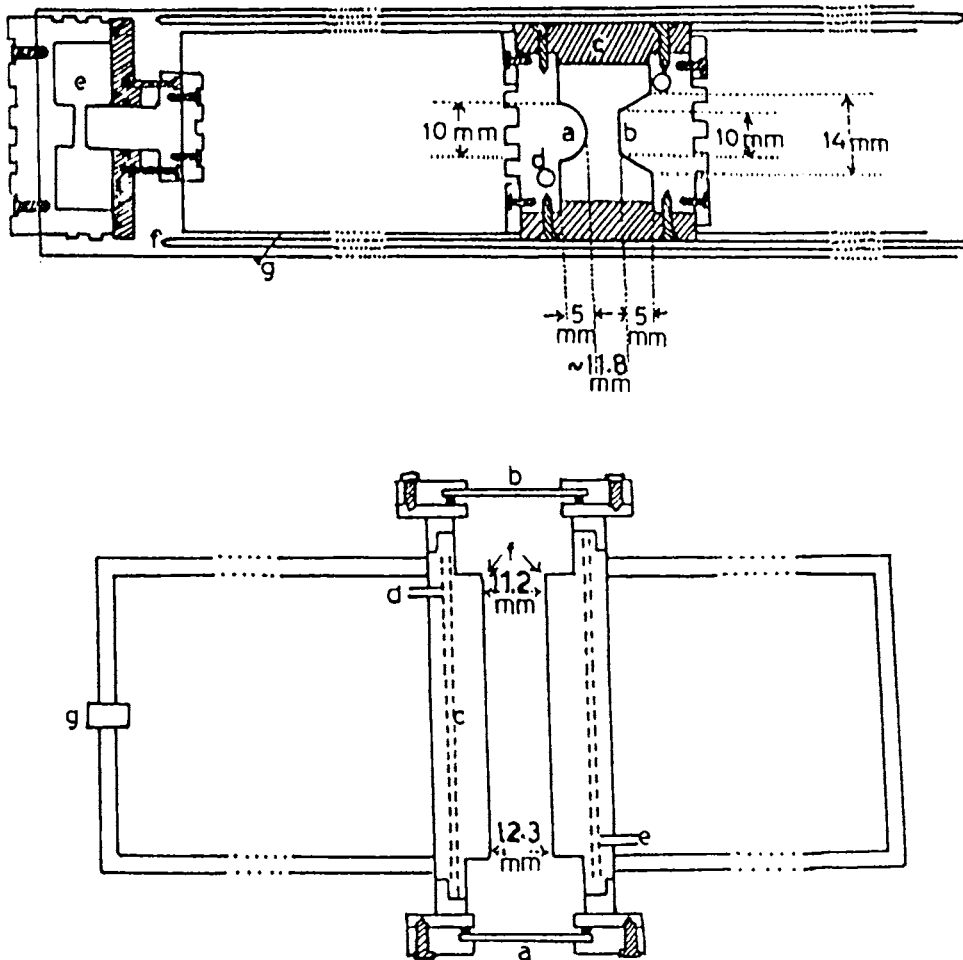


Fig.2.2. Laser cavity with spark gap and transmission lines.

(A) Side view

- a- cylindrical cathode
- b- plane anode
- c- perspex
- d- 1/4 inch hole of length 60 cm
- e- spark gap
- f- epoxy sheet
- g- copper lamina

(B) Front view

- a- quartz window
- b- aluminium coated mirror
- c- gas line
- d- gas inlet
- e- gas outlet
- f- electrodes
- g- spark gap

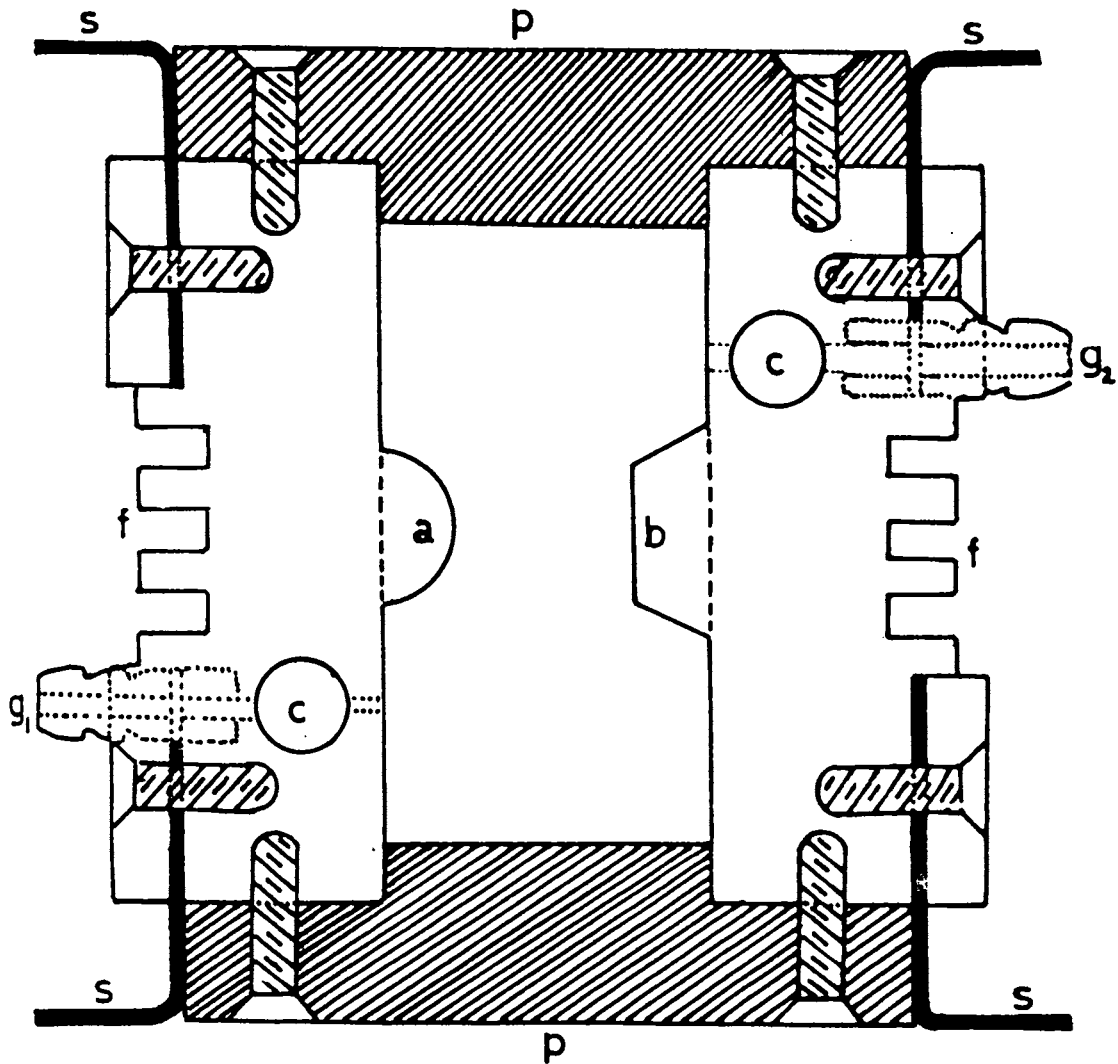


Fig.2.3. Cross-sectional view of the laser discharge channel.

a- cathode, b-anode, c-gas manifold,
 g₁ and g₂- gas inlet and outlet,
 f-cooling fin, p-perspex top and
 bottom, s-copper sheet as connecting
 leads.

and Fig. 2.3 show the details of the cross-sectional views of the laser discharge channel. A detailed description of the various constituents of the laser system is given in the following sections.

2.21. Laser cavity

The major engineering considerations in the design of the laser cavity is that the materials used for this purpose should withstand the effects of heating, ultraviolet radiation, high voltage and high peak current levels, while maintaining the vacuum inside the cavity. The laser cavity is made of two rectangular aluminium bars (60x5x1.6)cm separated by 1.2 cm thick perspex walls at the top and bottom. The two aluminium electrodes are 54 cm in effective length and form part of the cavity of the plasma tube so as to reduce the inductance. The cavity is held together by brass screws threaded into the perspex and sealed vacuum tight with teflon rope and a suitable adhesive (Araldite).

Theoretical analysis had shown that in order to have the interelectrode gap uniformly filled with plasma, it is

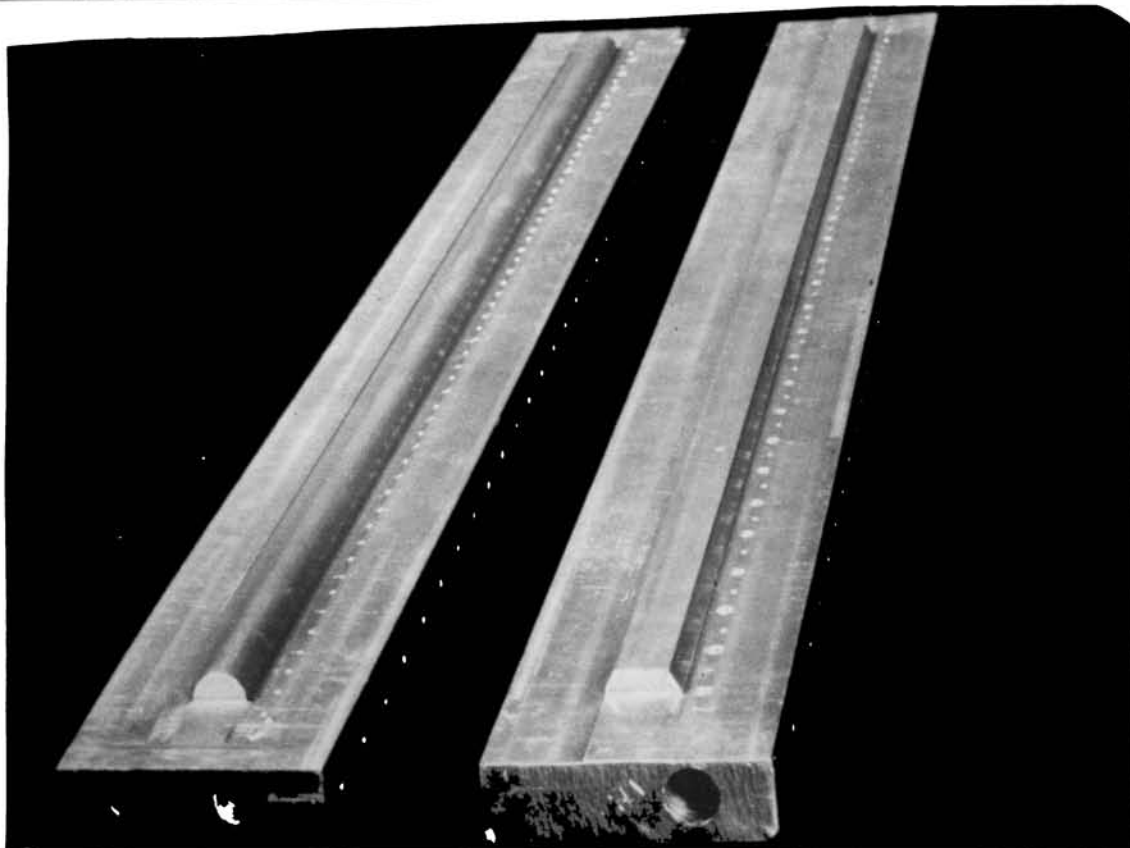


Fig.2.4. Electrodes: Cylindrical cathode and plane anode.

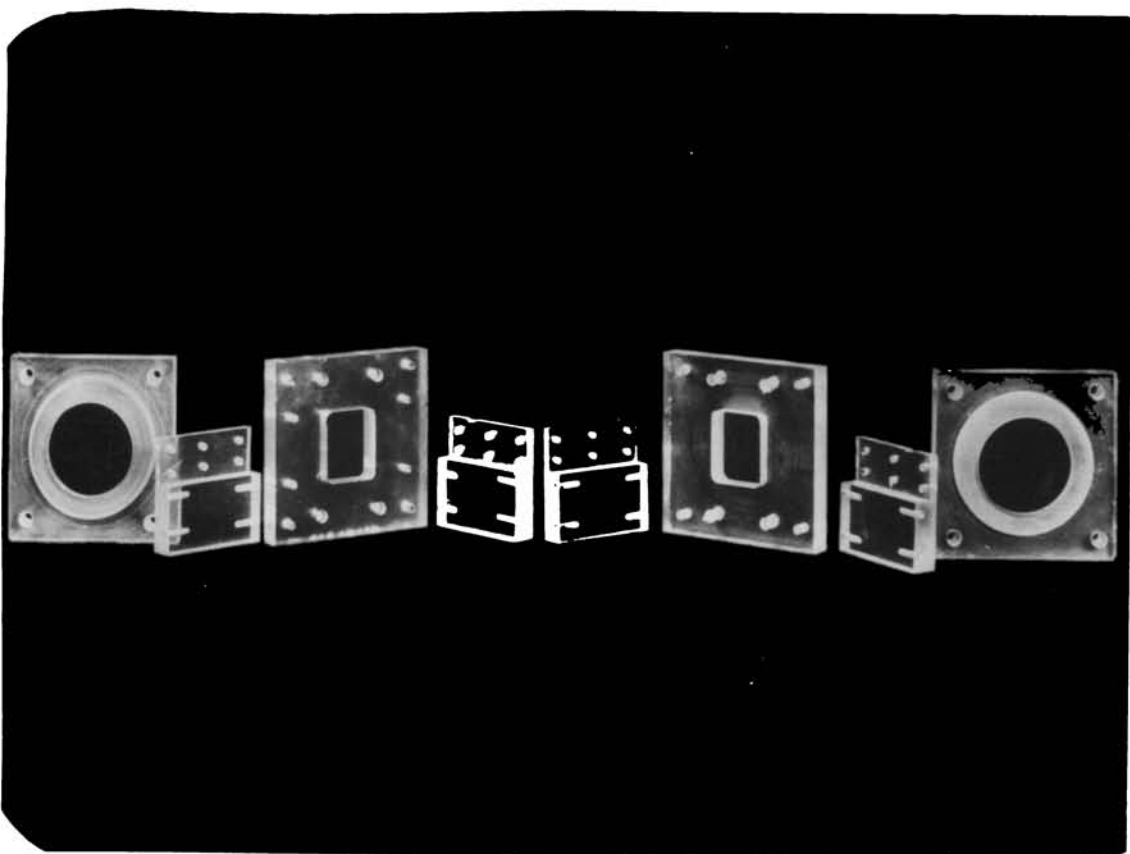


Fig.2.5. Perspex windows.

advisable to use a cylindrical cathode and plane anode [6]. Hence, a combination of cylindrical cathode and plane anode has been used as electrodes to obtain uniform and reproducible discharge. The cathode structure is of cylindrical aluminium electrode of 0.5 cm thick and 54 cm long and was machined with the help of a concave cutter. Anode dimensions are of the same values with flat tip milled in the aluminium bar (Fig.2.4). The cylindrical profile provides an intense electric field at the cathode surface to enhance the field emission and initiate many electron avalanches over the cathode surface.

The separation between the electrodes is 11.2 mm at the rear side and 12.3 mm at the front side (output side). Presumably, this type of tapered structure of the discharge tube results in the electrical excitation occurring first at the rear end and progressing towards the output end of the laser cavity. This travelling wave excitation can result in producing comparatively short laser pulses. Cooling fins on the outer parts of the electrodes which were black painted ensured effective heat dissipation.

Dielectric plates joining the electrodes were

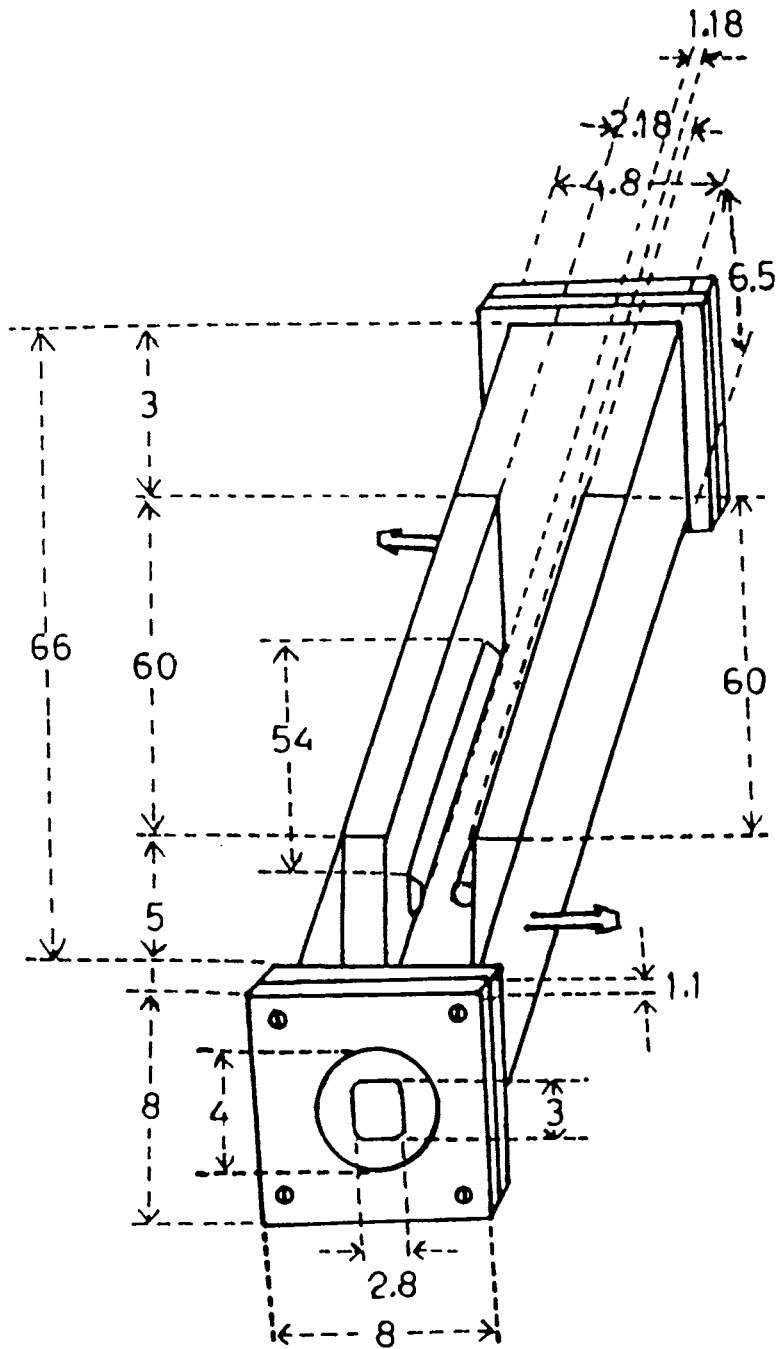


Fig.2.6. Dimensions of the laser cavity.
(all dimensions in mm).

made of perspex of size (66x4.80x1.20) cm which has a high thermal conductivity. The high thermal conductivity of the perspex enabled heat to be removed not only from the discharge zone adjacent to the electrodes, but also from the whole discharge volume, a considerable part of which is in contact with the perspex insulator.

The optical cavity of the laser employs two windows that are mounted on the ends. At either end, termination flanges are provided for holding the mirror and window (Fig.2.5) respectively. A partially reflecting mirror of 80 % reflectivity and a quartz window were used at the rear and the output end of the laser respectively.

The mirrors in their respective mountings are held against the 'O' rings in the flanges by means of square plates screwed on the flanges by four screws. The same four screws provide slight alignment capability of the mirrors. It is important that both these mirrors are adjusted to be parallel to each other and perpendicular to the optical axis of the discharge tube. The alignment can be done with a He-Ne laser by slightly varying the compression on the 'O'-rings

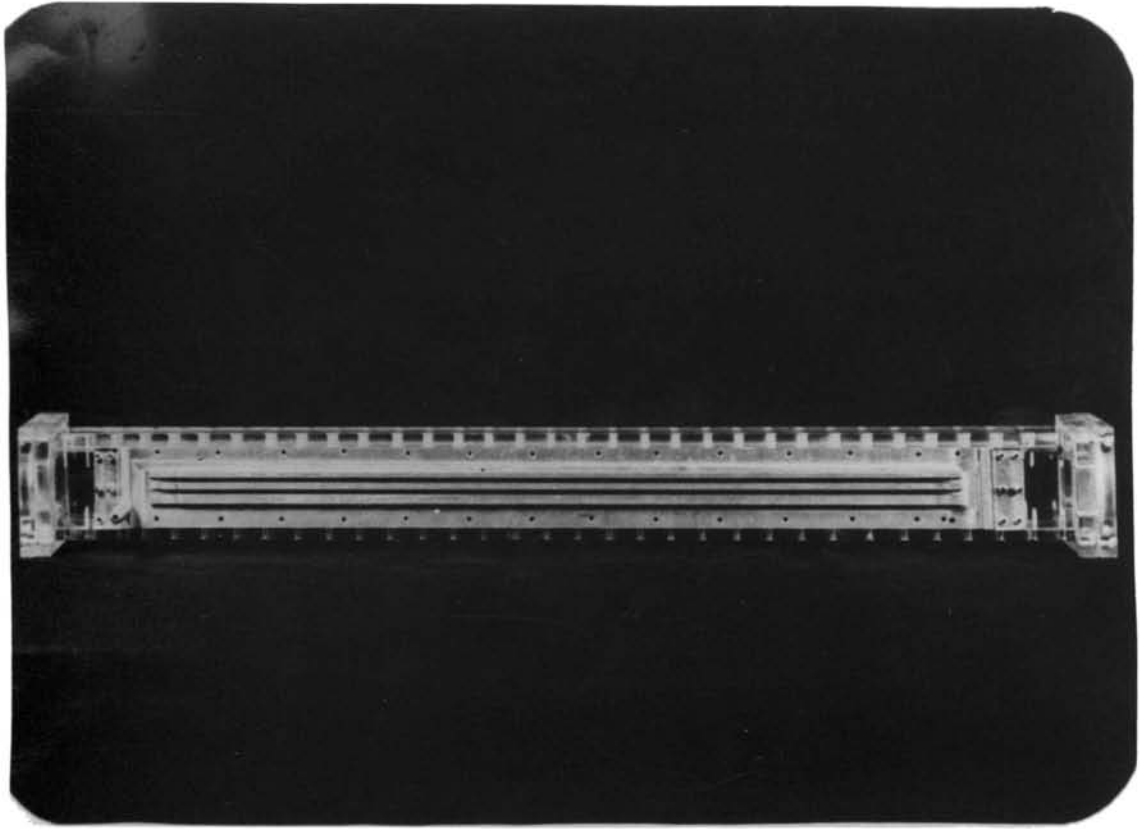


Fig.2.7. Side view of the laser cavity. (size;71x4.8x6.5)cm.

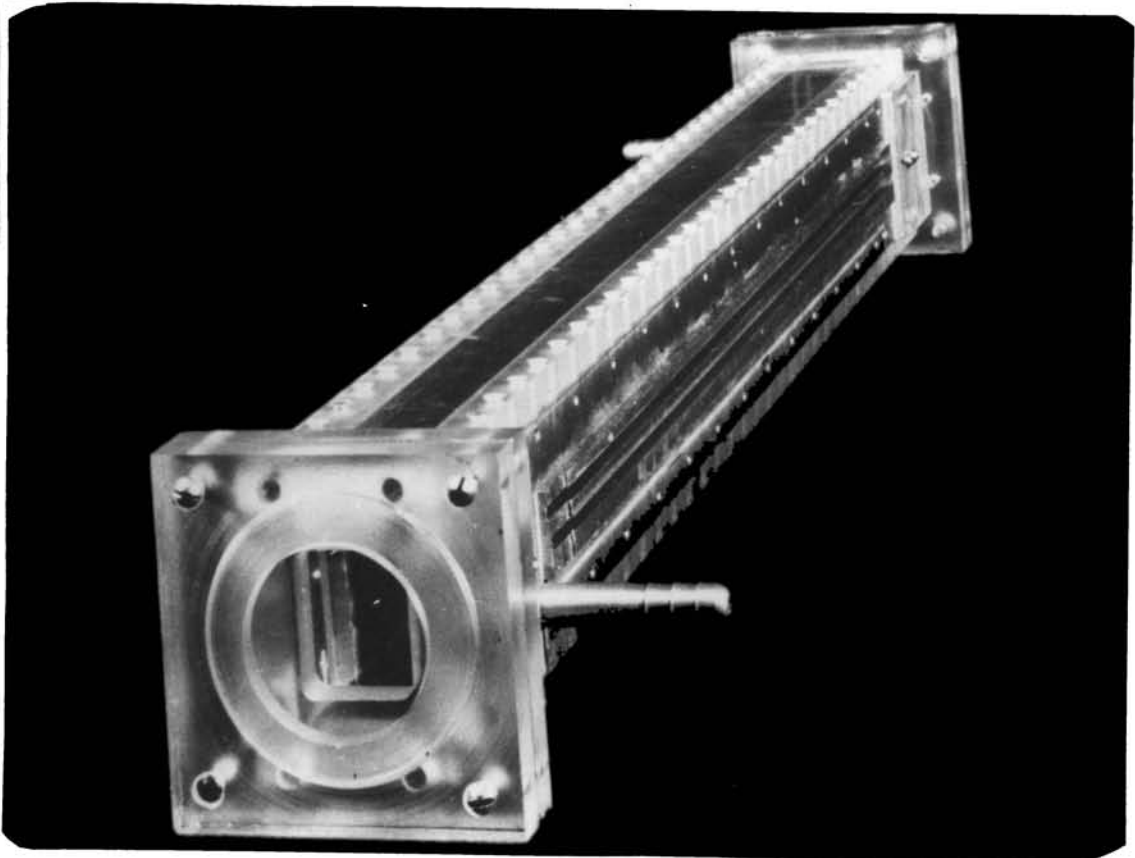


Fig.2.8. Front view of the laser cavity.

T

535.374:547.236:535.373

THO

The cross section of the discharge channel is (4 x 2.20) cm. It can be evacuated upto 10^{-2} torr using a rotary vacuum pump. The cavity has a demountable top to allow cleaning of electrodes. The plasma tube is provided with two gas port nozzles at either end for gas inlet and evacuation. Detailed cavity dimensions are as shown in Fig.2.6. The assembled laser cavity of the type shown in Fig.2.7 and Fig.2.8 have given satisfactory performance for many hundreds of hours of operation.

2.22. Gas flow

The nature of gas flow in the laser cavity is very important, particularly during the operation at high repetition rates. Too many ions or a non-uniform distribution of ions results in non-uniform discharge. Too many ions reduces the breakdown voltage in the gas. In both cases, the result is the reduction in the efficiency of laser device.

It is necessary that the residual ionization remaining due to the previous pulsed discharge should be distributed uniformly and with sufficient number density

throughout the gas flow in order to seed the next discharge [7]. To achieve this aim, the aluminium bars are drilled axially to form the gas chamber of 0.5 cm diameter. In order to maintain a uniform gas flow, 60 holes of different diameters ranging from 1 mm to 3 mm with 1 cm spacing are drilled on the inside surface of the electrodes (Fig.2.4) and these holes open into the gas chamber. Sufficiently uniform gas flow can be achieved with these holes distributed along each electrode and located so that these holes are not opposite to each other. Nitrogen gas is supplied through an inlet manifold fixed behind the electrode. The gas flows across the tube and is collected by an exhaust manifold in the other electrode.

The gas line consists of rubber tubings, needle valves and vacuum manometer. The nitrogen gas used is of commercial grade and the rubber tubes are used to connect the different parts of the laser system for the flow of the gas. The inlet from the gas cylinder is connected to a T-joint, one arm of which is used to pressurize the spark gap and the other arm contains a needle valve which will control the pressure in the cavity. The outlet from the needle valve also has a T-joint. One arm connecting a vacuum manometer and the other

leading to the inlet to the cavity.

The outlet from the cavity is connected by means of a rubber hose pipe to a nozzle for connection to the rotary vacuum pump. The spark gap pressure is controlled by the cylinder regulator as well as by the needle valve. The needle valve controls the pressure level in the cavity and can be directly noted on the vacuum manometer.

2.23. Spark gap

In a laser cavity, the electrical energy is stored by a high voltage/low inductance condenser of a few nanofarads. A triggering switch is used to transfer this energy into the discharge tube to excite the laser medium within a few nanoseconds. Thus the spark gap serves as a very fast switch which short circuits one of the capacitors capable of delivering several kilo amperes of current. Controlling large amount of currents for a very short duration of time with low switching inductance and low jitter has been examined by a good number of workers.

A variety of switches have been used to trigger the electronic circuit for excitation of the discharge. Some of them are simple air spark gap (spark-plug) [8 - 13] , pressurised spark gap [14-17], water spark gap [18], thyatron switching [11,19-23], and laser-triggered spark gap [24,25]. Thyatron switching gives uniform discharge with better pulse to pulse reproducibility [20,23]. However, due to their slow switching speed, thyatron-based switches have only limited applications. The other limitations for thyatron switches are higher inductance because of larger physical size, high cost and limited availability of indigenous components [26]. Apart from their simplicity and cost-effectiveness, spark gaps are the best means of switching high levels of stored energy with low loss and low inductance.

In order to have fast switching the total inductance in the discharge path must be very small [27]. The inductance generally increases with the number of mechanical contacts and decreases when operated under a gas pressure in the range of a few atmospheres. The intense sparking within the spark gap produces heat, thereby raising the temperature of the electrodes and the gas. The materials used should

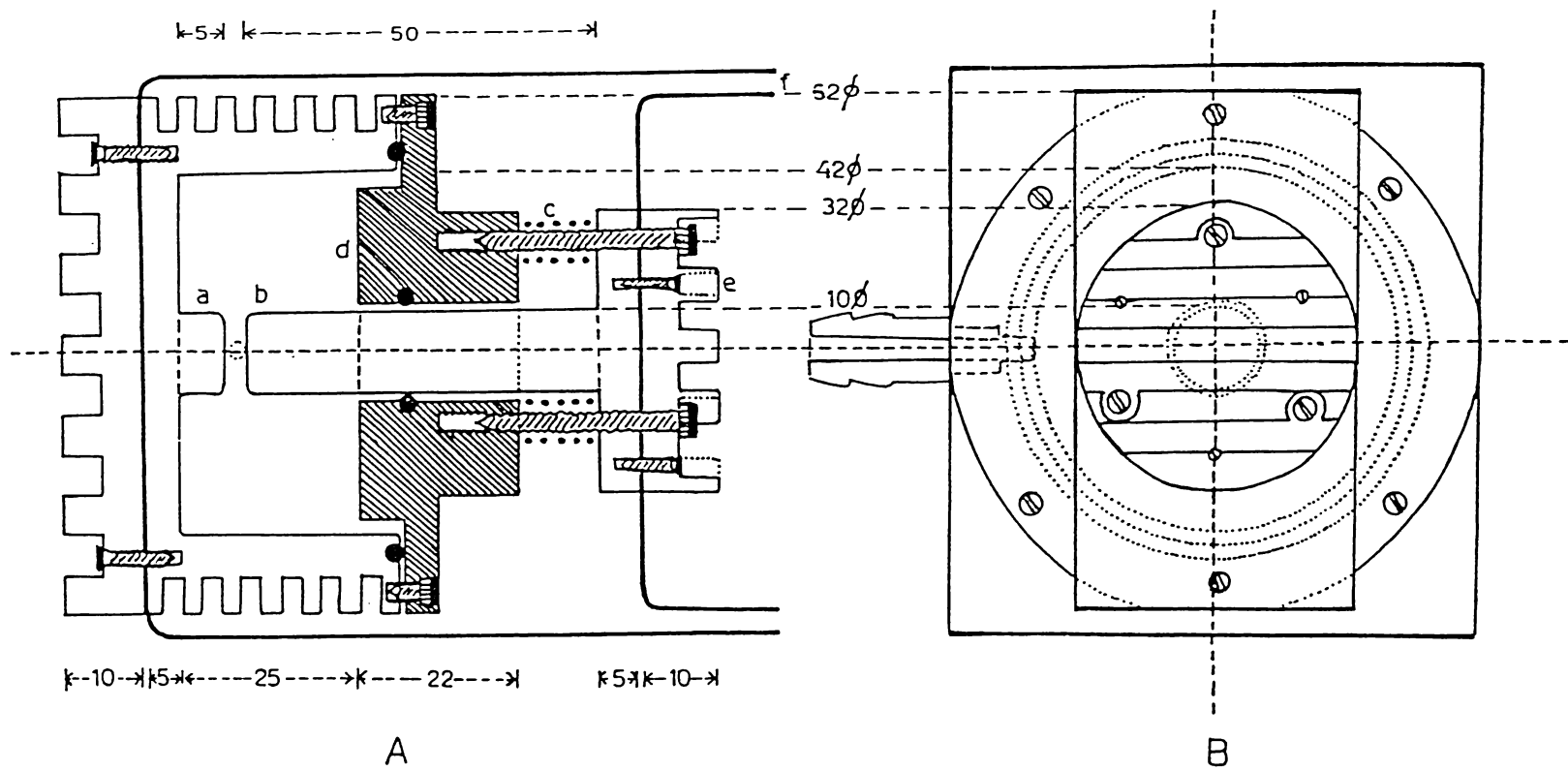


Fig.2.9. Mechanical construction of the free-running type spark gap switch.

(A) Cross section (B) Side view

- a- aluminium body with cathode
- b- anode
- e- cooling fins
- f- copper sheet as leads

therefore be able to withstand the high current and high voltage as well as the high temperature. These considerations impose some constraints on the materials that can be used for the fabrication of switching elements.

In the present work, a free-running type and a triggered spark gap switch were developed, details of which are given in the following sections.

2.23.1. Free-running type spark gap

The free-running type spark gap is a two electrode system. The spark gap dimensions were as shown in Fig.2.9. The electrodes were aluminium rods of 1 cm diameter and was machined in an aluminium block of outer diameter 6.2 cm and inner diameter 4.2 cm. The top and bottom electrodes are screwed on the copper strips and soldered to the top and bottom of the copper clad sheet. The spark occurs between the protruding tips in the two electrodes.

The spark gap was made air-tight by means of 'O' rings provided between the electrodes. It was pressurized by

means of nitrogen gas entering from an inlet in the bottom electrode and the pressure inside can be controlled by means of a needle valve. This works on 1-12 atmospheres of pressure and the gap can be adjusted with range 0-10 mm. Cooling fins were provided for heat dissipation.

2.23.2. Triggered spark gap switch

In the triggered spark gap switch, hylam sheet was used as the insulator in order to withstand higher temperatures. The electrodes were aluminium rods of 1 cm diameter. One of the electrodes that can move easily through the insulator is sealed off by two 'O'-rings, so as to ensure its axial movement. The trigger electrode is introduced through a hole coaxial to the cathode machined in an aluminium block. It is insulated from the electrode by a ceramic tube. Heat is removed by the fairly large surface area of the metal part in contact with the gas. Cooling fins are provided to enhance the efficiency of heat dissipation. Since no appreciable increase in temperature occurs during the operation, the pressure seals can withstand a pressure upto 12 atmospheres (1.2 MPa) , and material deterioration is very low.

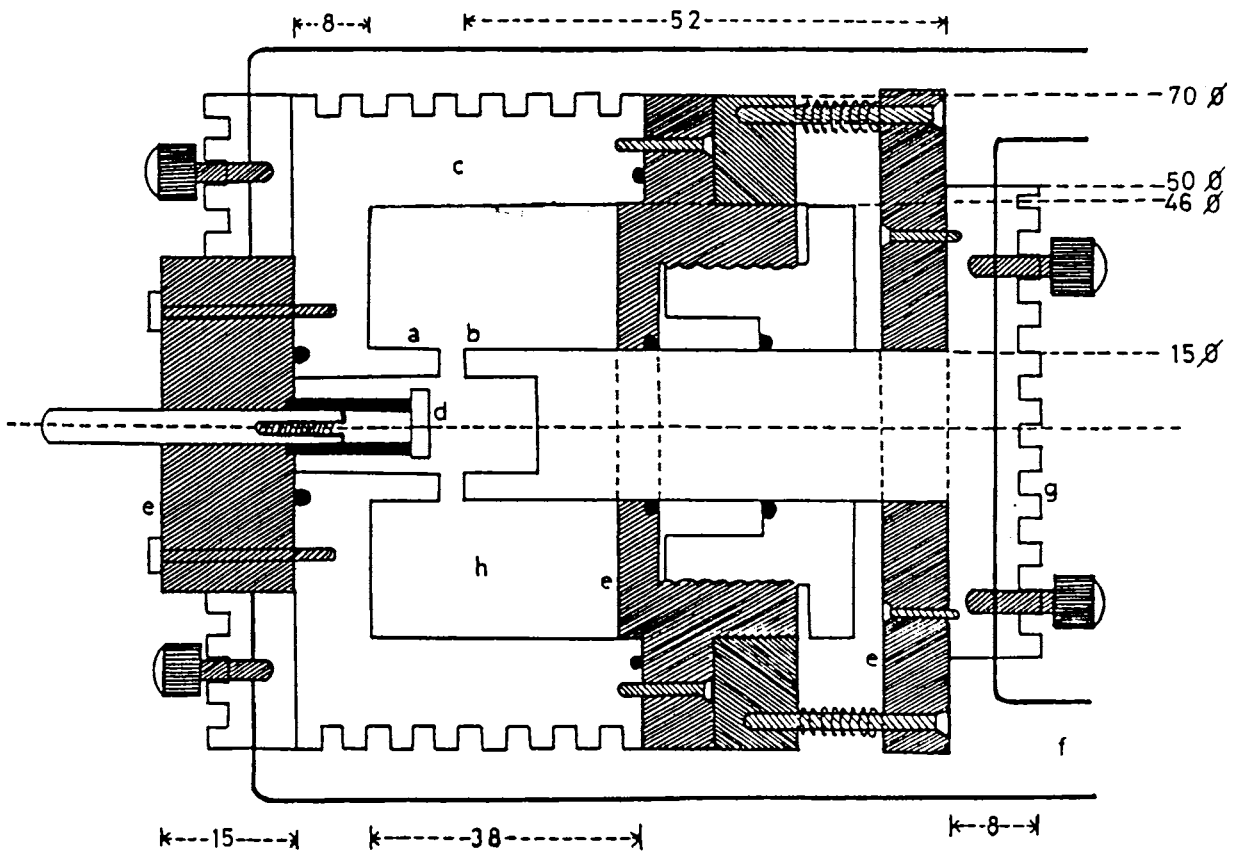


Fig.2.10 Sectional view of the triggered spark gap switch assembly (all dimensions in mm).
 a-cathode, b-aluminium body, d-trigger electrode, e-hylam, f-copper sheet as leads, g-cooling fin, h-pressurised N₂ gas.

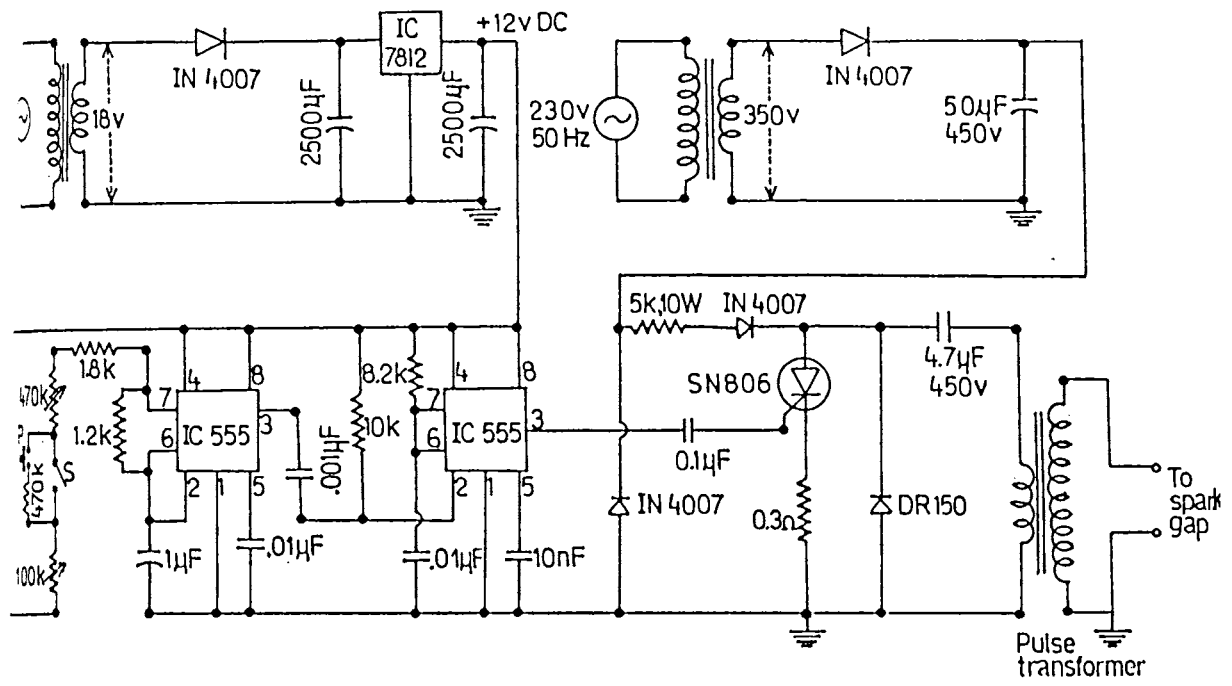


Fig.2.11. Trigger circuit.

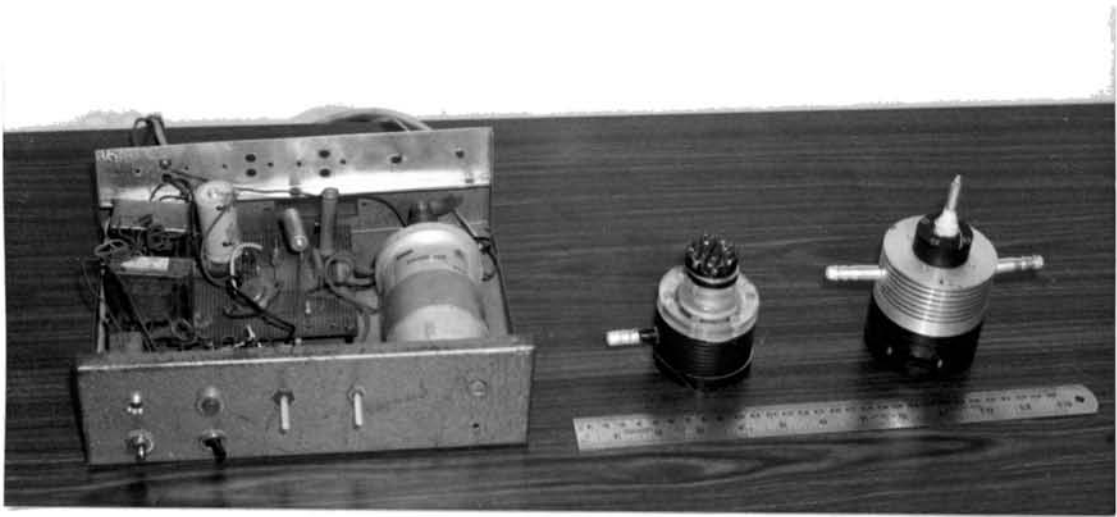


Fig.2.12. Trigger circuit assembly, free-running and triggered spark gap switches.

By sliding the electrodes through the O-ring seal, the electrode gap can be adjusted between 0 and 10 mm. Also the electrodes can be easily removed and cleaned because the internal assembly is removable (Fig.2.10.).

The design of the trigger circuit is as shown in Fig.2.11. The circuit consists of two ICs (NE 555) which generate pulses of 5 μ s duration with rise time of less than 1 μ s. The voltage pulse is fed to the gate of an SCR wired in the primary of a pulse transformer (an automobile ignition coil was used for this purpose) . The capacitor C is charged to about 450 V. The SCR is fired through the primary of the pulse transformer. The output of the secondary is a transient voltage of about 4 kV. This high voltage pulse is fed to the trigger pin of the spark gap. The pulse repetition frequency can be set between 0.1 Hz and 1 kHz. Provision for manual triggering is also included in the circuit. The circuit has safety provisions against current reversals and surge voltages. The photograph of the trigger circuit assembly, free-running spark gap switch and triggered spark switch were shown in Fig.2.12.

2.24. Energy storage capacitor

A double side copper clad glass epoxy sheet was used as the energy element/transmission line giving half the impedance of the single line. It has the additional advantage that the outer conductors are at ground potential, thus reducing electromagnetic interferences caused by the high voltage transient on the inner conductors and in the cavity. This feature also increases the safety of operation.

The transmission line consisted of double-sided copper clad fiber glass epoxy laminates (grade CFG 6/2DS, supplied by M/s. Formica India Ltd.) of dimensions (127 x 62) cm with thickness 1.6 mm which are charged to high voltage and can be discharged into plasma tube via a spark gap switch. The relative permittivity (ϵ) of epoxy sheet is 4.7 and it can sustain voltage of about 15 kV across it. A single Blumlein circuit is shown in Fig. 2.13.

Copper is etched from a 3 cm margin around the edges on both the top and bottom sides of the board to avoid flash over. An additional 10 cm wide copper is etched from the

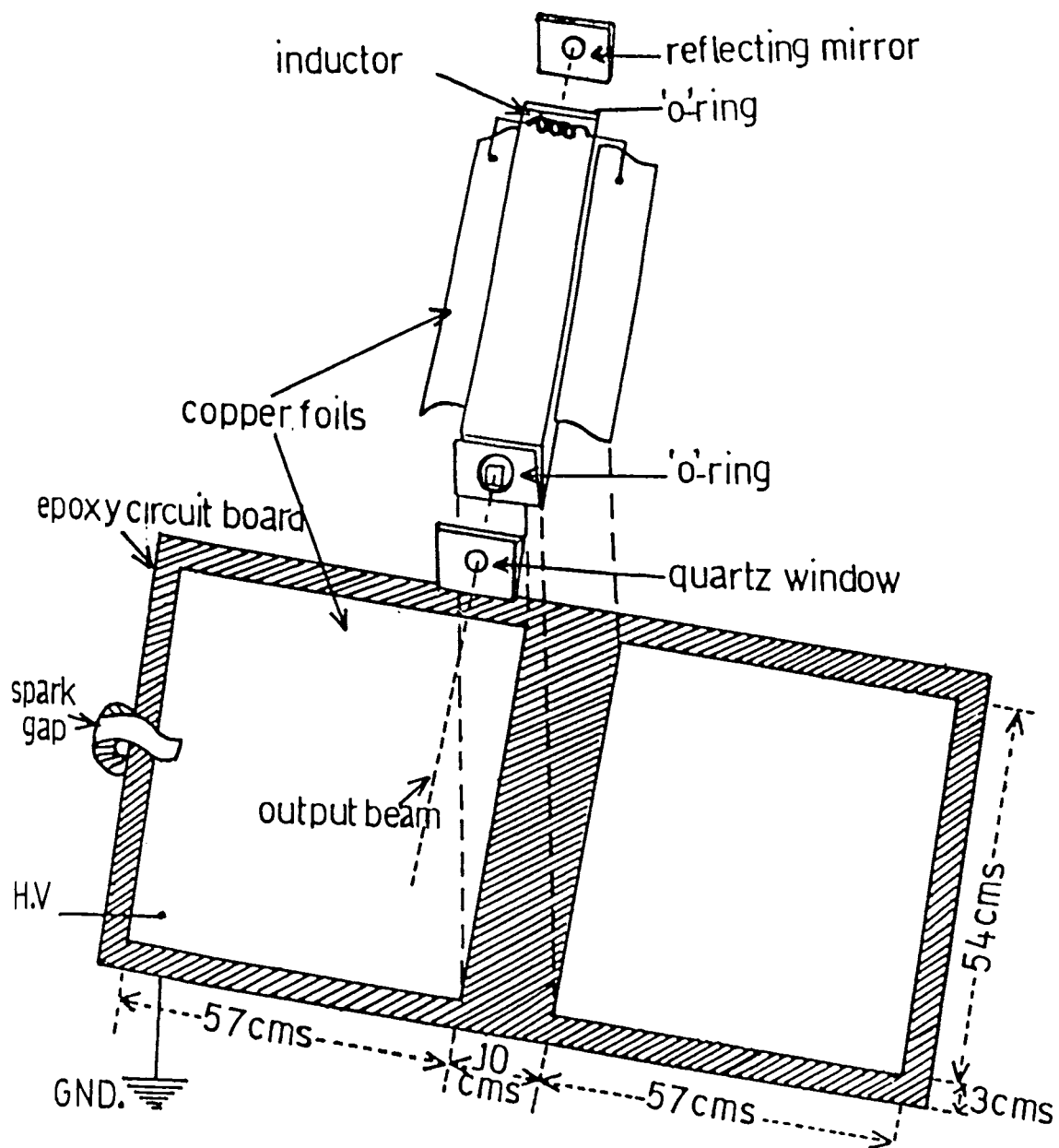


Fig.2.13. An exploded view of the N₂ laser.

middle of the two sheets to separate the capacitors across which the cavity is placed. Copper strips are soldered at the edges of these separated portions and screwed on to the aluminium side plates of the laser cavity as shown in Fig.2.13. The two parts were connected by an induction coil or high resistance (5K, 10W) to provide a charging path to the capacitor on the other side. The spark gap is located at one end of the sheet. The two electrodes of the spark gap are in electrical contact with the top and bottom copper cladding of the epoxy sheet. The high voltage cable from the power supply is connected to the inner conductors on the opposite side from the spark gap while the outer two surfaces of the sheets are connected together and maintained at the ground potential.

The maximum applied voltage of 12 kV was limited in the experiments which is well below the breakdown potential of the epoxy sheet. The principal failure one usually encounters is the electrical breakdown of the epoxy dielectric resulting in a pin hole puncture. Punctures can be repaired by removing copper from a 5mm circular area surrounding the puncture and sealing the hole with Araldite. It has been found that the double side copper clad sheets deteriorate with use.

To make it more failure-resistant and facilitate the operation even during humid weather, the sheets were carefully polished, with the edges well rounded to prevent corona discharge and the entire length of the edges were covered with Araldite. The capacitor plates are firmly and rigidly held together in order to maintain a uniform spacing and to prevent mechanical flexing of the plates during the charging and discharging cycles of the capacitor.

The characteristic impedance (Z), the capacitance (C), and propagation delay time (τ) of a double parallel plate transmission line is given by [1],

$$Z = Z_0 S / 2 \epsilon^{1/2} L \quad (\text{ohms}) \quad \dots (2.1)$$

$$C = 1.11 \epsilon L l / 2\pi S \quad (\text{PF}) \quad \dots (2.2)$$

and $\tau = 2 l \epsilon^{1/2} / c \quad (\text{sec}) \quad \dots (2.3)$

where,

Z_0 - the characteristic impedance of free space (377 ohm),

S - the thickness of the dielectric,

L - the width of the transmission line,

l - the length of the transmission line,

ϵ - the dielectric constant of the material,

c - the velocity of light ($c = 3 \times 10^{10}$ cm/sec.),

For the typical laser system, the sheet has $s = 0.16\text{cm}$, $L = 54\text{ cm}$, $l = 57\text{ cm}$, $\epsilon = 4.7$; so that the characteristic values were $Z = 0.26\text{ ohm}$, $C = 15.98\text{ nF}$ and $\tau = 8.24\text{ ns}$. Thus the line has a propagation delay time of 14.46 ns/m and can store sufficiently high electrical energy. For example, at 12 kV input voltage, the system can store an electrical energy ($CV^2/2$) of 1.15 J .

2.25. High voltage power supply

A switched mode power supply working as a capacitor charging unit was used in the present work [Hartley Measurements Ltd; (HML) Series 411-2230, UK]. It is capable of delivering a charging rate of 200 J/S . It has very accurate control of charging voltage coupled with low internal stored energy and high efficiency. It provides a constant rate of energy transfer to the load. Operation control includes separate power and charge controls, trigger, single shot and high voltage output adjustments. It is extensively protected against flash-over, short-circuit and voltage reversal transients which may occur in capacitor discharge circuits.

2.26. Electromagnetic shielding of the laser

The high voltage discharges associated with the operation of the laser generate a large amount of R.F. noises which cause disturbances in oscilloscopes and other detection instruments kept in the near vicinity. To overcome this problem, the whole laser assembly including the power supply, transmission lines, laser cavity and spark gap was enclosed in shields made of mild steel sheets and were separately earthed. This eliminated the electromagnetic interferences considerably.

2.27. Operation of the laser

After checking the power supply connections and the gas lines, the following steps were followed for operating the laser system. The rotary pump is switched "ON", and observed the vacuum manometer reading. It has finally reached near about 760 torr. The two stage pressure regulator of the nitrogen gas cylinder is opened and the pressure inside the spark gap is adjusted to about $1-2 \text{ Kg/cm}^2$. The needle valve connected to the spark gap is closed. Open the needle valve connected to the cavity so that the pressure inside the cavity is adjusted to about 90 torr. (This pressure has been found to give maximum power output in the system). The power supply is switched "ON". Slowly rotated the variac knob till the



Fig.2.14. Double-Blumlein nitrogen laser system.

voltmeter reads 9.3 kV (Maximum power at this voltage). At this stage, the UV laser output can be seen as a bright blue fluorescence on a white piece of paper. The beam profile is roughly rectangular. The pulse repetition rate can be controlled manually. To switch "OFF" the laser, following steps is to be carried out in order. Reduce the DC operating voltage to zero, switched off the power supply, cut-off the nitrogen gas supply, and switched off the rotary pump. Care is taken to open the air inlet valve of the vacuum pump so as to avoid oil to enter the vacuum lines.

The cost of the materials used in the fabrication of the laser works out to about Rs.20,000/-. The nitrogen laser constructed according to the present design has been found to operate satisfactorily for uninterrupted operations (Fig.2.14). The laser is continuously operated upto a period of four hours. The out power, when focussed was found to be more than sufficient to pump all of the commonly used visible wavelength laser dyes. The laser has been used as an excitation source to study the fluorescence of certain doped phosphors, details of which are given in later chapters. The performance evaluation of the laser is given in chapter 3.

REFERENCES

- [1] D.Basting, F.P.Schaffer and B.Steyer, Opto-Electron.,
4, 43 (1972).
- [2] B.Godard, IEEE J.Quantum Electron., QE-10, 147 (1974).
- [3] Thomas Baby, T.Ramachandran, K.Sathianandan, V.P.N.Nampoori
and C.P.G.Vallabhan, Rev.Sci.Instrum., 62(9), 2076 (1991).
- [4] Thomas Baby, T.Ramachandran, K.Sathianandan and
V.P.N.Nampoori,(communicated).
- [5] Thomas Baby, T.Ramachandran, P.Radhakrishnan,
V.P.N.Nampoori and C.P.G.Vallabhan, Measur.Sci. and Tech.,
2, 873 (1991).
- [6] A.V.Armichev, V.S.Aleinkov and T.B.Fogelson.,
Sov.J.Quant.Electron., 10, 592 (1982).
- [7] W.A.Fitzsimmon, L.W.Anderson, C.E.Reidhauser and Jan.M.Vrtilet
J.Quant.Electron., QE-12, 624 (1976).

- [8] E.E.Bergmann and N.Eberhardt, IEEE J.Quant.Electron.,
QE-9, 853 (1973).
- [9] J.Lawson, R.Coon and E.E.Bergmann, Bull.Am.Phys.Soc.,
18, 65 (1973).
- [10] I.Nagata and Y.Kimura, J.Phys.E: Sci.Instrum.,
6, 1193 (1973).
- [11] M.L.Pascu, A.Constantinescu, A.Pascu and G.Dumbraveanu,
Rev.Roum.Phys., 23, 569 (1978).
- [12] J.G.Small and R.Ashari, Rev.Sci.Instrum., 43, 1205 (1972).
- [13] J.G.Small, Laser Photochemistry, Tunable Lasers and other
topics., P.343, Santa Fe, New Mexico, U.S.A., 23 June-
4 July 1975, Addison-Wesley, Reading, MA (1976).
- [14] M.Geller, D.E.Altman and T.A.De Temple, Appl.Opt.,
7, 2232 (1968).
- [15] J.I.Levatter and Shao-Chin Lin., Appl.Phys.Lett.,
25, 703 (1974).
- [16] M.Maedan, T.Ydmashita and Y.Miyazo, Jap.J.Appl.Phys.,
17, 239 (1978).

- [17] S.Sankan and F.Shimizu, Rev.Sci.Instrum., 46, 1700 (1975).
- [18] E.G.Jones, S.Afr.J.Phys.,3, 49 (1980).
- [19] P.Schenek and H.Metcalf , Appl.Opt., 12, 183 (1973).
- [20] V.F.Tarasenko, Instrum.Exp.Tech., 17, 197 (1974).
- [21] R.Targ, IEEE J.Quant.Electron., QE-8, 726 (1972).
- [22] B.W.Woodward, V.J.Ehlers and W.C.Lineberger,
Rev.Sci.Instrum., 45, 1015 (1974).
- [23] K.Schildback and D.Basting, Rev.Sci.Instrum.,
45, 1015 (1974).
- [24] A.J.Schwab and F.W.Hollinger, Elektrotech.Z.(ETZ).,
A 96, 236 (1975).
- [25] D.D.Bhawalkar, S.S.Thattey, Lala Abhinandan, P.K.Bhadan,
Technical note on nitrogenlaser technology,
BARC, Bombay (1985).
- [26] A.J.Schwab and F.W.Hollinger, IEEE J.Quant.Electron.,
12, 183 (1976).

CHAPTER 3

PARAMETRIC STUDIES OF NITROGEN LASER

Abstract

The output power of the nitrogen laser depends on various parameters like cavity pressure, applied voltage, pulse repetition rate and other geometrical factors in the design. These parameters are studied on both the single and double-Blumlein circuits using free-running and triggered spark gap. It is found that the stability in repetition rate as well as pulse intensity is better for the triggered spark gap. The laser with free-running type spark gap at a charging voltage of 6.18 kV gave maximum efficiency of 0.51% , which is the second highest value reported so far. The dependence of the pulse width on spark gap distance and pressure are also described. Variation of efficiency with voltage and E/P ratios are also included in this chapter. The divergence of the beam as well as the variation of the power density distribution over the cross section of the discharge cell are also studied.

3.1. Introduction

A thorough knowledge of the optical as well as electrical characteristics of a laser is essential if one is to build a system with maximum possible efficiency and good long term stability. Many researchers have reported [1-3] that travelling wave excitation of the gas is the ideal method for attaining maximum efficiency.

As explained earlier, in a travelling wave excited laser, the discharge starts at one end of the laser cavity and propagates towards the other end with a velocity nearly equal to the velocity of light [4]. Hence spontaneously emitted photons in the direction of laser axis sees maximum inversion and gets amplified to sufficient power levels in a single pass-which is the main principle behind the superradiant mode of operation of the nitrogen laser. High power buildup is possible by this method because the gain for $C^B\Pi_u \longrightarrow B^B\Pi_g$ transition is quite high owing to the short life time (about 20 ns, in effect) of the upper laser level. With a view to understand the nature and characteristics of the N_2 lasers

using a Blumlein circuit, two different transmission lines and spark gaps were built and their performance were studied.

3.1.1. Blumlein circuit and E/P requirements

Blumlein circuit is simply a high voltage pulse generator (Fig.1.4) where the energy storage capacitors have the same value (ie; $C_1 = C_2$). Just before the spark gap is fired, the full charging voltage V_0 appears across the spark gap, while the voltage across the laser tube remains zero. When the spark gap fires, the LC circuit consisting of the capacitance C_2 and spark gap inductance L_s (plus the stray inductance) begins to oscillate at $\omega = (L_s C_2)^{-1/2}$. At this instant the voltage across the laser tube also starts oscillating at the same frequency and the voltage rises to a maximum value of $2V_0$ due to the reflection of the voltage wave at the laser channel. In actual operating conditions, this voltage will not reach $2V_0$ because the N_2 gas will breakdown at a lower voltage, near V_0 . For practical purposes, the peak value of V_0 can be taken as the breakdown voltage and can be used for the calculation of the instantaneous electric field E

using the relation,

$$E = \frac{2^{1/2} V_0}{d} \quad (\text{Volt/cm.}) \quad \dots (3.1)$$

where d is the electrode separation in cm. In the present design, the average value for $d = 1.18$ cm.

Once the discharge is struck between the electrodes, the voltage falls off rapidly due to the development of a highly conducting plasma. The electrons in the nitrogen discharge may be assumed to be in a steady state with the instantaneous electric field. Since the maximum output power of nitrogen lasers occur with E/P ratios in the range 60-135 volts/cm.torr (Table.3.2), the laser plasma can be described in terms of an electron temperature given by [5],

$$\alpha V_d = N_{\text{gas}} \int_0^\infty g(T_e, v) \sigma_i(v) 4\pi v^3 dv \quad \dots (3.2)$$

where, α - Townsend ionization coefficient

V_d - the drift velocity

N_{gas} - ground state gas density

$g(T_e, v)$ - normalized Maxwell-Boltzmann distribution

$\sigma_i(v)$ - velocity dependent ionization cross section for the nitrogen molecule.

For nitrogen lasers with E/P in the range 20 to 150 V/cm.torr; Fitzsimmons et al.[5] had shown that,

$$V_d = 2.9 \times 10^5 (E/P) \text{ cm/s} \dots\dots(3.3)$$

$$\alpha/P = 1.4 \times 10^{-8} (E/P)^{3.7} (\text{torr.cm})^{-1} \dots(3.4)$$

$$\text{and, } KT_e = 0.11 (E/P)^{0.80} \text{ eV} \dots\dots(3.5)$$

The effective electron temperature calculated using eqn. (3.5) enables one to predict the observed rates of ionization in nitrogen, which would be very much nearer to the excitation rates of the $C^3\Pi_u$ and $B^3\Pi_g$ states, as these states lie very close to the ionization limit.

3.1.2. The pulse forming net works

Two typical transmission lines were made that can be used with the same laser cavity. For the first type of the transmission lines, conventional Blumlein circuit configuration ($C_1 = C_2$) has been employed, while in the second type, two double sided copper clad sheets are used, one above and the other below the cavity, so as to double the storage capacity. The length and width of the line was 57 cm

and 54 cm respectively for the two cases.

The transmission lines were made as described in chapter 2.. The capacitance, characteristic impedance and propagation delay time calculated using eqns. (2.1), (2.2) and (2.3), for the two circuits are given in Table 3.1.

Table 3.1 Nitrogen laser characteristics

Laser Characteristics	Single Blumlein	Double Blumlein
Characteristic impedance Z (ohm)	0.52	0.26
Capacitance C (nF)	7.99	15.98
Propagation delay time τ (ns)	8.14	8.14
Pulse width (FWHM) (ns)	2.5	3
Stored energy at 9.3 kV (mJ)	345.5	691
Output energy/pulse at 9.3 kV (mJ)	0.084 (at 13.7 pps)	0.21 (at 8.8 pps)
Peak power output at 9.3 kV	335	700
Efficiency = $\frac{E_{out}}{E_{stored}}$ (%)	0.2	0.31

The lines and the spark gap were soldered to the laser one after the other and the various parameters were studied. The dependence of output power on parameters such as operating pressure, voltage and repetition rate were studied on both the single and double-Blumlein circuits.

Table 3.2 Nitrogen laser discharge parameters

Transmission line		Applied voltage V_0 (kV)	Electric field E (volt/cm.)	Optimum pressure P (torr)	Optimum E/P (volt/cm.torr)	Electron temp. KT_e (eV)
Single Blumlein circuit	Free	6.3	7550	80	94.4	4.2
	run-	7.8	9348	120	77.9	3.6
	ing	9.3	11146	110	101.3	4.4
		10.5	12584	120	104.9	4.6
Double Blumlein circuit	Free	3.9	4674	80	58.4	2.8
	run-	6.18	7407	90	82.3	3.7
	ing	9.3	11146	90	123.8	5.2
Double Blumlein circuit	Triggered	7	8389	70	119.8	5.06
		9	10786	80	134.8	5.56
		11	13183	100	131.8	5.46

The laser plasma can be described in terms of an electron temperature given by eqn. (3.5). The maximum output power of nitrogen laser occur with E/P ratios in the range 60-135 V/cm.torr (Table 3.2).

The electron density in the discharge plasma increases rapidly when E/P is greater than about 100 V/cm.torr. As the discharge begins to load the electrical circuit, the voltage across the plasma tube falls suddenly to a very low value with the emergence of optical output when E/P passes through a value of about 80 V/cm.torr ($T_e = 4$ eV) [5,6]. The electrical power to the laser is a maximum when the impedance of the discharge is equal to the impedance of the driving electrical circuit. The inductance of the plasma discharge changes with the change in the pressure in the plasma tube. It has been observed that the optimum E/P value also changes with pressure. Influence of these parameters gives rise to the variation of pulse energy as a function of plasma tube pressure. A change in the applied voltage changes E/P ratio so that the maximum point shifts to a new value.

3.2. Methods of measurement

In the present work, a pulse repetition rate of 10 pps has been chosen. The important parameters measured in the present work are the pulse width, the pulse energy, the peak power, efficiency, laser beam size and beam divergence. The methods and the experimental procedures adopted are given below.

3.2.1 Pulse width

The pulse width was measured using photodiodes (HP-2-4207 Hewlett Packard) which have a rise time of less than 1 ns, and have wide dynamic range (1% linearity over 100 dB). The photodiode circuit is shown in Fig.3.1. The whole circuitry including the photodiode and the load resistor were soldered onto a printed circuit board and enclosed in an aluminium housing with a window to pass the laser emission. A reverse bias of 15 V is applied to the photodiodes and the outputs are terminated in 50 ohm load for fast response and minimum pulse distortion. The mounts are earthed and the

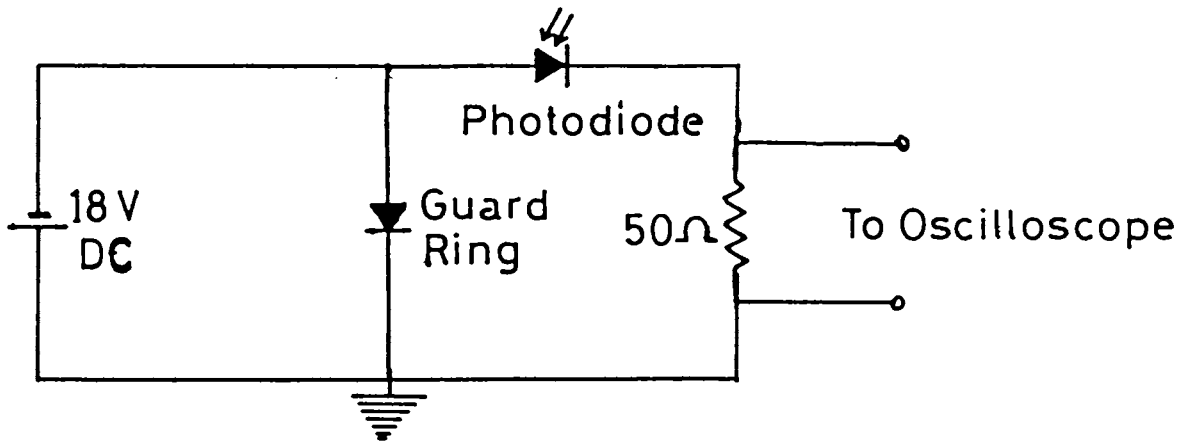


Fig.3.1 Photodiode circuit.

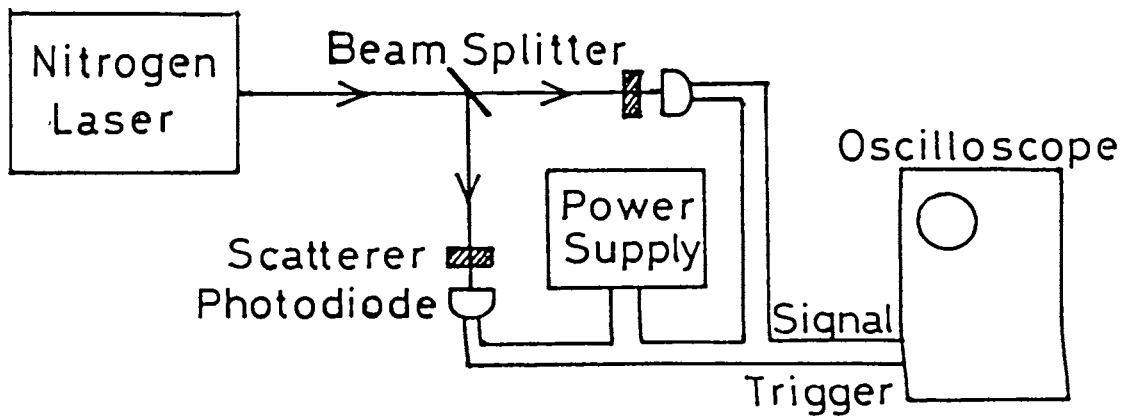


Fig.3.2. Pulse width measurement using photodiode.

output signal was taken out using a shielded cable from the BNC termination on the rear side of the housing.

The experimental setup used to measure the pulse width is shown in Fig.3.2. Nitrogen laser beam is splitted

Table.3.3. Pulse width (FWHM) for various pressures and voltages.

Pressure (torr)	Voltage (kV)	FWHM (ns)
50	7	3.8
	9.3	3.8
	11	3.6
70	7	3.6
	9.3	3.4
	11	3.2
90	7	3.6
	9.3	3
	11	3
110	7	3.4
	9.3	3
	11	3

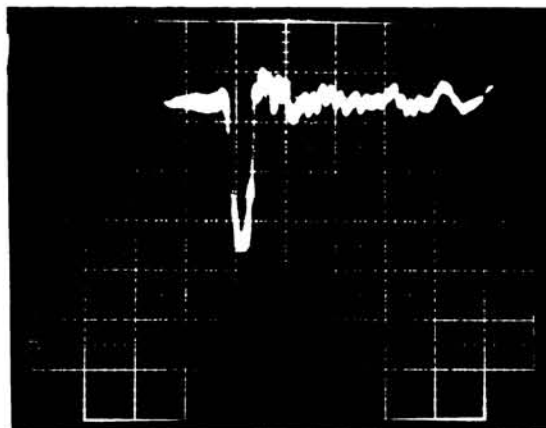


Fig.3.3. Nitrogen laser pulse shape.
Sweep speed : 5 ns/div and
gain : 0.5 V/div.

using a beam splitter made of plane quartz plate. One part of the pulse falls on the photodiode through a scatterer. The output of the photodiode (signal) is given to the 466 DM 44 Tektronix storage oscilloscope. The other pulse, reflected from the quartz plate falls on another photodiode. The output of the photodiode is given to the oscilloscope for triggering.

The pulse width (FWHM) was measured as a function of pressure and voltage (Table 3.3). The pulse width at FWHM was 3 ns for the double-Blumlein circuit as shown in Fig.3.3.(9.3 kV; 90 torr) The average width of the pulses at the base is about 8 ns, which corresponds closely to the propagation delay time of the storage line ($\tau = 8.24$ ns). The result agrees with those reported by Mehendale and Bhawalkar [4] who also obtained a value of about the same as that of the propagation delay time of the transmission line. Since the propagation delay time of the storage line is smaller than that which is possible with the conventional designs, the laser gave slightly short duration pulses.

3.2.2. Pulse energy and peak power output

The average power of the laser was measured

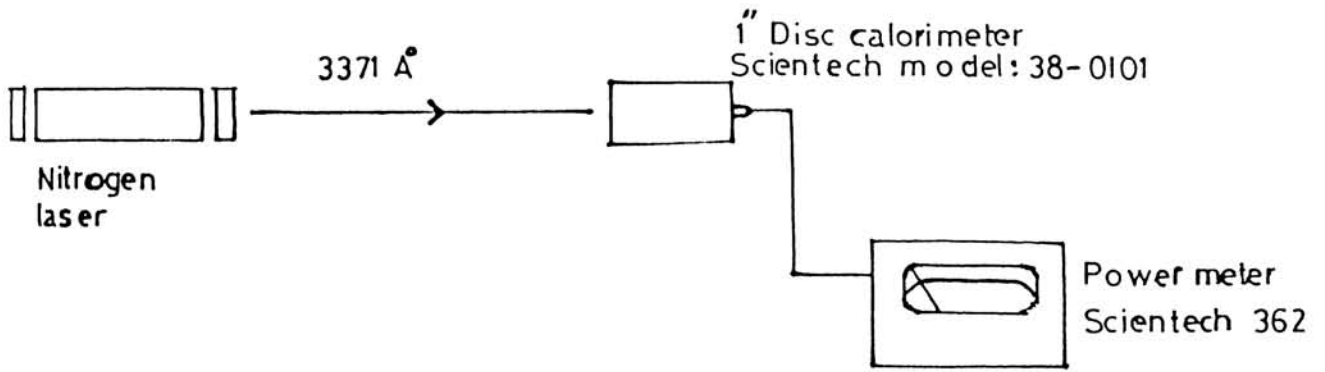


Fig.3.4 Output measurement set up.

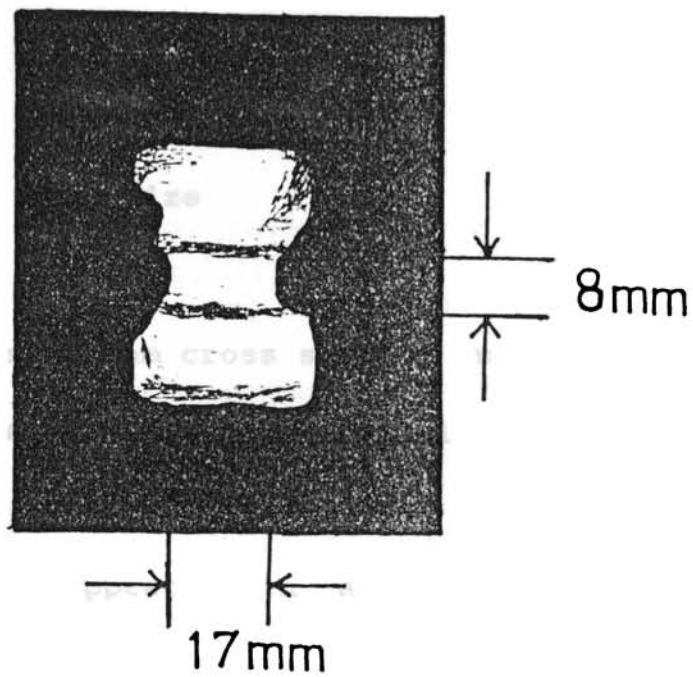


Fig.3.5 Nitrogen laser beam size
(exit window)

using a Scientech model 38-0101 volume absorbing 1 inch disk calorimeter (thermopile) and displayed by a laser powermeter (Scientech model 362). The experimental set up is shown in Fig.3.4. The energy per pulse was obtained by dividing the average power by repetition rate from which the peak power was obtained by dividing the energy/pulse by the pulse width at FWHM. As the pulse width variation with pressure was not appreciable, we have used the pulse width at 90 torr for the calculation of peak power output. For the double-Blumlein circuit, the output energy/pulse at 9.3 kV was 0.21mJ at a rep. rate of 8.8 Hz and the peak output power obtained was 700 kW.

3.2.3. Divergence and beam size

The laser beam cross section is rectangular with dimensions of (1.7 x 0.8) cm outside the exit window (Fig.3.5). Due to the particular configuration of the laser cavity, two values of divergence appeared in a plane containing the electrodes and in a perpendicular plane. The half-angle divergence is measured in the following way. The beam width

parallel to a particular plane is taken at different points. If the widths of the two points are h_1 and h_2 and the distance between them is d , the half angle divergence θ can be calculated as,

$$\theta = \frac{(h_2 - h_1) / 2}{d} \quad \text{radian.}$$

Same procedure is used to measure the divergence for both the planes. The horizontal divergence of the beam at half angle is 24 mrad while the vertical divergence is 3.5 mrad at half angle.

3.2.4. Efficiency

The overall efficiency was calculated by dividing the optical output energy per pulse by the stored electrical energy ($CV^2/2$). For the double-Blumlein circuit, the overall maximum conversion efficiency obtained was 0.51 % at a charging voltage of 6.2 kV, which is remarkably high for an N_2 laser as compared to the earlier reports. The high power and better conversion efficiency obtained using the present design is attributed to the low inductance of the system. It

may be noted that the highest value (1%) reported so far for laser action in nitrogen is by Godard [2].

3.3. Experimental observations

3.3.1. Dependence of laser pulse energy on the spark gap pressure

The pressure in the spark gap affects the inductance of the discharge circuit. It is observed that the higher the pressure in the spark gap, the lower will be the inductance. The optimum output power obtained is at around 2 atmospheres of pressure. The variation of pulse energy with the spark gap pressure at a plasma tube pressure of 80 torr (10.6 kPa) for different voltages is shown in Fig.3.6.

3.3.2. Variation of pulse width with spark gap distance

As shown in Fig.3.7; the variation of pulse width with spark gap distance is not appreciable. Ishikawa et al.[8] have reported that changing the electrode spacing may

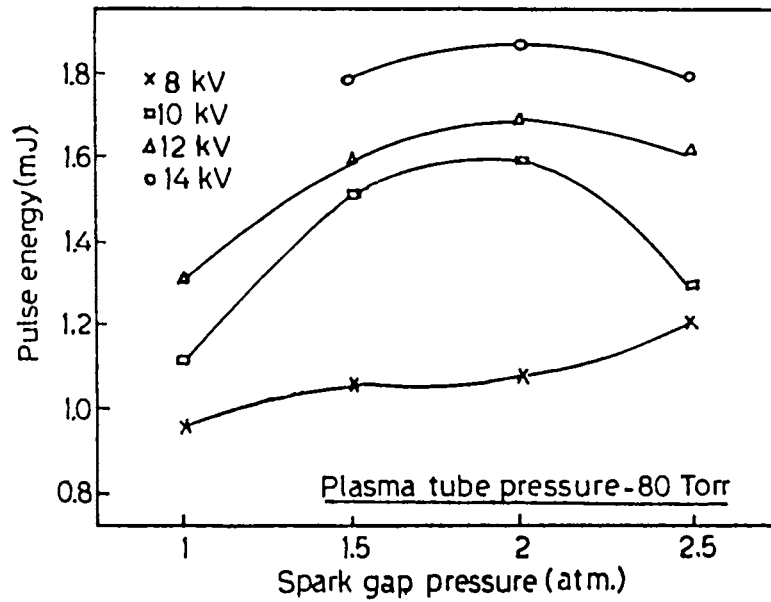


Fig.3.6 Variation of pulse energy with spark gap pressure for different voltages (in kV): The plasma tube pressure is 80 torr.

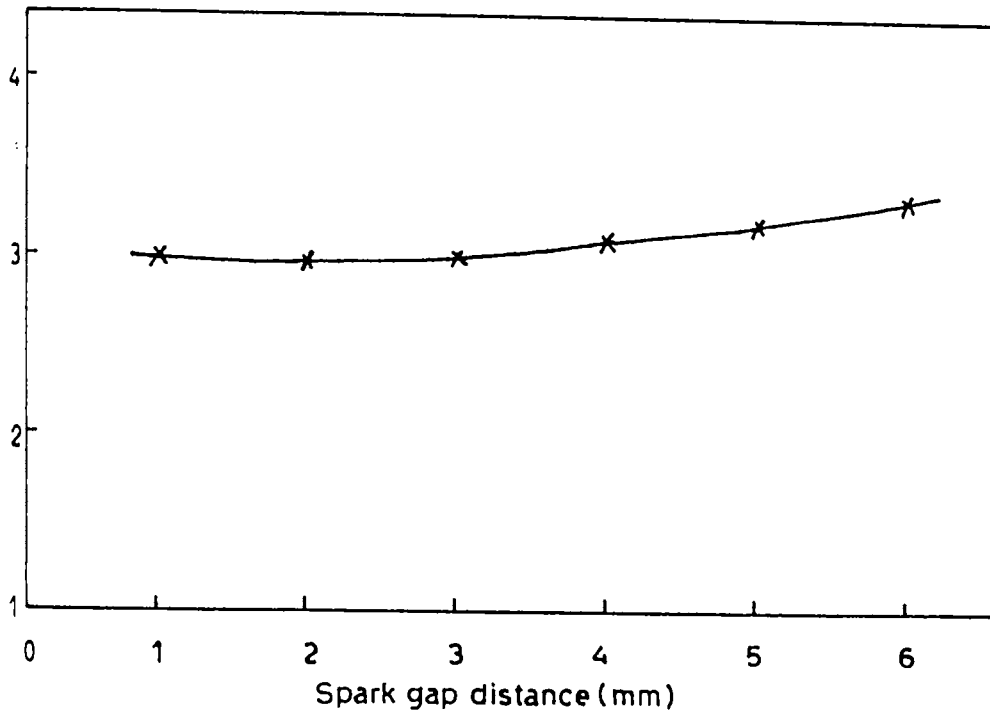


Fig.3.7 Variation of pulse width with spark gap distance.

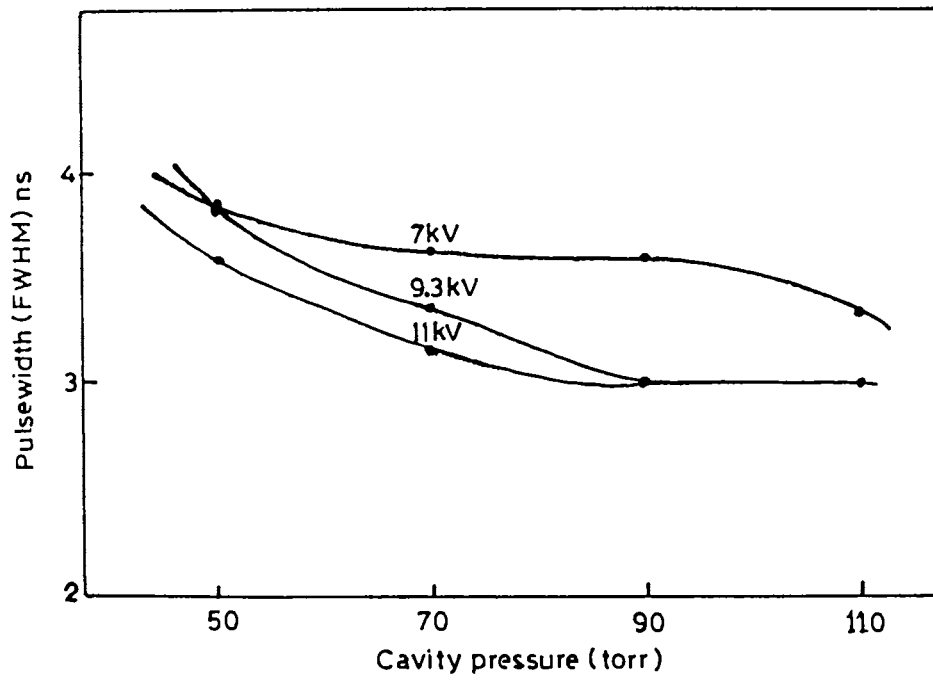


Fig.3.8 Variation of pulse width with cavity pressure.

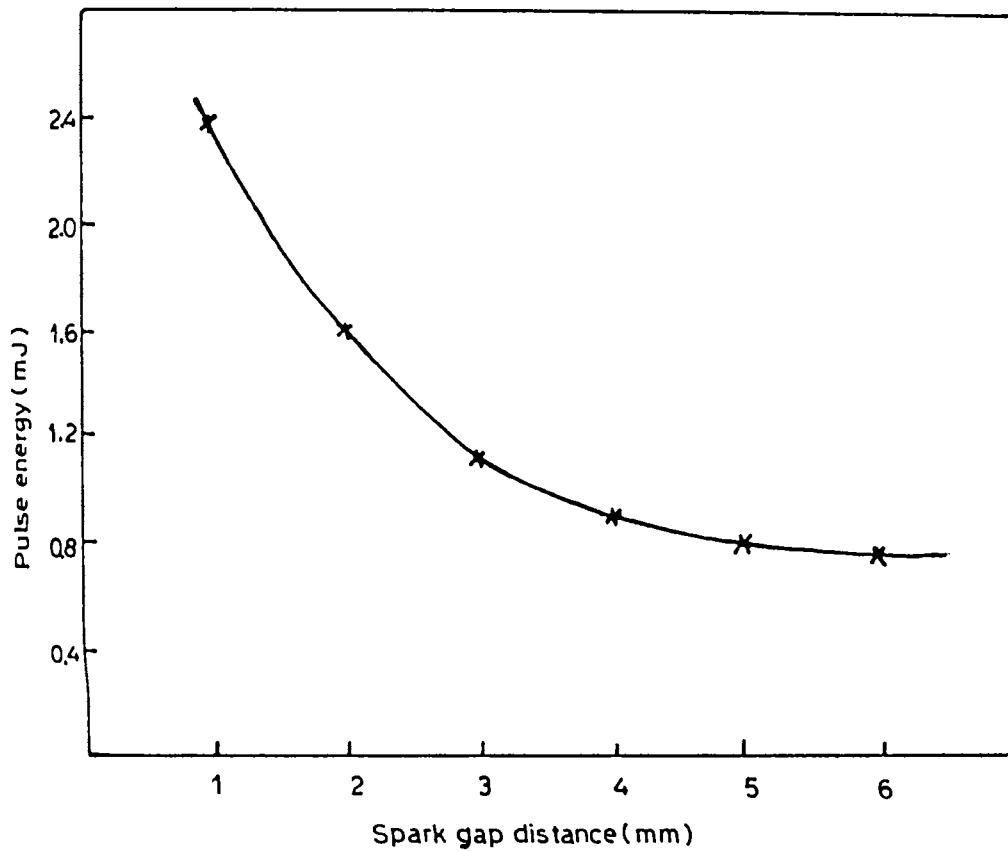


Fig.3.9. Variation of laser power with spark gap distance.

influence the readings as it affects the discharge inductance of the spark gap. No experimental data have been reported on the power increase and reduction of the pulse width of N_2 lasers with decreasing the gap of the spark gap switches, although the behaviour has been predicted [9,10].

3.3.3. Variation of pulse width with cavity pressure

As described earlier in Table 3.3, pulse width (FWHM) for various pressures is shown in Fig.3.8 . The result shows that the pulse width slightly decreases as the pressure is increased.

3.3.4. Variation of laser power with spark gap distance

As seen in Fig. 3.9, laser output power decreases with increasing the spark gap distance. This may be due to the reduction of the residual inductance of the gap switch.

3.3.5. Variation of output peak power with the pressure

The dependence of the output peak power with

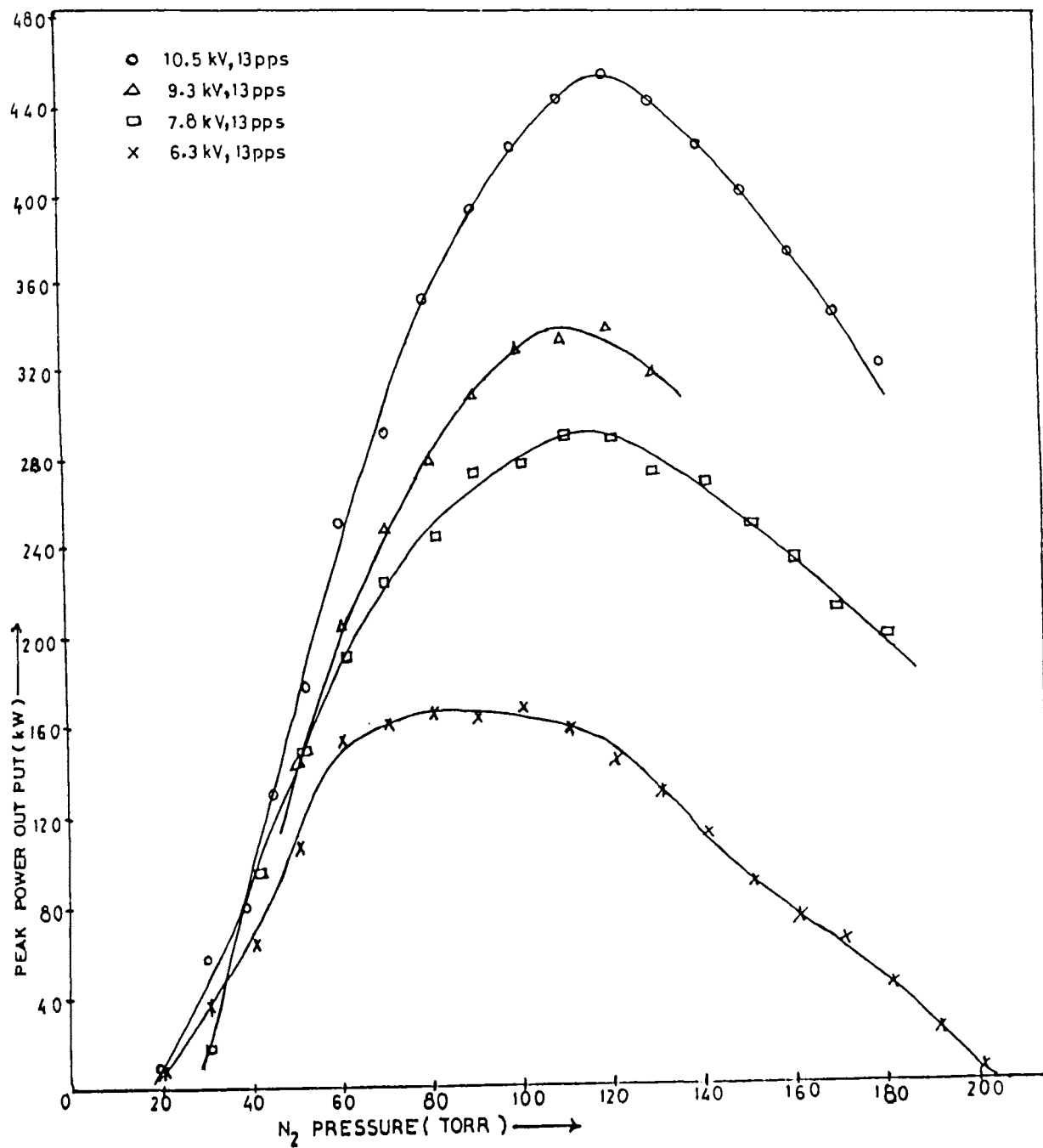


Fig.3.10 Variation of output peak power with pressure for single-Blumlein circuit (free-running spark gap).

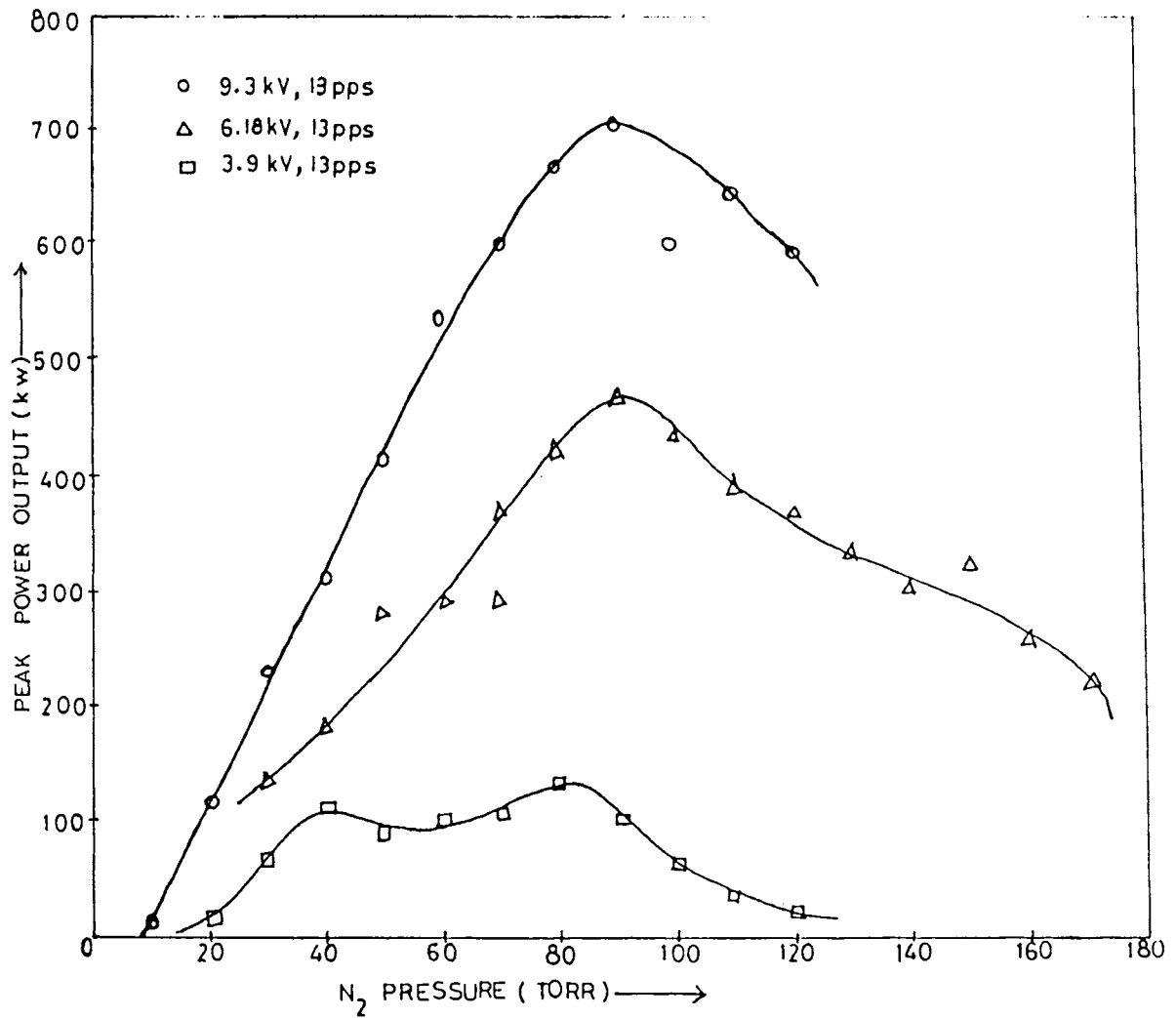


Fig.3.11 Variation of the output peak power with pressure for double-Blumlein circuit (free-running spark gap).

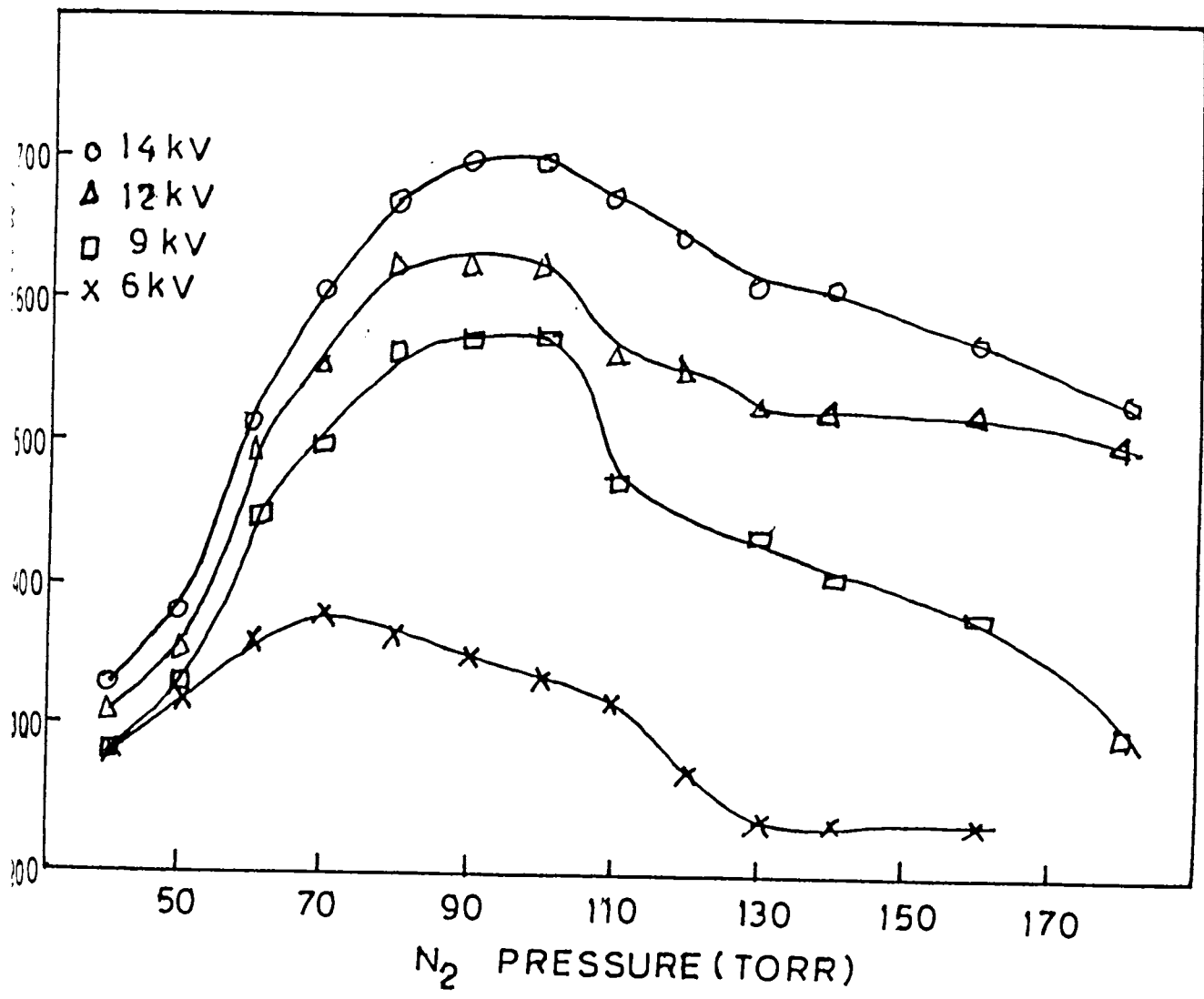


Fig.3.12 Variation of output peak power with pressure for double-Blumlein circuit (triggered spark gap).

nitrogen pressure for different charging voltages is shown in Fig. 3.10 for single Blumlein circuit (free running spark gap) and for the double-Blumlein circuit (free-running spark gap) (Fig.3.11). The readings were taken in the pressure range of 10 to 200 torr when the transmission lines were charged to 3.9-10.5 kV. With the free-running spark gap, lasing is obtained for a wide range of plasma tube pressures from 10 torr to 180 torr. The firing voltage of the spark gap is adjusted by changing the electrode spacing.

In the case of double-Blumlein circuit (triggered-spark gap), lasing is obtained when the plasma tube pressure is in the range 40-180 torr (Fig.3.12). Above 180 torr, streaming and arcing in the discharge region ultimately stops the lasing. The typical curves for 6kV, 9kV, 12 kV and 14kV are given in Fig.3.12. By using a triggered spark gap switch, the experimental conditions could be set more accurately.

As seen from the three figures, for a fixed voltage, the energy per pulse and hence the output power increases with pressure, reaches a maximum and then decreases

with further increase in pressure. The present results are in good agreement with the previous observations by many authors. It was observed that the optimum laser output was obtained when the E/P values are in the range 60-135 V/cm.torr. The initial increase in the laser power with increasing pressure is due to the fact that the number of molecules available for inversion keeps on increasing as the pressure is increased, with electron temperature of the plasma remaining fairly high. At high N_2 pressures, the electron temp. T_e is low, hence both the rate of ionization and excitation fall reducing the output power due to onset of arcing, while at low pressures though the electron temp. is high, the number of molecules available for laser action is small and hence the output power decreases.

3.3.6. Variation of output power with voltage

Fig.3.13 and Fig.3.14 shows the change in output peak power with voltage at different N_2 pressures for the single and double-Blumlein circuits (free-running) and Fig.3.15 for the double-Blumlein circuit (triggered spark gap) respectively. It is seen that the variation in output power

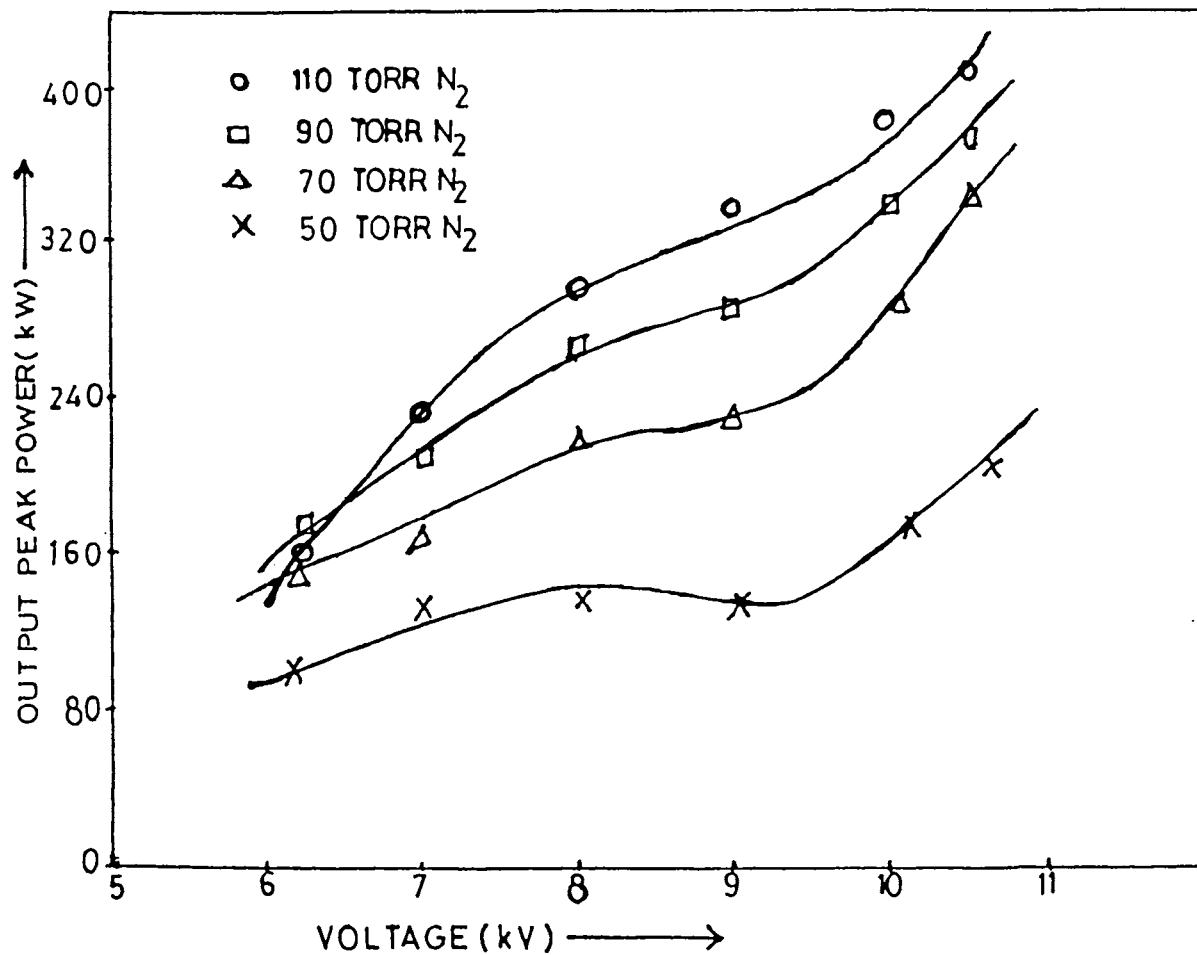


Fig.3.13 Variation of output peak power with voltage for single-Blumlein circuit (free-running spark gap switch).

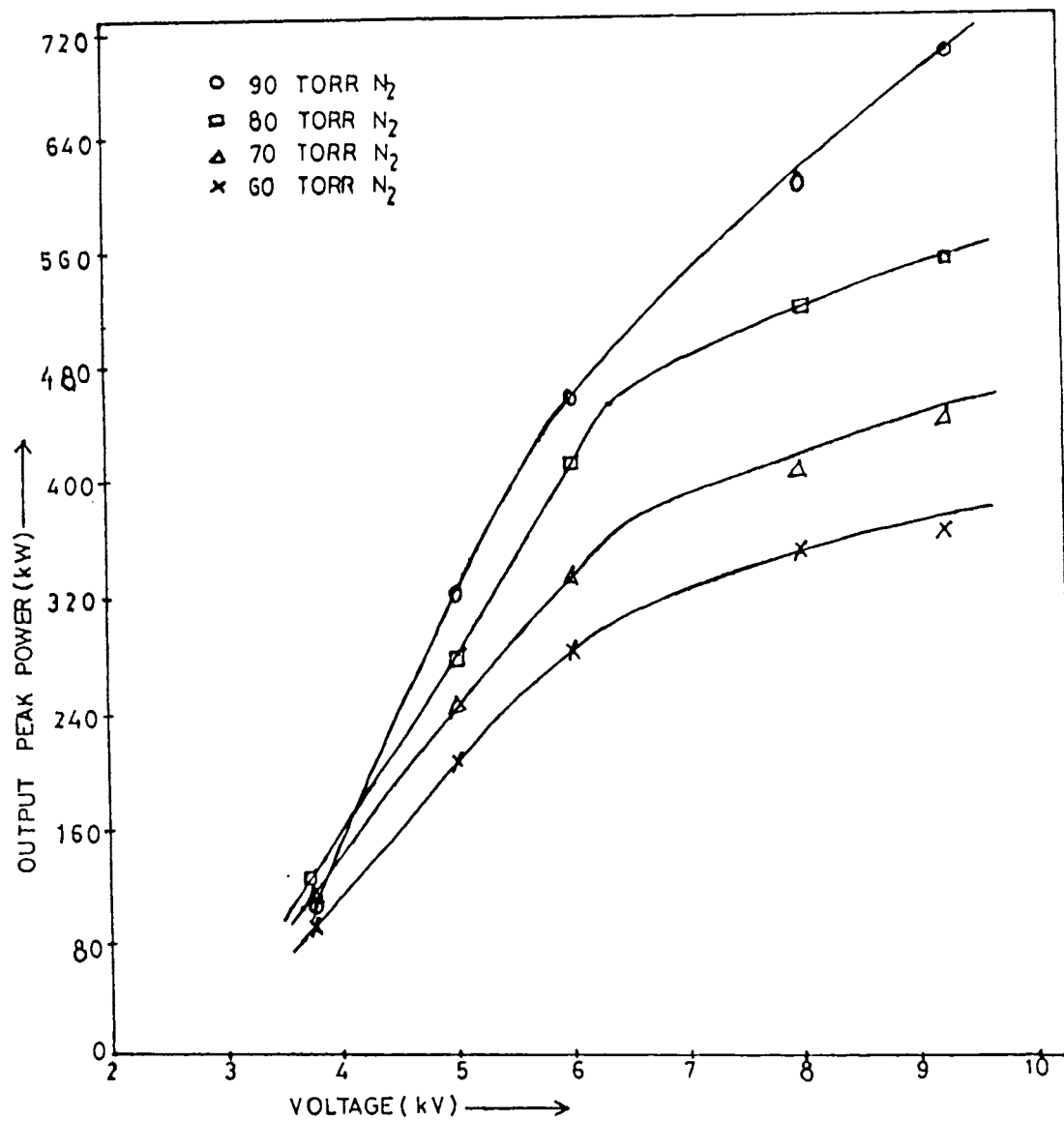


Fig.3.14 Variation of output peak power with voltage for double-Blumlein circuit (free-running spark gap).

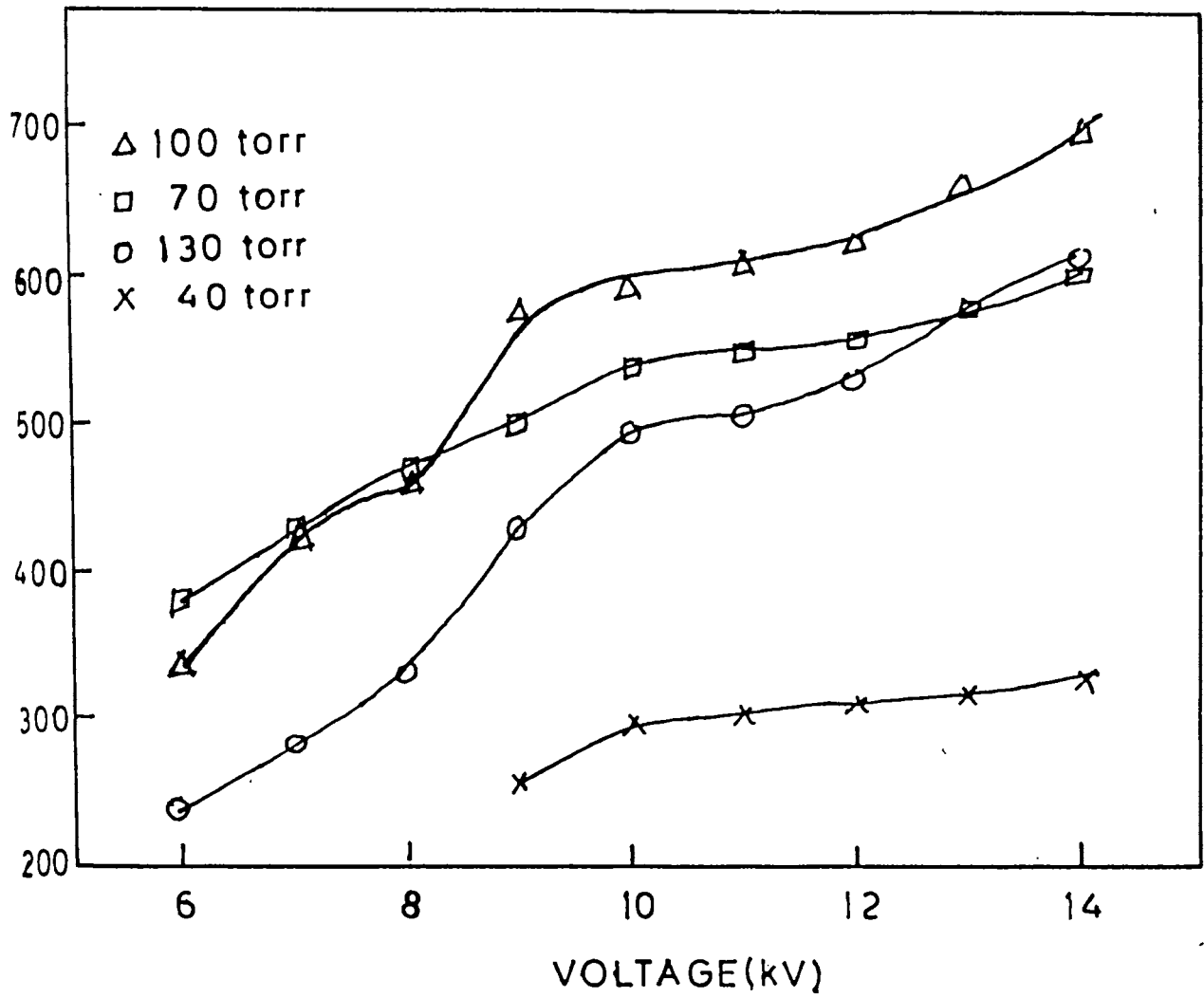


Fig.3.15 Variation of output peak power with voltage for double-Blumlein circuit (triggered spark gap).

is not linear with voltage. The rate of increase of power with charging voltage is rapid at higher pressures.

The variation of output peak power with the applied voltage at corresponding optimum pressure shows a non-linearity in the graph, unlike the results reported by many workers [3,4,7,11-13] except Ritcher et al.[14]. Following Ritcher and co-workers, the non-linearity can be explained on the basis of the voltage dependence of electron temperature.

The absolute value of output power is propotional to N_0 :

$$W_p \propto \phi_+ (\lambda, t_p) N_0 \dots\dots\dots(3.6)$$

where, $N_0 \propto \sigma (T_e) N_e \dots\dots\dots(3.7)$

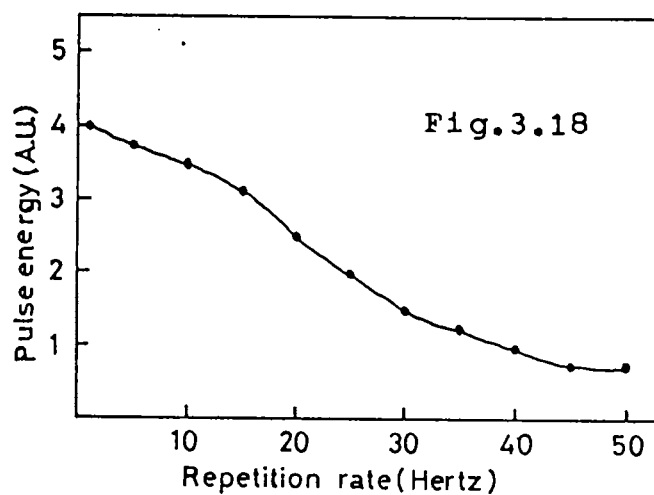
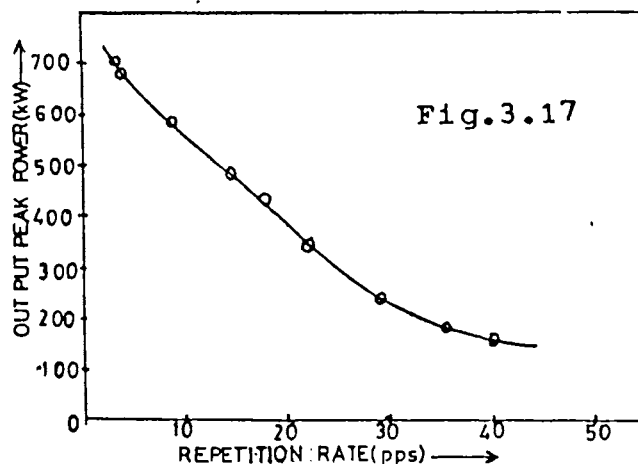
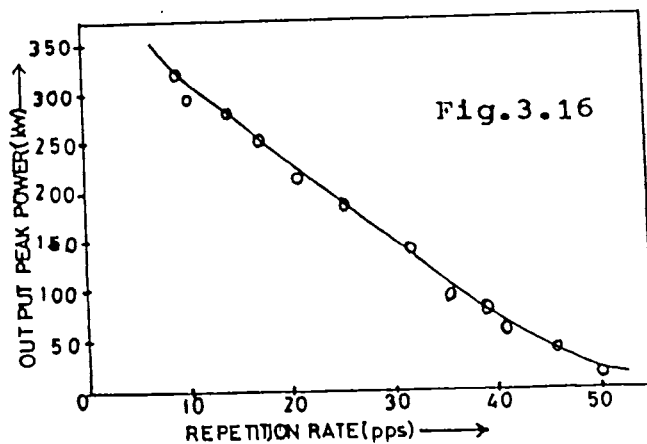
Here N_e is the electron density, σ is the sum of the electron excitation cross section to the upper and lower laser levels, and $\phi_+ (\lambda, t_p)$ is the value of the output peak photon density. The above equation shows that W_p increases linearly with N_e . It means that the output power increases as

the voltage applied to the storage capacitor increases. The dependence of T_0 with voltage shows a saturation at higher discharge voltage. The deviation from non-linearity originates from the voltage dependence of T_0 and therefore also $\sigma(T_0)$ which in turn depends on the charging voltage.

3.3.7 Variation of power with repetition rate

The dependence of output power with the pulse repetition frequency for the three different conditions are shown in Fig.3.16, Fig.3.17 and Fig.3.18. The variation of average power with repetition rate for the two configurations are shown in Fig.3.19 and Fig. 3.20 respectively.

In all the cases, the pulse energy is drastically reduced with an increase in the pulse repetition frequency. It may be due to the change in the initial pre-ionization conditions prevailing in the plasma tube before each pulse.[15]. After the gas pressure in the plasma tube is adjusted in the range of tens of torrs, a high voltage applied across the electrodes of the plasma tube by the firing



Variation of output power with repetition rate:
 Fig. 3.16. Single-Blumlein circuit (free-running spark gap), Fig. 3.17. Double-Blumlein circuit (free-running spark gap), Fig. 3.18-Double-Blumlein circuit (triggered spark gap).

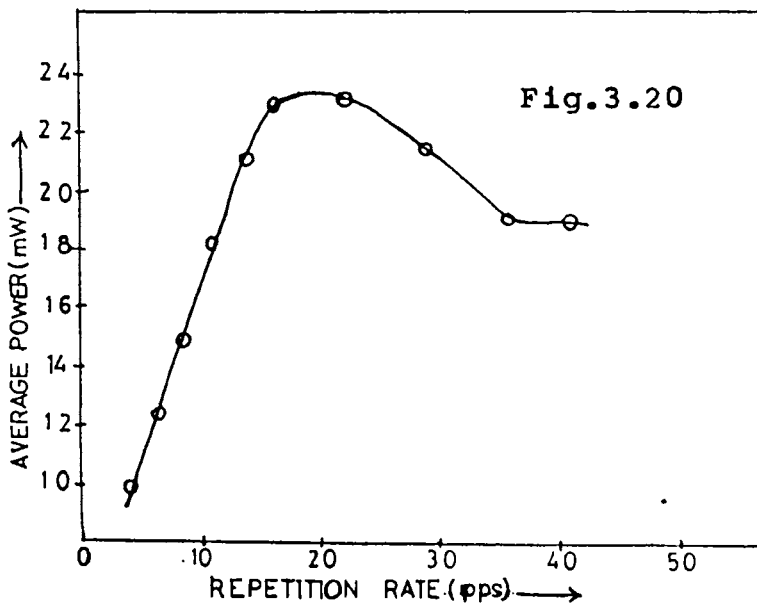
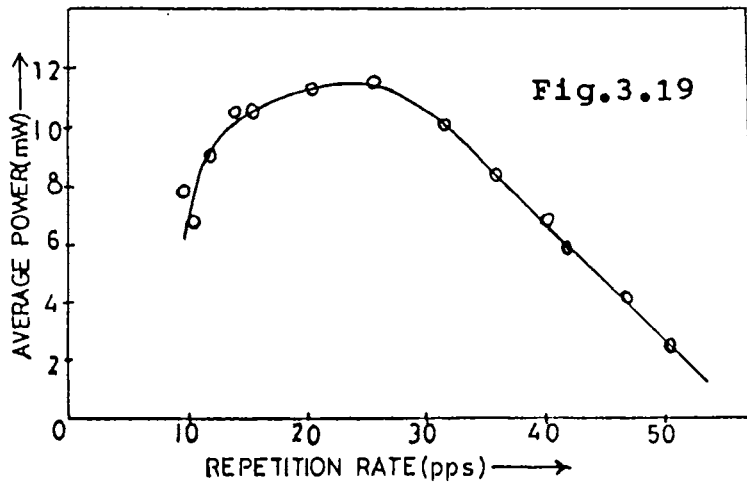


Fig.3.19 Variation of average power with repetition rate for single-Blumlein circuit (free-running spark gap).

Fig.3.20 Variation of average power with repetition rate for double-Blumlein circuit (free-running spark gap).

of the spark gap. The voltage increases till a discharge develops in the plasma tube producing a highly conducting plasma. The actual firing voltage depends upon the pressure and the initial ion density in the plasma tube [16,17]. For a constant pressure, the higher the actual firing voltage, the higher the optical output. It can be shown that there is a reduction in the firing voltage as the repetition rate increases. The ions remaining in the plasma tube after a pulse play the pre-ionization role for the next pulse. Thus by increasing the time interval between two successive pulses, that is, by decreasing the pulse repetition rate, the initial ion density (pre-ionization) for each pulse is reduced. The lower the initial ion density, the higher the actual starting voltage and consequently the higher the power of the laser beam. An increase in the gas flow rate enhances the rate of removal of the remaining ions from the discharge area resulting into increase in the power output. Therefore in order to obtain high repetition rates, one may increase the gas flow rate.

3.3.8. Variation of overall efficiency with the voltage and E/P ratios

The net electrical to optical efficiency is one

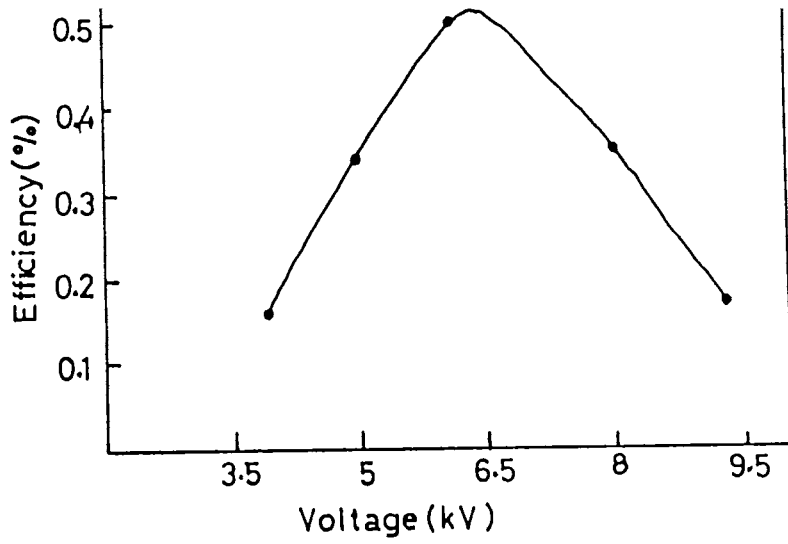


Fig. 3.21

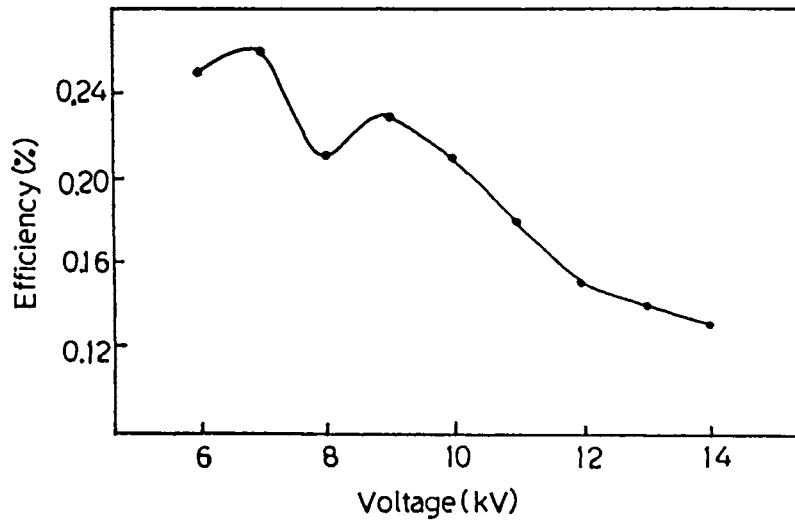


Fig. 3.22

Fig.3.21 Variation of maximum efficiency with voltage (free-running spark gap).

Fig.3.22.Variation of maximum efficiency with voltage (triggered spark gap).

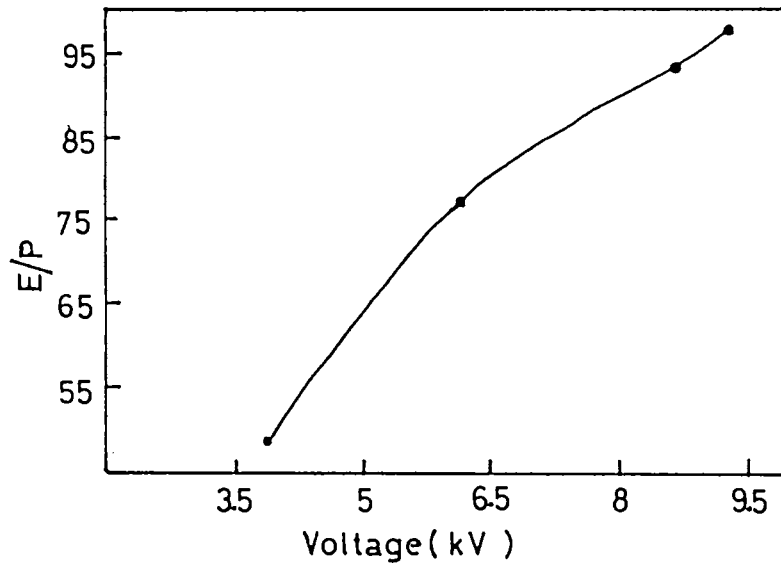


Fig.3.23 Variation of optimum E/P with voltage (free-running spark gap)

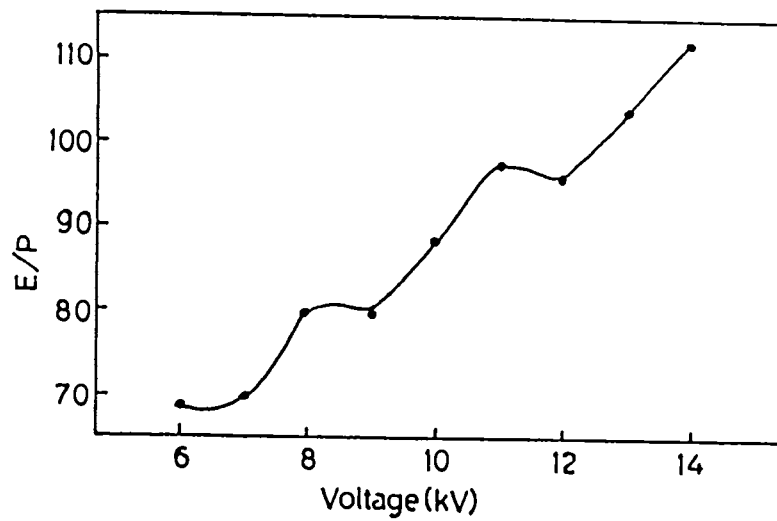


Fig.3.24 Variation of optimum E/P with voltage (triggered spark gap).

of the most important parameters in a laser. It determines the optimum operating conditions for the maximum life of the system. The overall efficiency obtained under different plasma tube pressure conditions but with the same voltage is calculated. The values are plotted against the corresponding voltages as shown in Fig.3.21. and 3.22.

The E/P ratio is plotted against the voltage (Fig.3.23 and 3.24). It is found that the overall efficiency is higher when a free-running spark gap is used instead of a triggered spark gap. It is also observed that the optimum E/P value increases with voltage.

The maximum efficiency obtained is 0.51% at a charging voltage of 6.18 kV. To the author's knowledge, this value appears to be the second highest one reported so far for the transverse electric nitrogen lasers. It may be noted that the highest efficiency (1%) reported so far for laser action in nitrogen is by Godard [2]. Other typical values reported are 0.039 % by Bergmann [18]. 0.05 % by Mehendale and Bhawalkar [4], 0.065% by Sam [19], 0.025% by Fitzsimmons et al.[5] and

0.3%-0.4% by Schwab et al. [20].

3.3.9 Variation of the power density over the cross section of the laser electrodes

The interelectrode separation in a transversely excited (TE) N_2 laser is much smaller in comparison with that in an axially excited laser, and very little studies of the non uniform population inversion in the laser channel have been made. In the case of nitrogen laser applications, the distribution of the output power over the cross section of the beam is very important [21]. Many authors have reported that the intensity distribution in the N_2 laser beam along the interelectrode gap was found to be asymmetric [22,23]. This asymmetry in the intensity distribution has been interpreted in terms of strips parallel to the electrode length in the interelectrode region with different degrees of population inversion. The population inversion in each strip has been assumed to be the same. This nonuniformity of population inversion can be discussed with the help of ionizing wave fronts propagating between the two electrodes. This was

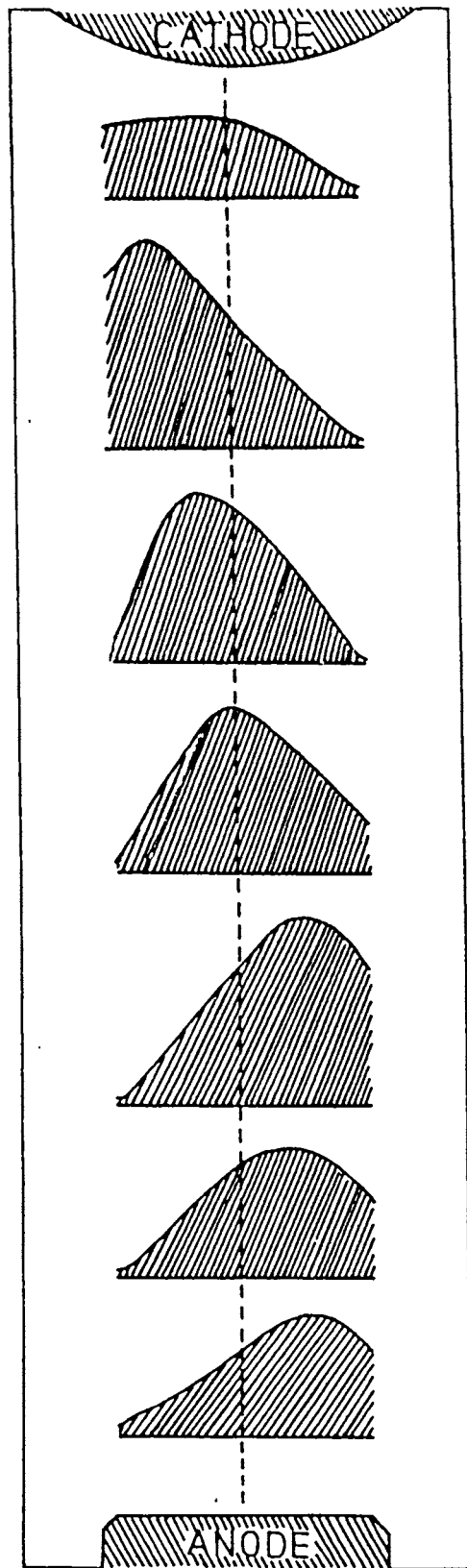


Fig.3.25 Variation of the power density distribution over the cross section of the laser electrodes.

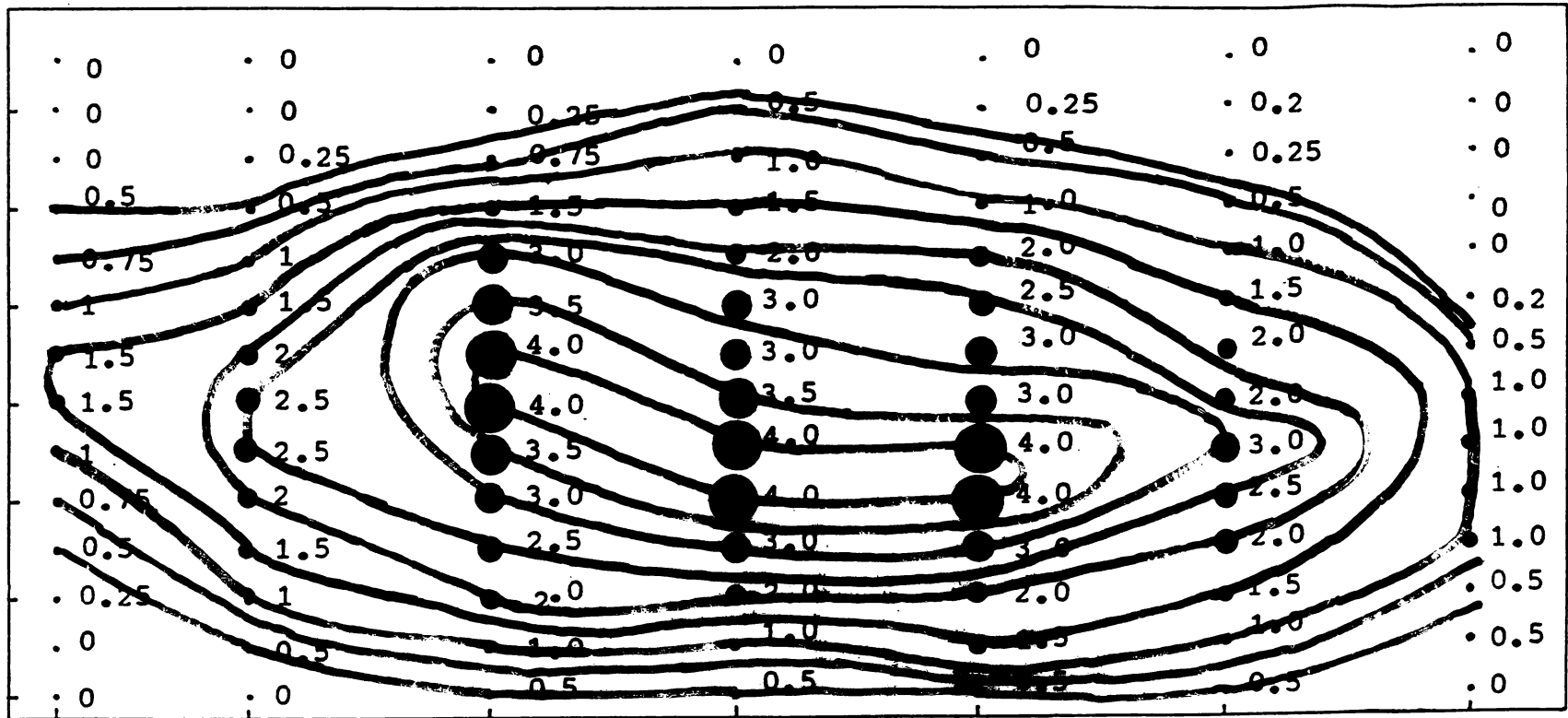


Fig. 3.27. ISO-intensity contour of the laser beam cross section.

first suggested by Loeb [24] to account for the formation of luminous pulses in electrical breakdown.

The laser operated using the double-Blumlein circuit was charged by 9.3 kV (pressure:90 torr) and triggered by the spark gap switch. The intensity distribution along the horizontal and vertical direction in the laser beam cross section was measured by an HP-2-4207 Hewlett Packard photodiode and a 466 DM44 Tektronix storage oscilloscope. The photodiode was fixed in a travelling microscope, at one metre away from the laser output window and could be moved horizontally as well as vertically. The laser beam was attenuated by inserting a 1 cm thick transparent perspex plate before falling on the photodiode. As seen in Fig.3.25, the position of the intensity maximum is shifted towards the edges of the electrodes.

The peak intensity is at the centre of discharge cavity at midway between the cathode-anode separation. The position of the peak shifts from above the middle line of the cross section near the cathode to lower side near the anode, thus gives rise to a helical type pattern for peak position.

This non uniformity is due to the off centering of the peak intensity of the emission cross section of the beam profile. This is clear from the intensity contour as given in Fig.3.26.and 3.27 respectively.

REFERENCES

J.D.Shipman, Jr., Appl.Phys.Lett., 10, 3 (1967).

B.Godard, IEEE J.Quant.Electron., QE-10, 147 (1974).

D.Basting, F.P.Schafer and B.Steyer, Opto-Electr.,
4, 43 (1972).

S.C.Mehendale and D.D.Bhawalkar, BARC Technical Note (1976).

W.A.Fitzsimmons, L.W.Anderson, C.E.Riedhauser and
Jan.M.Vrtilek, IEEE J.Quant.Electron., QE-12, 624 (1976).

A.G.Englehardt, A.V.Phelps and E.G.Risk, Phys.Rev.,
135, 1566 (1964).

Kazuhito Ishikawa, Shinzo Muto and Hidenori Matsuzawa,
Appl.Phys.Lett., 50(14), 889 (1987).

J.I.Levatter and S.Lin, Appl.Phys.Lett., 25, 703 (1974).

A.J.Schwab and F.W.Hollinger, IEEE J.Quant.Electron.,
QE-12, 183 (1973).

- [10] M.Geller, D.E.Altman and T.A.De Temple, Appl.Opt.,
7, 2232 (1968).
- [11] E.E.Bergmann, Appl.Phys.Lett., 31, 661 (1977).
- [12] J.P.Singh and S.N.Thakur, J.Sci.Ind.Res., 23, 227 (1978).
- [13] P.Richter, J.D.Kimel and G.C.Moulton, Appl.Opt.,
15, 756 (1976).
- [14] P.Persephonis, Opt.Comm., 62, 265 (1987).
- [15] T.Mitani and T.Nakaya, J.Phys.D., 11, 2071 (1978).
- [16] T.Mitani, J.Appl.Phys., 52, 3159 (1981).
- [17] E.E.Bergmann, Appl.Phys.Lett., 28, 84 (1976).
- [18] C.L.Sam, Appl.Phys.Lett., 29, 505 (1976).
- [19] A.J.Schwab and F.W.Hollinger, IEEE J.Quant.Electron.,
QE-12, 183 (1976).
- [20] A.V.Armichev, V.S.Aleinkov, T.B.Fogel'son, Sov.J. Quant.
Electron., 10(5), 592 (1980).
- [21] J.P.Singh and S.N.Thakur, Ind.J.Phys., 55, 422 (1981).

[22] C.Lal and S.N.Thakur, *Appl.Opt.*, **21**, 2317 (1982).

[23] Leonard.B.Loeb, *Science.*, **148**, 1417 (1965).

CHAPTER 4

EFFECT OF ADDITIVES ON N₂ LASER PERFORMANCE

Abstract

The effect of additives on N₂ laser performance was studied by many workers and briefly reviewed as an introduction of this chapter. The additive gases selected for the present study are oxygen, argon, 1,2-dichloroethane, carbon tetrachloride and thionyl chloride. A maximum increase of 40% was observed for the organic additive SOCl₂.

1.1. Introduction

The technology of N_2 laser has undergone many modifications to obtain higher output powers. A large part of the effort in this direction has been towards modifying the electrode design and electrical circuitry. It is an experimental fact that even with the extremely selective excitation provided in the N_2 system, in order to achieve high power output and conversion efficiency, we have to add certain other gases to the N_2 system. The effect of the presence of an additional gas in the laser plasma cavity on the position and pulse width of the laser transitions in the UV and IR regions have been studied by several workers [1-33]. TABLE 6 lists the effect of certain additive gases on the power output of a high power N_2 laser. The results obtained by various authors do not agree in certain cases.

It is interesting to investigate the role played by the additive gases in enhancing the power output efficiency of the N_2 laser, because there are at present a number of

Table.1. The effect of additives on laser performance.

Sl.No.	Additive gas	P _{out}	References
1(a)	Ar	decrease decrease	Mehendale et.al(1976) Mau-Song Chou et al(1981)
(b)	He	increase increase nil	Kurnit et al. (1975) Mehendale et al.(1976) Mau-Song Chou et al.(1981)
(c)	Ne	nil	Mau-Song Chou et al.(1981)
2(a)	(C ₂ H ₅) ₃ N	increase no increase	Kurnit et al. (1975) Mehendale et al.(1976)
(b)	(C ₃ H ₇) ₃ N	no increase	Mehendale et al.(1976)
(c)	(C ₄ H ₉) ₃ N	no increase	Mehendale et al.(1976)
3	C ₃ H ₈	increase	Tetsuya Mitani (1981)
4	CCl ₂ F ₂	increase	Tetsuya Mitani (1981)
5	C ₄ H ₁₀	increase	Tetsuya Mitani (1981)
6	CF ₄	decrease	Collier et al.(1978)
7	F ₂	increase increase	Armadillo et al.(1982) Shin Sumida et al.(1979)
8	NF ₃	increase	Rothen et al.(1979)
9	BF ₃	increase	Mehendale et al.(1982)
10.	SF ₆	increase	Levatter et al.(1974)

conflicting theories which try to explain the function of these gases. The most widely used additive has been SF₆. The output power at 337.1 nm shows a significant change in the presence of SF₆. The exact mechanism of the appearance of additional laser transitions and changes in the laser pulse width are not very well understood so far. It is reported that fluorine containing compounds are cumbersome in handling and that they corrode the electrodes.

There are different opinions regarding the role of SF₆ (and other molecules) in increasing the output power. Some authors feel that the increase in power is due to the increase in the pumping rate of the C-state (v =0) [23], and to deactivation of A and B states of N₂ [5,11] and others feel that SF₆ or its discharge products lead to a modification of the electron energy distribution that improve C-state population and deactivation process is not important [15]. Wang [24] feels that an increase of output power by the addition of a small amount of SF₆ is due to the increase in breakdown time and breakdown voltage.

Both SF_6 and CF_4 have also been thought to be involved in the quenching of the $v = 1$ level of the $B^3\Pi_g$ state, leading to the lasing of the (0,1) band and its higher sequence number. The lengthening of the (0,1) pulse appears to be due to prolonged population inversion resulting from continued quenching of the $v = 1$ level when a 300 ns electrical pulse was used [3]. Possibly, $v = 2$ and $v = 3$ levels are also quenched leading to the appearance of the (1,2) and (1,3) levels in the laser spectrum.

One of the possible ways to induce additional population inversion between the lasing levels is by quenching the lower lasing level through collisional excitation transfer to an additive. This method is especially useful in the case of the nitrogen lower lasing level ($B^3\Pi_g$) which has a larger life time (8 μ s) than that of the upper lasing level ($C^3\Pi_u$) (40 ns), thereby causing a bottle neck for population inversion to be maintained for durations larger than 20 ns. The penning ionization mechanism, which has been utilized in metal vapor lasers to produce the ions in an excited state, can well be suited to depopulate the lower laser level and create a larger

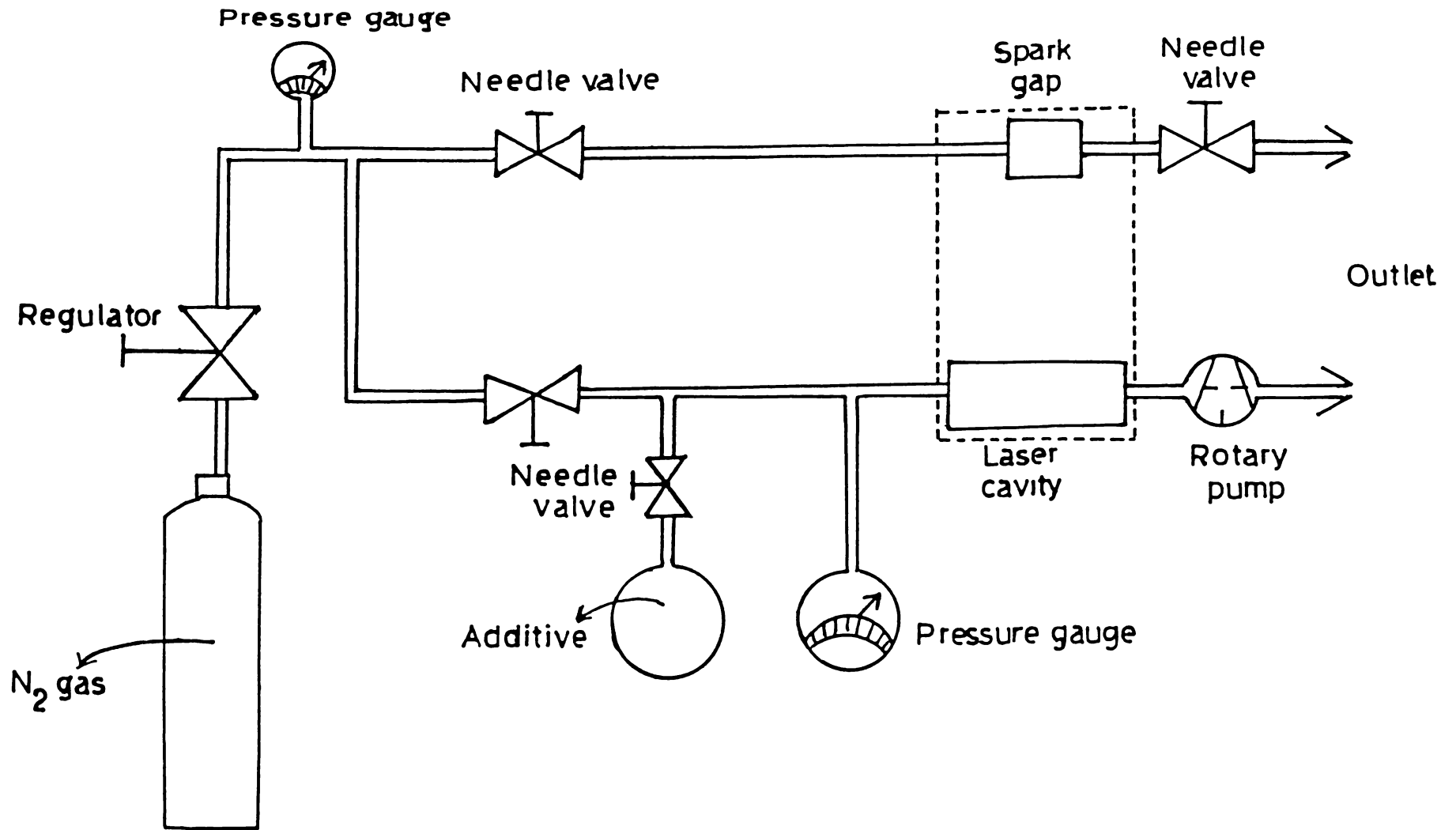


Fig.4.1 Experimental set up used for power enhancement of N_2 laser with additives.

population inversion. The energy level of N_2 ($B^3\Pi_g$) is sufficiently high (7.35 eV) compared to the ionization potential (IP) of some of the organic compounds [25].

4.2. Experimental set up

The gas supply to the laser cavity was modified as shown in Fig.4.1. The partial as well as the total pressure can be read on the manometer. Needle valves were used to control the partial pressures of N_2 and the additive. The laser was operated using the triggered spark gap switch. Keeping the N_2 pressure at a fixed value, the pressure of the additive was varied (1,2 and 4 torr) and the variation in the average power was measured using a Scientech calorimeter. The nitrogen pressure was varied in steps of 10 upto 170 torr. The repetition rate was fixed at 10 Hz. The pulse shape is recorded on a 100 MHz Tektronix storage oscilloscope using HP-2-4207 photodiode of rise time \sim 0.3 ns. The additives selected for the present study are oxygen, argon, 1,2-dichloroethane, carbon tetrachloride and thionyl chloride. The applied voltage was kept constant at 9.3 kV.

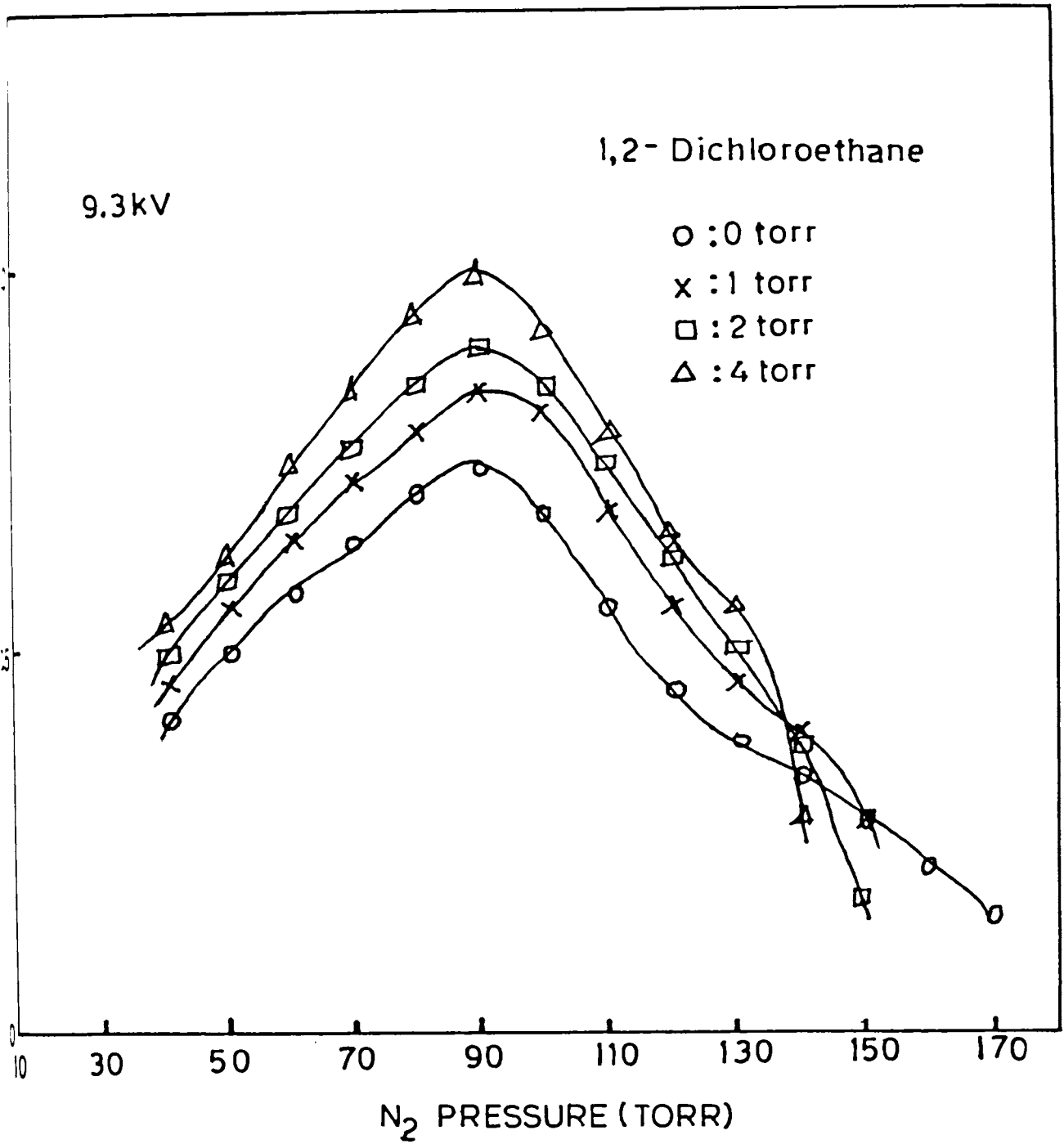


Fig.4.2. Variation of laser energy with pressure of 1,2-Dichloroethane for different pressures of N₂.

4.3. Variation of power on adding additives

4.3.1. Power variation with O₂ and Ar

Oxygen and Argon didnot show any appreciable effect on laser performance in the discharge system. Introduction of Ar and O₂ suppresses the lasing action as reported by Bergmann et al.[34]. However, Arutyunyan and Galechyan [20] have observed the highest output energy with the addition of 5%, 15%, and 25% oxygen to N₂ gas at total pressure of 70,50 and 30 torr respectively.

4.3.2. Power variation with 1,2-Dichloroethane (CH₂Cl-CH₂Cl)

The effect of addition of 1,2-dichloroethane to N₂ was studied over a range of N₂ pressures, keeping the applied voltage constant at 9.3 kV. The variation of output power with pressure of added 1,2 - dichloroethane (1,2 and 4 torr) is shown in Fig.4.2 for different pressures of N₂ and also that of N₂ alone. At higher pressures, the increase was less. There was no observable change in the pulse duration

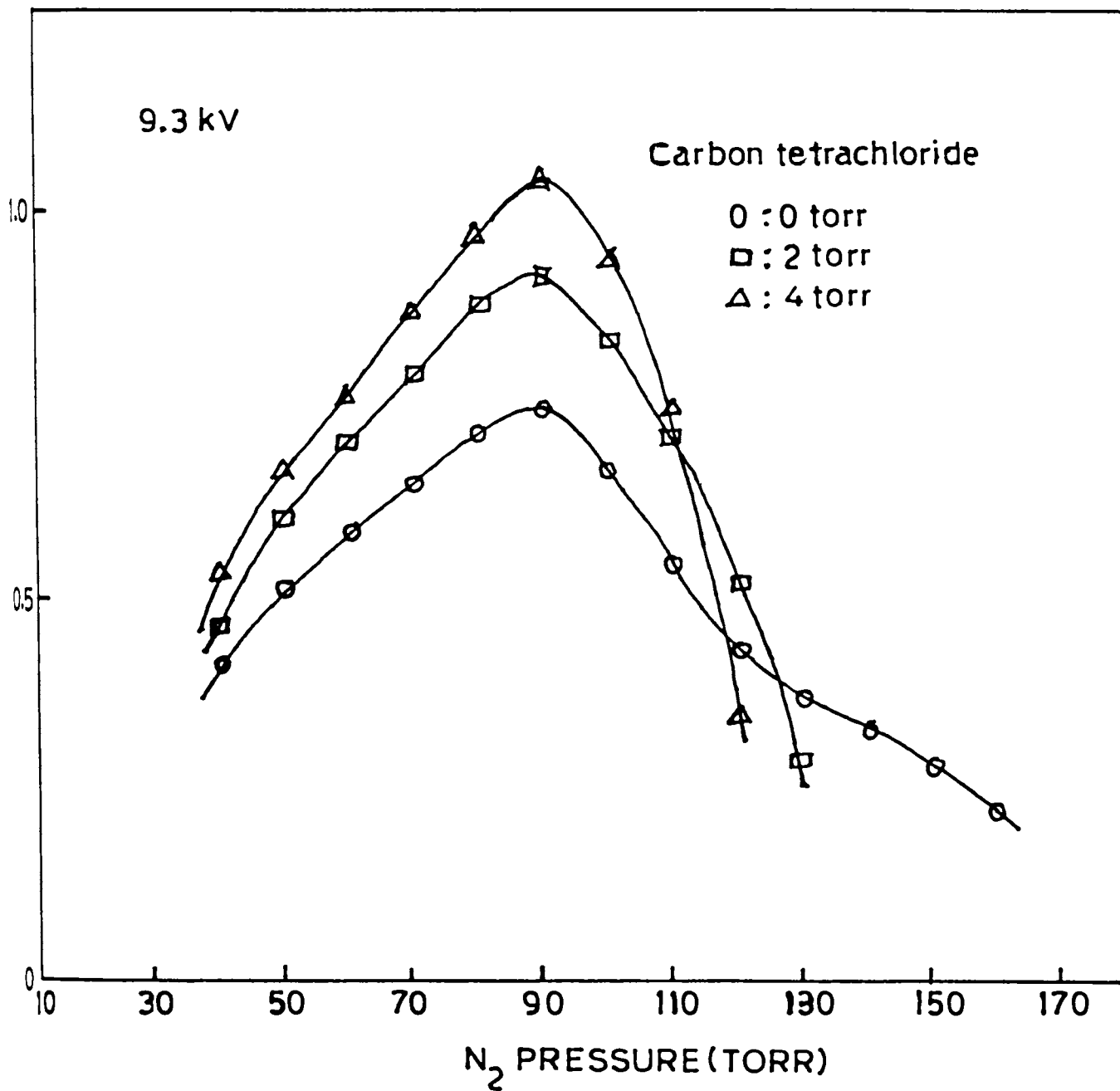


Fig.4.3.Variation of laser energy with pressure of carbon tetrachloride for different pressures of N₂ .

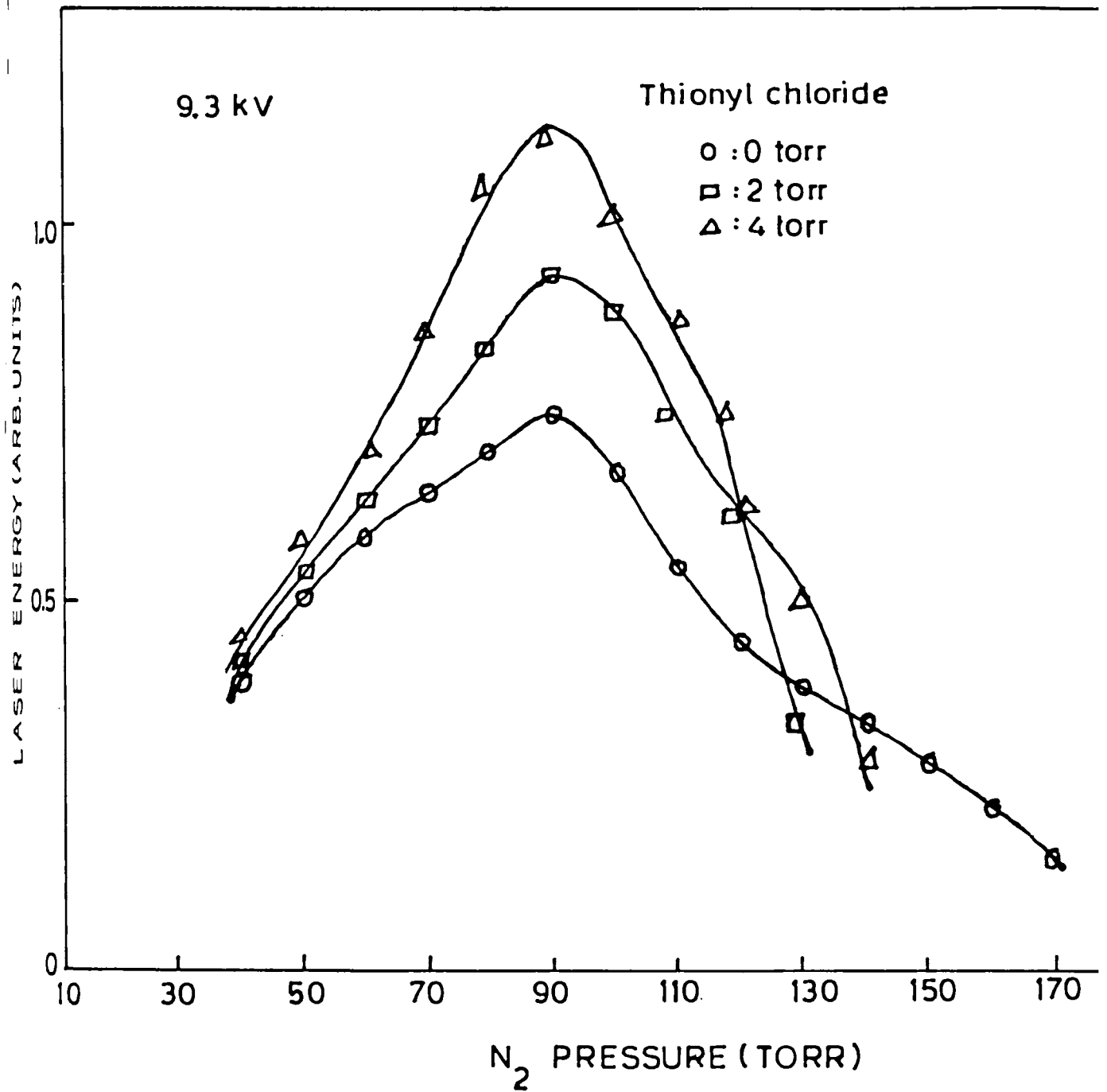


Fig.4.4. Variation of laser energy with pressure of thionyl chloride for different pressures of N₂.

for a pressure of 90 torr with 4 torr of 1,2-dichloroethane, the laser energy is increased by 25% .

4.3.3. Power variation with Carbon Tetrachloride (CCl_4)

The variation of output energy for different pressures of CCl_4 (2 and 4 torr) was measured and plotted as shown in Fig.4.3. A maximum increase of 30% was observed for 4 torr of CCl_4 . No appreciable change in the pulse width was observed.

4.3.4. Power variation with Thionyl Chloride (SOCl_2)

A maximum increase of 40% was observed at 90 torr of N_2 and 4 torr of SOCl_2 (Fig.4.4). The decrease in power output is notable at higher N_2 pressures. No variation in pulse width was obtained.

The present studies show that the additive gases enhances the emission intensity (except for Ar and O_2) without affecting the pulse width. Unlike in the case of some of the

earlier studies [34], we observe that there is an optimum partial pressure of the additive gas at which the maximum power enhancement is obtained. The molecules of the additive gases get dissociated in the plasma discharge so as to enhance the number of species in the discharge medium. This (on colliding with N_2 at lower laser level), brings about the faster deexcitation of N_2 to the ground state, thereby enhancing the laser power. However, at higher number densities of the "dopants", various species formed with nitrogen (like CN, NO, NS, CO etc.) bring down the number of active centres (N_2 molecules) in the medium resulting into the decrease in the output power of N_2 laser.

REFERENCES

- [1] R.P.Akins and Shao-Chi Lin, *Appl.Phys.*, **28**, 221 (1976).
- [2] E.Armandillo, G.Salvetti, R.Marchetti and E.Penco,
Lett.Nuovo Cemento., **31**, 140 (1981).
- [3] F.Collier, G.Theill and P.Cottin, *Appl.Phys.Lett.*,
32, 739 (1978).
- [4] R.Cubeddu and S.M.Curry, *IEEE J.Quant.Electron.*,
QE-9, 499 (1973).
- [5] R.F.Heidner III, D.G.Sutton and S.N.Suchard, *Chem.Phys.Lett.*,
37, 243 (1976).
- [6] R.S.Kunabenchi, M.R.Gorbal and M.I.Savadatti, *Am.J.Phys.*,
50, 568 (1982).
- [7] J.I.Levatter and Shao-Chi Lin, *Appl.Phys.*, **25**, 703 (1974).
- [8] M.C.Lin, *Int.J.Chem.Kinet.*, **5**, 173 (1973).
- [9] S.C.Mehendale and D.D.Bhawalkar, *J.Appl.Phys.*,
53, 6444 (1982).

- [10] A.Rothem and S.Rosenwaks, Opt.Comm., 30, 227 (1979).
- [11] S.N.Suchard, D.G.Suttan and R.F.Heidner, III, IEEE J. Quant. Electron., QE-11, 908 (1975).
- [12] S.Sumida, M.Obara and T.Fujioka, Appl.Phys.Lett., 34, 31 (1979).
- [13] H.M.von Bergmann, V.Hasson and D.Preussler, Appl.Phys.Lett., 27, 553 (1975).
- [14] H.M.von Bergmann and V.Hasson and J.Brink, J.Appl.Phys., 47, 4532, (1976).
- [15] C.S.Willett and D.M.Litynski, Appl.Phys.Lett., 26, 118 (1975).
- [16] D.Basting, F.P.Schaffer and B.Steyer, Opto-Electr., 4, 43 (1972).
- [17] M.Hugenschmidt and J.Wey, Opt.Comm., 29, 191 (1979).
- [18] T.Kobayashi, M.Takemura, H.Shimizu and H.Inaba, IEEE J. Quant.Electron., QE-8, 579 (1972).
- [19] N.A.Kurnit, S.J.Tabbs, K.Bidhichand, L.W.Ryan,Jr., and

- J.Javan, IEEE J.Quant.Electron., QE-11, 174 (1975).
- [20] G.G.Arutyunyan and G.A.Galechyan, Sov.Phys.Tech.Phys.,
26, 94 (1981).
- [21] O.Judd, IEEE J.Quant.Electron., QE-12, 78 (1976).
- [22] Yu.I.Bychkov, M.N.Kostin, V.F.Losey and V.F.Tarasenko,
Instrum.Exp.Tech., 21, 1093 (1979).
- [23] A.Maeda, T.Ydmashita and Y.Miyazoe, Jap.J.Appl.Phys.,
17, 239 (1978).
- [24] C.P.Wang, Rev.Sci.Instrum., 47, 92 (1976).
- [25] Kumar, S.V.Krishna and S.K.Mitra, J.Appl.Phys.,
60(6), 2177 (1986).
- [26] S.C.Mehendale and D.D.Bhawalkar, BARC Technical
Note., (1976).
- [27] Mau-Song Chou and Gerald A.Zawadzkas, IEEE J.Quant.
Electron., QE-17, 77 (1981).
- [28] Tetsuya Mitani, Appl.Phys., 52, 3159 (1981).

- [29] E.Armandillo and A.J.Kersley, Appl.Phys.Lett.,
41,611 (1982).
- [30] J.Itani, K.Kagawa and Y.Kimura, Appl.Phys.Lett.,
7, 503 (1975).
- [31] P.Akins Robert and S.C.Lin, Appl.Phys.Lett.,28,221(1976).
- [32] Tsunenori Arai, Minoru Obara and Tomoo Fujioka,
J.Appl.Phys., 51, 3556 (1980).
- [33] L.Y.Nelson, G.J.Mullaney and S.R.Byron, Appl.Phys.Lett.,
22, 79 (1973).
- [34] C.Sudha Kartha, Ph.D Thesis, Cochin University (1984).

CHAPTER 5

FLUORESCENCE IN SrS:Ce AND SrS:Eu PHOSPHORS

Abstract

The method of preparation of SrS phosphors doped with rare earths are given in this chapter. Nitrogen laser induced fluorescence emission spectra of Ce³⁺ and Eu²⁺ phosphors in the visible region are recorded and discussed. For Ce³⁺, a prominent peak at 408 nm and a shoulder at 450 nm are observed. A band with line structure in the region 350-430 nm and a new broad band at 460 nm are observed for Eu²⁺ ion.

5.1. Introduction

Alkaline earth sulphide phosphors activated by rare earth elements are of considerable practical importance after the discovery of infrared stimulation and sensitized luminescence [1,2]. Fluorescence emission characteristics of phosphors such as CaS, SrS and BaS have been done using conventional UV excitation sources [3-7]. Amongst the series of alkaline earth sulphide phosphors, SrS is the least studied. This chapter deals with the results obtained from the study of the fluorescence emission of SrS phosphors doped with Ce and Eu using N_2 laser as a source of excitation.

5.2. Sample preparation

The samples were prepared with the use of procedures that, to a large extent, have been worked else where [8,9]. High purity $SrSO_4$ (Reidel, Germany) was used as the base material. A number of samples with varying dopant concentrations were prepared by doping the base material with



Fig.5.1. The sample cell.

the required amounts of rare earth oxide (99.99% purity from IRE, India) and carbon (reducing agent) in the presence of sodium thiosulphate as flux. The mixture was fired at 950^o C for about one hour. Efficient phosphors were obtained by quenching the fired samples to room temperature. The powder thus obtained was converted into pellets of 10 mm radius and 3 mm thickness.

5.3. Sample cell

The pelletised samples under study are mounted inside a cell. The sample holder and the cell assembly are shown in Fig.5.1. The metallic cell has four quartz windows at right angles to each other. The sample holder consists of two flat round copper discs which can be tightened with the sample in between, using brass screws. The cell can be evacuated by connecting it to a vacuum pump through a side tube. The cell can be used for the fluorescence measurements at LNT and RT. It can be evacuated to a pressure of 2×10^{-5} torr.

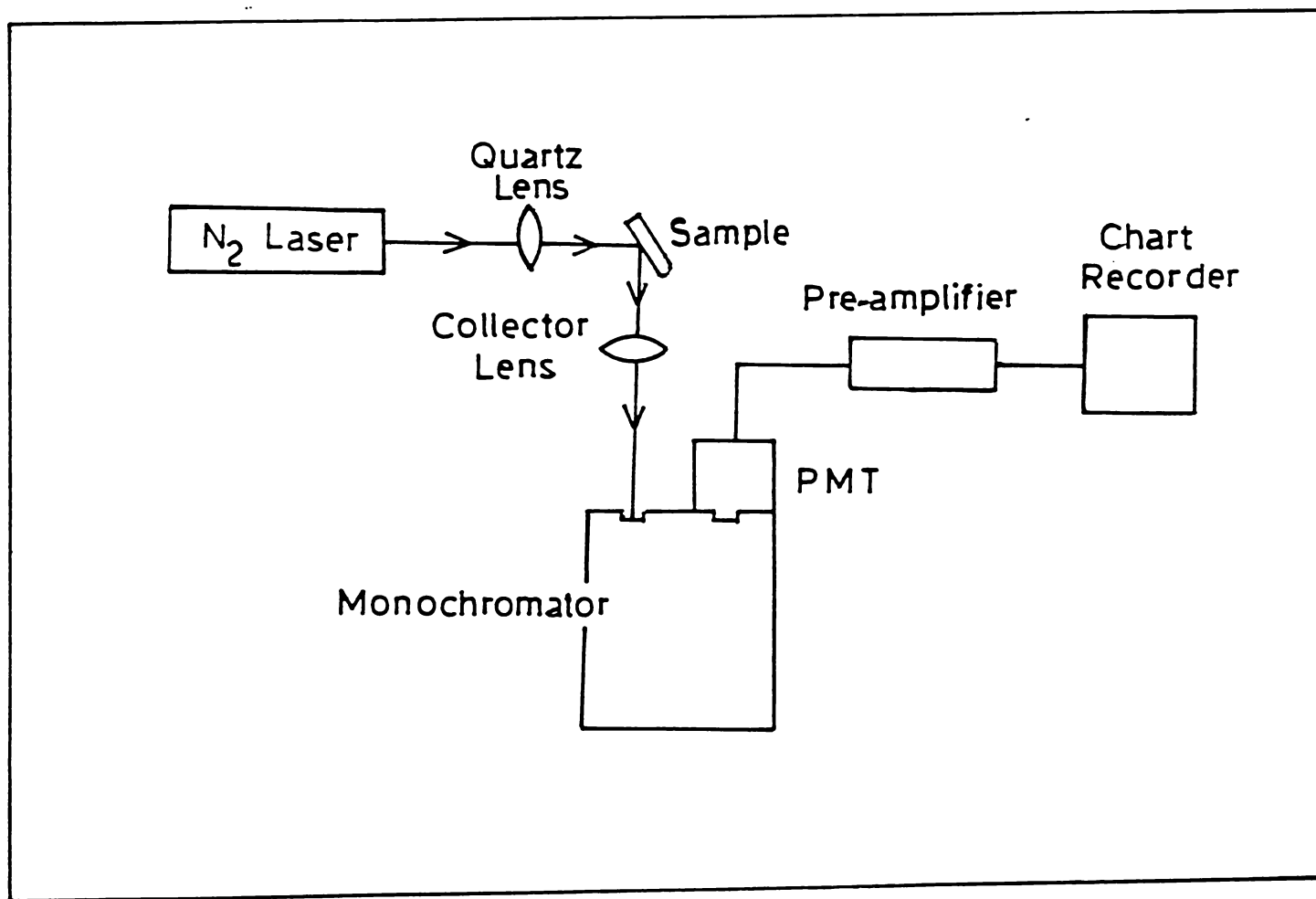


Fig.5.2 Schematic diagram of the apparatus used for recording the fluorescence spectra.

5.4. Experimental set up

The schematic diagram of the experimental set up is shown in Fig.5.2. The phosphors were excited using the pulsed N_2 laser. The N_2 laser beam is focussed on to the sample and fluorescence emission is collected in a direction perpendicular to that of the laser beam, and focussed on to the slit of a 0.5 m Jarrel Ash monochromator. The diffracted light is detected by a EMI 9683 KQB photomultiplier tube (PMT) having an S-20 cathode attached directly in front of the exit slit. The photocurrent produced in it is amplified using a low-noise high gain preamplifier and recorded on a strip chart recorder (Omnigraphic) (Fig.5.3).

5.5. SrS:Ce phosphors

Luminescence properties of cerium activated sulphides were studied by many workers [10, 11]. In the present study, cerium was introduced into SrS in the form of cerium oxide. All the measurements were carried out at room temperature.

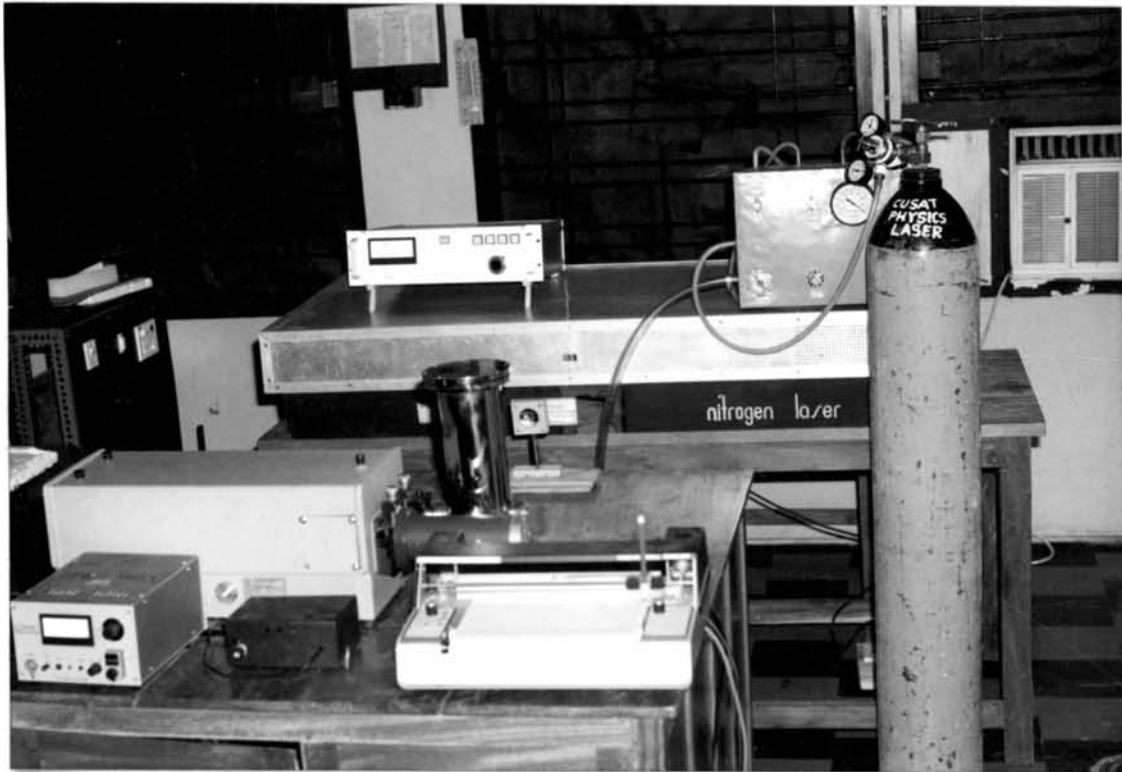


Fig.5.3. Experimental set up for recording the fluorescence spectrum.

Two types of SrS:Ce phosphors were prepared [12]. In type I, the concentration of flux was varied from 2% to 50% by wt. and the cerium concentration was kept constant at 2% by wt. In type II, the flux concentration was kept constant at 35% by wt., while cerium concentration was varied from 0.1% to 1.4% by wt.

In the case of undoped SrS sample, only a broad band at 520 nm was observed (Fig.5.4). Fig.5.5 shows that the emission spectra of the SrS:Ce phosphors for various flux concentrations. The fluorescence emission intensity increases with the flux concentrations upto 40% by wt. (sample 5 of Fig.5.5) and then decreases for higher flux concentrations. The decrease in intensity is due to the concentration quenching. Further it was observed that, with increasing flux, a shoulder is developed at higher wavelength side of the main band.

The number of luminescent centres increases with the increase of cerium concentrations resulting into the increase in fluorescence emission showing maximum intensity for

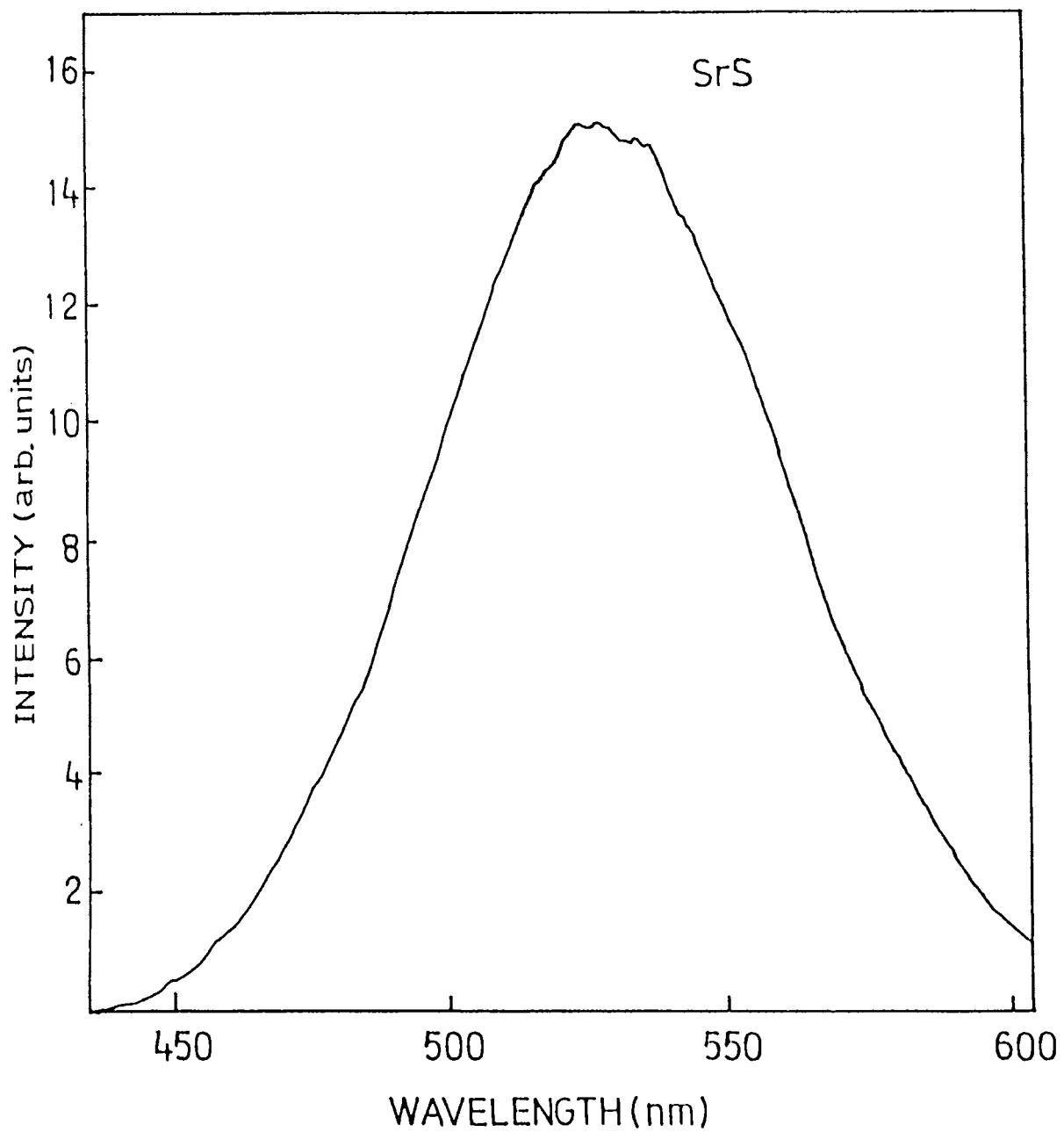


Fig.5.4 Fluorescence emission spectrum of undoped SrS sample.

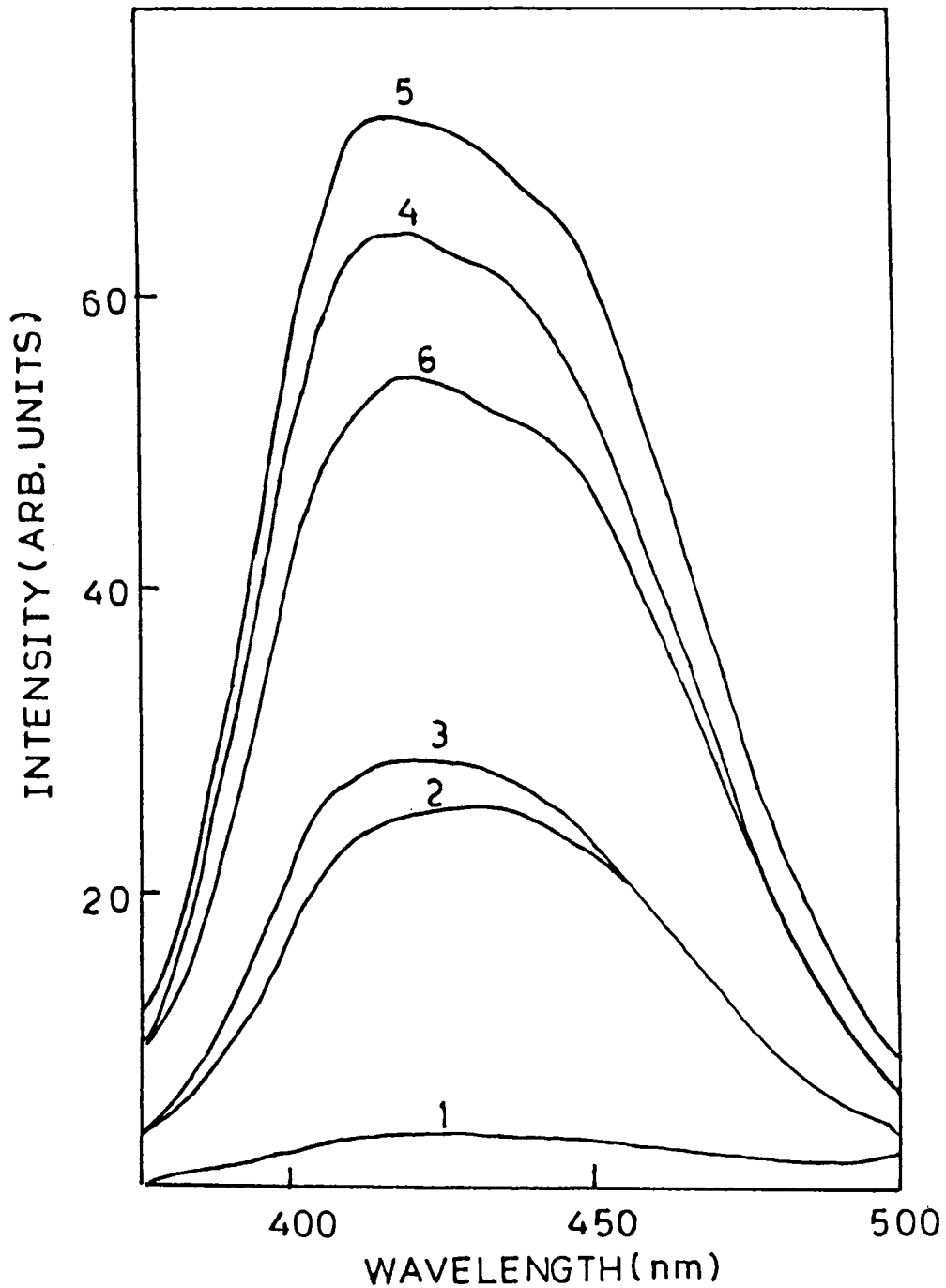


Fig.5.5. Fluorescence emission spectra of SrS:Ce ((Type I) phosphors with different flux concentrations (in wt.%): (1) 2%, (2) 10%, (3) 25%, (4) 35%, (5) 40% and (6) 50% with Ce at 2%.

the sample 5 (Ce:1%) as shown in Fig.5.6. Usual concentration quenching of the fluorescence emission is observed at higher concentrations. The emission spectra consist of a prominent peak at 408 nm and a shoulder at 450 nm. These two bands are well developed as the concentration is decreased. A more resolved spectrum of Ce:0.1% is shown in Fig.5.7. No perceptible shift in peak wavelength with the change of activator concentration was detected.

The two luminescence bands observed can be ascribed to transitions from the lowest level of the 5d configuration, to the levels ${}^2F_{5/2}$ and ${}^2F_{7/2}$ of the 4f configuration of the cerium ion. It is seen that there are no observed crystalline field splittings in the emission spectra. The SrS has a NaCl type of structure and if we assume that the rare earth is located in a substitutional site, then the Ce^{3+} will experience a cubic field potential [10].

According to Freed [13], a pair of excited states measured in Ce^{3+} salts in the form of chloride and ethylsulphate single crystals, can be assigned to the terms of

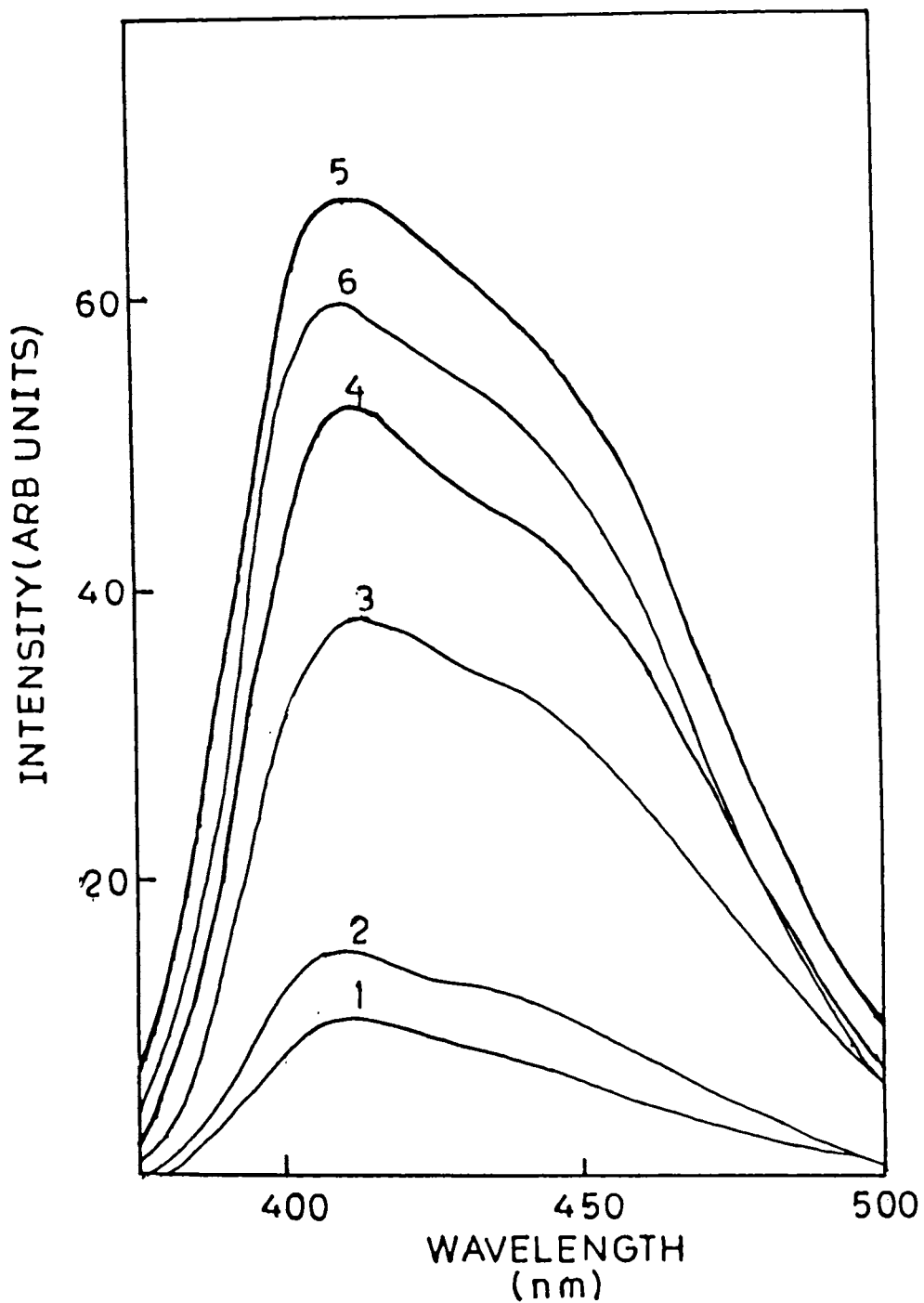


Fig.5.6 Fluorescence emission spectra of SrS:Ce (Type II) phosphors with different Ce concentrations (in wt.%): (1) 0.1%, (2) 0.2%, (3) 0.4%, (4) 0.8%, (5) 1% and (6) 1.4%.

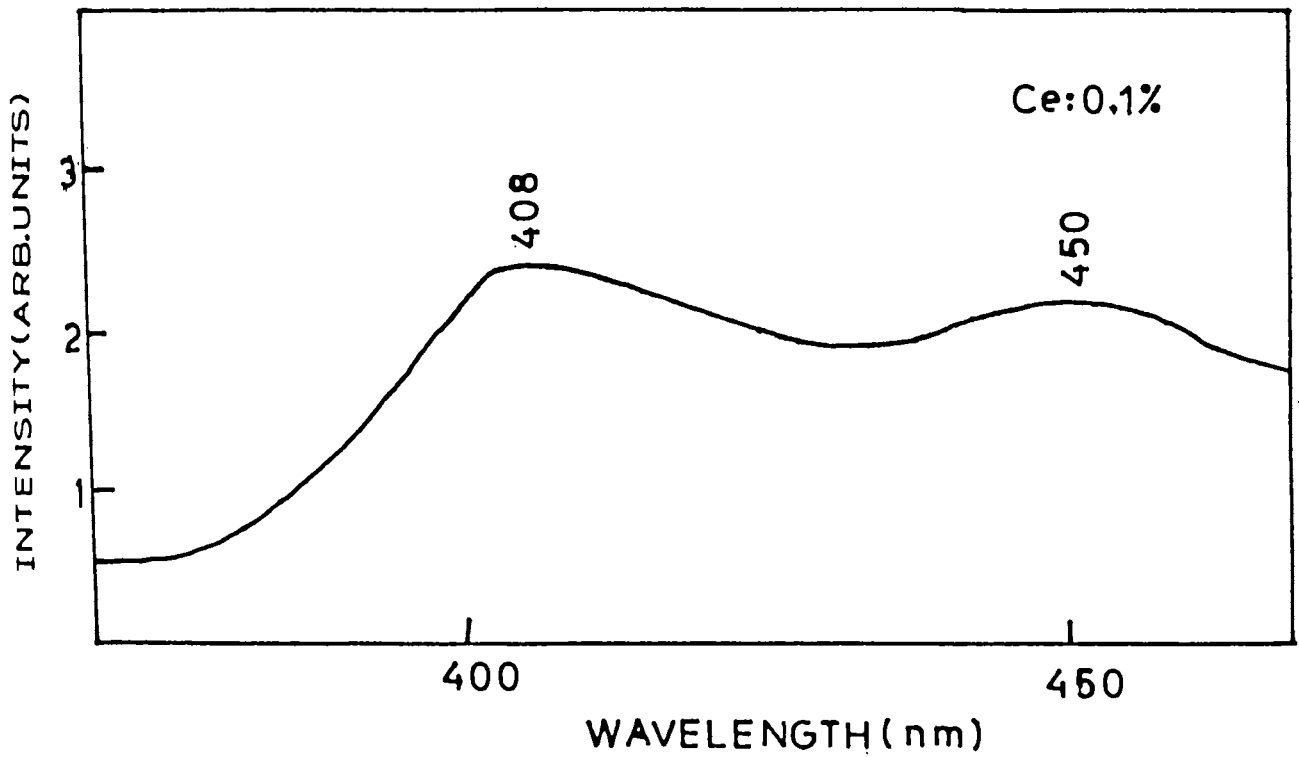


Fig.5.7 Fluorescence emission spectrum of SrS:Ce (Ce:0.1%).

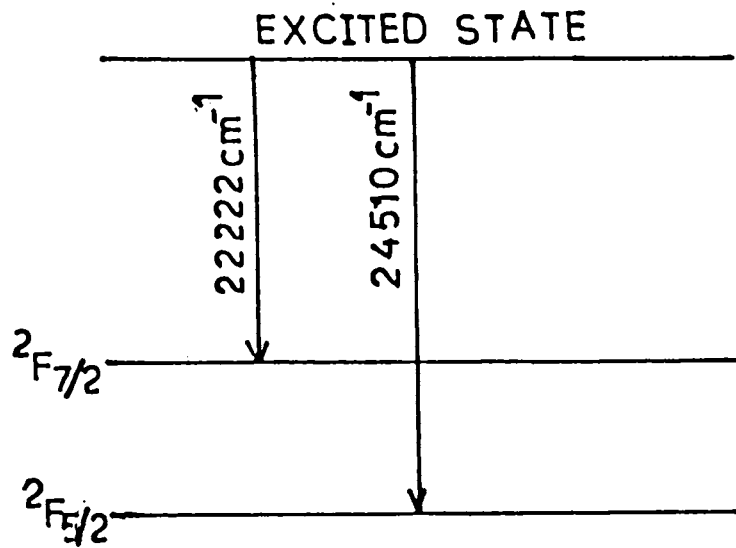


Fig.5.8 Energy level diagram of Ce³⁺.

$^1D_{3/2}$ and $^2D_{5/2}$. It can be seen that the separation between the $^2D_{3/2}$ and $^2D_{5/2}$ level is not large compared to a reasonable joint crystal field splitting of these two levels. The best approximation to the true picture appears to be one in which the upper levels are so smeared out and mixed that one need only talk about one broad excited state [10]. With this conclusion, we can represent the levels of Ce^{3+} in SrS as shown in Fig.5.8.

5.6. SrS:Eu phosphors

In recent years, it has become apparent that in certain hosts, Eu^{2+} exhibits fluorescence emission spectrum characterized by sharp lines. The presence of such sharp line spectra has caused detailed experimental measurements and theoretical analysis by various workers. The luminescence properties of Eu^{2+} activated alkaline earth phosphors (e.g. Ca, Sr and Ba) have been studied and it was found that the emission spectrum constitutes of a $4f^7(^6P) - 4f^7(^8S)$ line spectrum in the near ultraviolet region [14-19].

Przibram [20] claimed that in the divalent europium halides, the fluorescent emission consists of a blue band and sharp lines in the red region. This was in contrast with the results of Gobrecht [21] who attributed the blue band to Eu^{2+} and red lines to Eu^{3+} . Freed and Katcoff [22] had results essentially in agreement with Przibram with their work on EuCl_2 . On the other hand, Brauer [23] reported that the emission from Eu^{2+} and Eu^{3+} falls in the same wavelength region. According to Brauer, Eu as a trace, is divalent in the alkaline earth sulphides and trivalent in the alkaline earth oxides. Jaffe and Banks [25] have also reported similar results. Keller [25] had shown that Eu^{2+} can be converted into Eu^{3+} and vice versa by changing the conditions of firing. Further more, under certain conditions, samples can be obtained which have measurable amounts of both divalent and trivalent europium.

Thus the investigation on Eu phosphors is surprisingly rare, and a few publications are not always in agreement with each other. Our investigations were intended to clarify the reported contradictions and to interpret the optical spectra of Eu^{2+} in the SrS:Eu phosphor system.

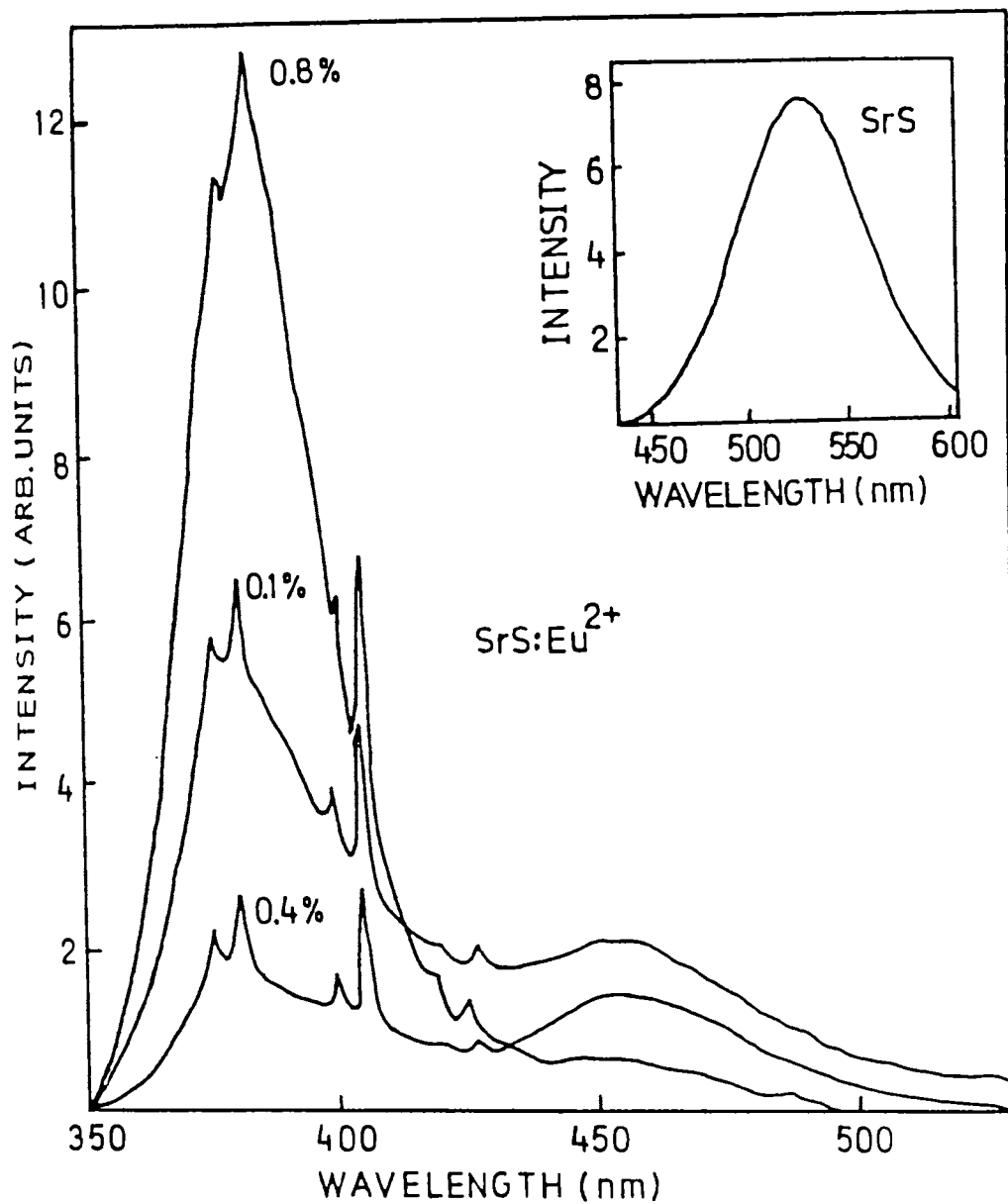


Fig.5.9 Fluorescence emission spectra of SrS:Eu²⁺ phosphors for different Eu concentrations (in wt.%): (1)0.1%, (2)0.4%, and (3)0.8%. Inset shows the fluorescence emission spectrum of undoped SrS.

probable energy level scheme is also given from the observed spectra [26].

Europium was introduced into SrS in the form of europium oxide . The fluorescence emission spectra of SrS:Eu²⁺ are shown in Fig.5.9. Spectra reveal several narrow lines which are superimposed on the broad band emission peaking at 380 nm and a broad band at 460 nm. The 460 nm band is not observed using conventional UV excitation sources. The band intensity at 380 nm gets enhanced at the cost of 460 nm. The 460 nm band disappears completely at 0.8 % of Eu concentration. There is no perceptible shift in peak wavelength of both the bands with the change of activator concentrations. In the case of undoped SrS sample, only a broad band at 520 nm is observed (inset of Fig.5.9). The sample doesnot show any characteristic fluorescence emission in the red region. This indicates that Eu goes into the SrS lattice as Eu²⁺.

The phosphors exhibit a broad band resulting from the 5d \longrightarrow 4f transition as well as sharp line emission which has been assigned to 4f (6P_i) \longrightarrow 4f ($^8S_{7/2}$) transitions

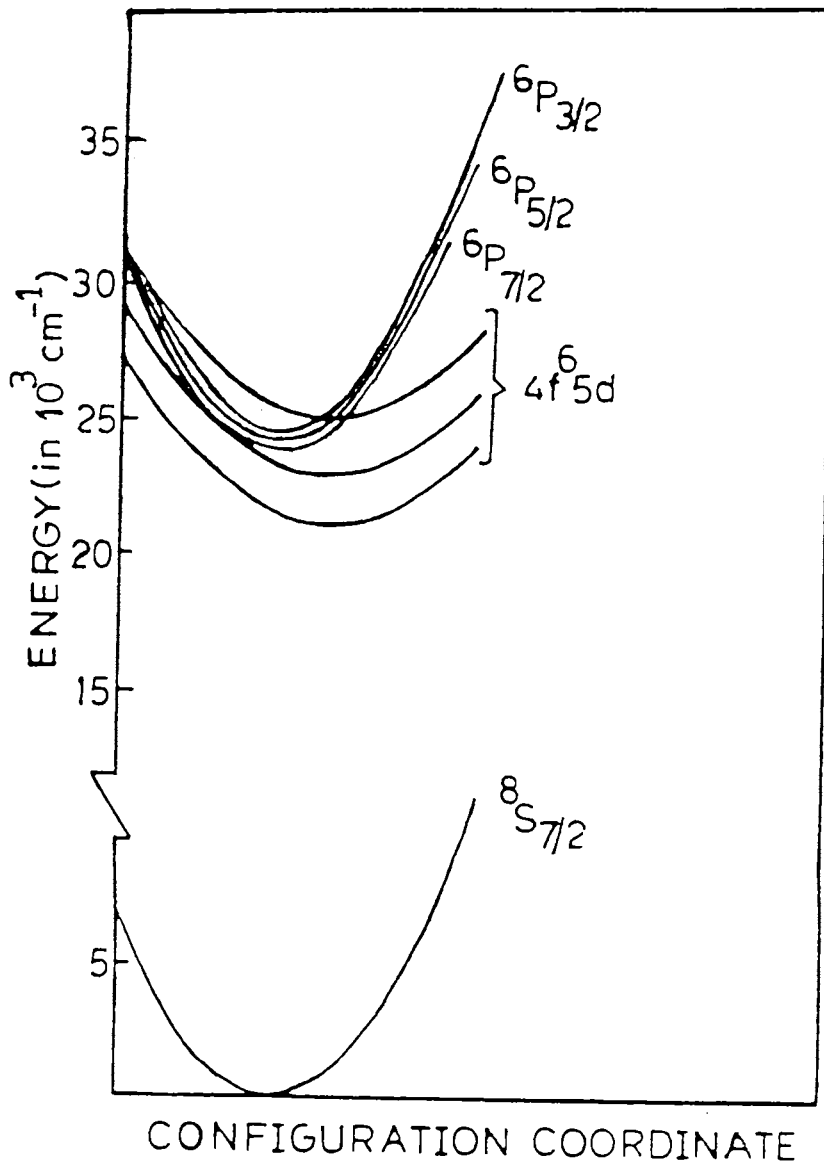


Fig.5.10 Schematic configuration coordinate diagram of Eu^{2+} . Curves were placed as indicated in the text. Stark splitting is not shown.

(here $i = 3/2, 5/2$ and $7/2$). As in the case of fluorite type crystals doped with divalent europium [27], the broad band in the optical spectra of alkaline earth sulphides is due to the transition from the $4f^7 (^8S_{7/2})$ ground state to the states in the $4f^6 5d$ configuration of the Eu^{2+} ion. The presence of both $5d \rightarrow 4f$ and $4f \rightarrow 4f$ transition indicates the proximity of the lowest excited $5d$ and $4f^7 (^6P_{7/2})$ levels [17,28].

A schematic configuration coordinate diagram of Eu^{2+} in which the lowest excited $5d$ and $4f^7 (^6P_i)$ levels are included is shown in Fig.5.10. The diagram is similar to that proposed by Blasse [29] except that 6P_i level was fixed lower than that of $4f^6 5d$. Our observations show that 6P_i should lie above $4f^6 5d$. The change in relative position of the $5d$ and 6P_i levels is due to the difference in host lattice. Strong $5d \rightarrow 4f$ band emission occurs when the $5d$ level is significantly lower than $^6P_{7/2}$ level while the $4f \rightarrow 4f$ line emission appears when the reverse is true. Both $5d \rightarrow 4f$ and $4f \rightarrow 4f$ transition occurs when the energy levels are close together as in the present case. Thus the broad band at 460 nm is attributed to the $5d \rightarrow 4f$ transition, while the band with

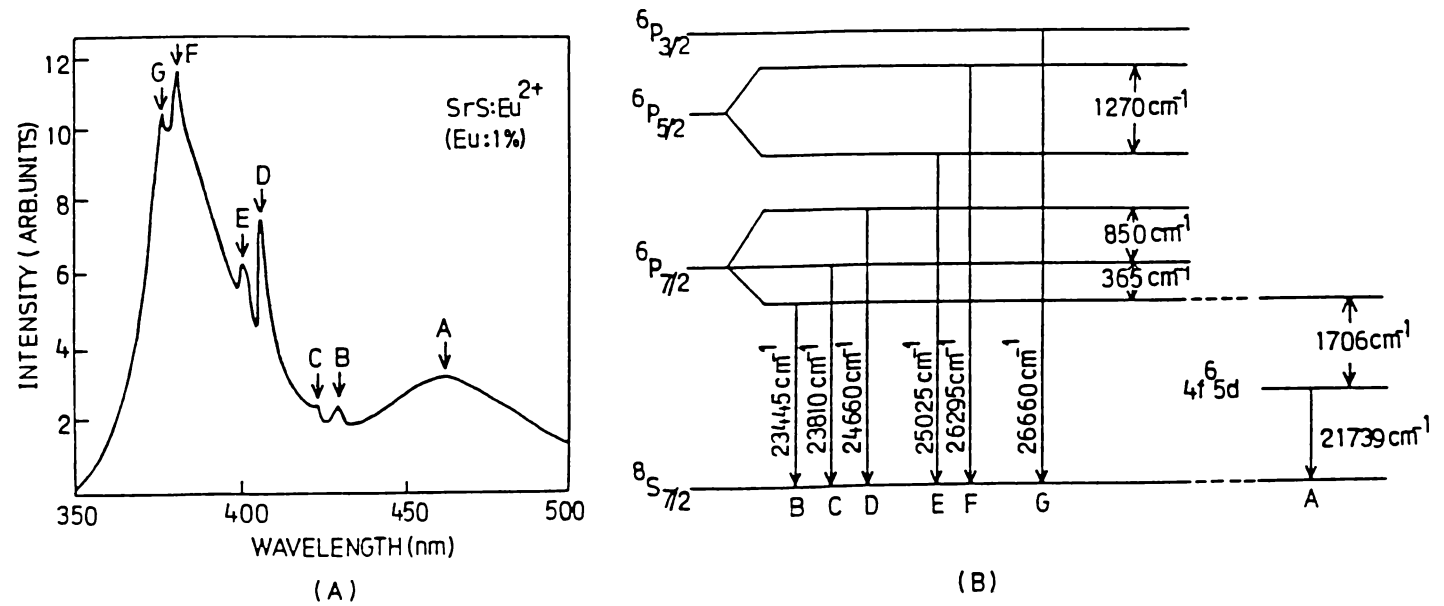


Fig.5.11 (a) Fluorescence emission spectrum of SrS:Eu²⁺ (Eu:1%).
 (b) Energy level scheme showing the various sublevels which give rise to the fluorescence emission spectrum of Eu²⁺.

line structure in the region 350-430 nm corresponds to ${}^6P_i \rightarrow {}^8S_{7/2}$ transitions. This implies that 5d level lies at about 1706 cm^{-1} lower than the ${}^6P_{7/2}$ state [Fig. 5.11.(b)].

The wavelengths and assignments of the observed fluorescence emission in the 350-430 nm region are given in Table 5.1. In order to identify the various sublevels giving rise to the six lines occurring in the ${}^6P_i \rightarrow {}^8S_{7/2}$ an analysis of the spectrum has been carried out. It is found that the six lines can be attributed to transitions from various Stark

Table 5.1. Wavelength and assignments of 6P levels of Eu^{2+} .

Group	Wavelength (nm)	Wavenumber ($\nu \text{ cm}^{-1}$)	
		Observed	Calculated
${}^6P_{7/2} \rightarrow {}^8S_{7/2}$	427.3	23403	23445
	420.0	23810	23810
	404.9	24697	24660
${}^6P_{5/2} \rightarrow {}^8S_{7/2}$	399.6	25025	25025
	380.3	26295	26295
${}^6P_{3/2} \rightarrow {}^8S_{7/2}$	375.1	26660	26660

levels of ${}^{\sigma}P_{7/2}$, ${}^{\sigma}P_{5/2}$ and ${}^{\sigma}P_{3/2}$ to ${}^8S_{7/2}$. The present analyses show that ${}^{\sigma}P_{7/2}$ and ${}^{\sigma}P_{5/2}$ split into triplet and duoblet, respectively, due to the crystal field interactions while ${}^{\sigma}P_{3/2}$ and ${}^8S_{7/2}$ do not show any splitting. The relevant energy level diagram is shown in Fig.5.11(b).

In conclusion, we have observed a new broad band ($5d \rightarrow 4f$) as well as sharp line emissions ($4f \rightarrow 4f$) of divalent europium doped in SrS phosphors. The energy level scheme for these transitions in Eu^{2+} ion is also presented.

REFERENCES

- 1] S.Rothschild, Z.Phys., 35, 557 (1934).
- 2] R.Tomaschek, Reichsber Phys., 1, 139 (1944).
- 3] S.P.Keller, J.Chem.Phys., 29, 180 (1958).
- 4] D.Sharma and Amar Singh, Ind.J.Pure and Appl.Phys., 7, 310 (1969).
- 5] P.S.Kanari, Ind.J.Pure and Appl.Phys., 10, 131 (1972).
- 6] P.R.Lalitha, V.R.Rao and V.P.N.Nampoori, Proc.of the DAE Symp. on NP and SSP., 22C, 331 (1979).
- 7] P.R.Lalitha, V.R.Rao and V.P.N.Nampoori, Curr.Sci., 49, 881 (1980).
- 8] S.P.Keller, J.E.Mapes and G.Cheroff, Phys.Rev., 108, 663 (1957).
- 9] R.P.Rao and P.R.Rao, Bull.Mater.Sci., 5, 29 (1983).
- 10] S.P.Keller, J.Chem.Phys., 29, 180 (1958).

- [11] S.Asano, N.Yamashita and T.Ohnishi, Phys.Stat.Sol.,
(6) 99, 661 (1980).
- [12] Thomas Baby, Reethamma Thomas and V.P.N.Nampoori, Proc.
opf the DAE Symp.on Quant.Electron., P.180, (1985).
- [13] S.Freed, Phys.Rev., 386, 2122 (1931).
- [14] J.L.Sommerdijk, J.M.P.J.Verstegen and A.Bril, J.Lumin.,
8, 502 (1974).
- [15] J.M.P.J.Verstegen and J.L.Sommerdijk, J.Lumin.,
9, 297 (1974).
- [16] J.M.P.J.Verstegen, J.L.Sommerdijk and A.Bril, J.Lumin.,
9, 420 (1974).
- [17] B.Tanguy, P.Merle, M.Pezat and C.Fouassier, Mater.Res.
Bull., 9, 831 (1974).
- [18] A.L.N.Stevens, J.Lumin., 17, 121 (1978).
- [19] G.Blasse, A.Bril and J.de Vries, J.Electrochem.Soc.,
115, 977 (1968).
- [20] K.Prizibram, Z.Physik., 107, 709 (1937).

- [21] H.Gobrecht, *Ann.Physik.*, **28**, 673 (1937).
- [22] S.Freed and S.Katcoff, *Physica.*, **14**, 17 (1948).
- [23] P.Brauer, *Z.Naturforsch.*, **6a**, 561 (1951).
- [24] P.M.Jaffe and E.Banks, *J.Electrochem.Soc.*,
102, 518 (1955).
- [25] S.P.Keller, *J.Chem.Phys.*, **30**, 556 (1959).
- [26] Thomas Baby and V.P.N.Nampoori , *Solid State Commun.*,
(1991). In press.
- [27] J.Hernandez.A, W.K.Cory and J.Rubio.O, *J.Chem.Phys.*,
72(1), 198 (1980).
- [28] T.Kobayasi, S.Mroczkouski and J.F.Owen, *J.Lumin.*,
21, 247 (1980).
- [29] G.Blasse, *Phys.Status Solidi.*, **55**, 131 (1973).

CHAPTER 6

CRYSTAL FIELD ANALYSIS OF SrS:Sm, SrS:Dy AND SrS:Er PHOSPHORS

ABSTRACT

The fluorescence emission spectrum of SrS:Sm, SrS:Dy and SrS:Er has been recorded using nitrogen laser excitation and analyzed in detail using a parametrized model. The splitting pattern of the energy levels in SrS lattice is evaluated using crystal field theory.

6.1. Effect of crystal field on the spectra of ions

When an atom in a proper ionized state is located in a crystal, it is subjected to various inhomogeneous electric fields produced by the ligands. This results either in the splitting of energy levels, or modification of energy levels which are essentially brought about due to perturbation caused by the interaction between ligands and impurity ions. Interaction of the doped ions with host lattice also modifies the lattice energy. Introduction of dopants will change luminescence characteristics of phosphors due to the change in the distribution of self activated centres and some times due to the appearance of new centres. The problem of the influence of the surrounding ion on the energy levels of the central ion in a crystal field was first studied by Bethe [1]. He assumed the point charge crystal field model and used a group theoretical method to predict the multiplicities of the various degenerate levels from a knowledge of the symmetry of the environment of the ion.

6.2. Theoretical calculation

According to Lea et al.[2] for the 4f states of the rare earth ions, within the manifold of angular momentum J composed of f-electron wave functions, the most general operator equivalent potential with cubic point symmetry may be written as:

$$\mathcal{H} = B_4 (O_4^0 + 5 O_4^4) + B_6 (O_6^0 - 21 O_6^4) \dots (6.1)$$

where,

$$\begin{aligned} O_4^0 &= 35 J_z^4 - [30J(J+1) - 25] J_z^2 - 6J(J+1) + 3J^2(J+1)^2 \\ O_4^4 &= 1/2 (J_+^4 + J_-^4) \\ O_6^0 &= 231 J_z^6 - 105 [3J(J+1) - 7] J_z^4 \\ &\quad + [105 J^2(J+1)^2 - 525J(J+1) + 294] J_z^2 - \\ &\quad - 5J^3(J+1)^3 + 40J^2(J+1)^2 - 60J(J+1) \\ O_6^4 &= 1/4 [11 J_z^2 - J(J+1) - 38] (J_+^4 + J_-^4) \\ &\quad + 1/4 (J_+^4 + J_-^4) [11 J_z^2 - J(J+1) - 38] \end{aligned}$$

with x,y,z axes chosen along the <100>, <010> and <001> direction. The coefficients B_4 and B_6 are factors which determine the scale of the crystal field splittings. They are linear functions of $\langle r^4 \rangle$ and $\langle r^6 \rangle$, the mean fourth and sixth

powers of the radii of the orbital corresponding to magnetic electron, and thus depend on the detailed nature of the magnetic ion wave functions. Since these are very difficult to calculate quantitatively, it is customary to regard the coefficients B_4 and B_6 as parameters to be determined empirically.

For the numerical calculation of the eigen values, for each J-manifold the $(2J+1) \times (2J+1)$ matrix is written down using the operator equivalent matrix element tabulated by Stevens [3]. These tables contain factors common to all the matrix elements, viz., $F(4)$ and $F(6)$, and these are separated out in the present calculation in order to keep the eigen values in the same numerical range for all ratios of the fourth and sixth degree terms. Then the Hamiltonian can be written as,

$$\mathcal{H} = B_4 F(4) \frac{O_4^0}{F(4)} + B_6 F(6) \frac{O_6^0}{F(6)} \dots (6.2)$$

where,

$$O_4^0 = [O_4^4 + 5 O_4^4] \quad \text{and}$$

$$O_6^0 = [O_6^0 - 21 O_6^4]$$

In order to cover all possible values of the ratio between the fourth and sixth degree terms, we put

$$B_4 F(4) = W x \quad \dots\dots(6.3)$$

$$B_6 F(6) = W (1 - |x|) \quad \dots\dots(6.4)$$

where x is a dimensionless parameter which can have values between -1 and $+1$ and W is a scale factor. It follows that,

$$\frac{B_4}{B_6} = \frac{x}{1 - |x|} \frac{F(6)}{F(4)} \quad \dots\dots(6.5)$$

so that $B_4/B_6 = 0$ for $x = 0$, while $B_4/B_6 = \pm \infty$ for $x = \pm 1$.

Rewriting equation (6.2), we have

$$\mathcal{H} = W \left[x \frac{O_4}{F(4)} + (1 - |x|) \frac{O_6}{F(6)} \right] \quad \dots\dots(6.6)$$

The term expressed in the square bracket represents a matrix whose eigenvectors correspond to the most general combination of fourth and sixth degree crystal fields, and whose eigen values are related to the crystal field energy levels by a scale factor W defined by eqn. (6.3) and (6.4). The diagonalization of the matrix was performed and for each J manifold x was allowed to take values $0, \pm 0.2, \pm 0.4, \pm 0.6, \pm 0.8, \pm 1.0$.

One can find the sign of the scale factor W and that of the parameter x directly from the signs of B_4 and B_6 as follows:

- (i) From eqn.(6.4), from which the sign of W is determined by the sign of B_6 since $(1-|x|)$ is always positive for $-1 < x < +1$
- (ii) From eqn.(6.5) which shows the sign of x is determined by the sign of B_4/B_6 ; since $F(6)$ and $F(4)$ are both positive for all J 's. The sign of B_4 and B_6 can be found out from the point charge crystal field model for the geometrical coordination factors A_4 and A_6 . There are three types of cubic corresponding to 4,6, or 8 equidistant charges Ze . For each of these, the point charge model gives the parameters as shown in Table 6.1. Here R is the distance of the coordinating charges

Table.6.1. Point charge model parameters [Ref. 2].

Type of coordination	$B_4 = A_4 \langle r^4 \rangle \beta$	$B_6 = A_6 \langle r^6 \rangle \gamma$
Tetrahedral (4)	$-7/36 Ze^2/R^5 \langle r^4 \rangle \beta$	$+1/18 Ze^2/R^7 \langle r^6 \rangle \gamma$
Octahedral (6)	$+7/16 Ze^2/R^5 \langle r^4 \rangle \beta$	$+3/64 Ze^2/R^7 \langle r^6 \rangle \gamma$
Cubic (8)	$-7/18 Ze^2/R^5 \langle r^4 \rangle \beta$	$+1/9 Ze^2/R^7 \langle r^6 \rangle \gamma$

Table 6.2. Values of multiplicative factors of β and γ [Ref.2]

Rare earth ion	$\beta \times 10^{-4}$	$\gamma \times 10^{-6}$	β/γ
Ce ³⁺	63.492	0	α
Pr ³⁺	-7.3462	60.994	-12.044
Nd ³⁺	-2.9111	-37.988	7.6632
Pm ³⁺	4.0755	60.781	6.7052
Sm ³⁺	25.012	0	α
Eu ³⁺	0	0	0
Gd ³⁺	0	0	0
Tb ³⁺	1.2244	-1.1212	-109.20
Dy ³⁺	-0.59200	1.0350	-57.200
Ho ³⁺	-0.33300	-1.2937	25.740
Er ³⁺	0.44400	2.0699	21.450
Tm ³⁺	1.6325	-5.6061	-29.120
Yb ³⁺	-17.316	148.00	-11.700

Z_e from the magnetic ions, e is the charge on the electron, r is the radius of the ion, β and γ are the Steevens multiplicative factors. The numerical values of β and γ for RE³⁺ are given in Table 6.2. The calculated values of $\langle r^n \rangle$ in units of Bohr radi using 4f wave functions are given below.

Table.6.3. Calculated values of $\langle r^n \rangle$ [ref.3].

Rare earth ion	$\langle r^2 \rangle$	$\langle r^4 \rangle$	$\langle r^6 \rangle$
Ce ³⁺	1.200	3.455	21.226
Pr ³⁺	1.086	2.822	15.726
Nd ³⁺	1.001	2.401	12.396
Sm ³⁺	0.883	1.897	8.775
Eu ³⁺	0.938	2.273	11.670
Gd ³⁺	0.785	1.515	6.281
Dy ³⁺	0.726	1.322	5.102
Er ³⁺	0.666	1.126	3.978
Yb ³⁺	0.613	0.960	3.104

The scale and pattern of the crystal field splittings are determined from the coefficients B_4 and B_6 given by ,

$$B_4 = A_4 \langle r^4 \rangle \beta \quad ; \quad B_6 = A_6 \langle r^6 \rangle \gamma \quad \dots\dots\dots(6.7)$$

where $\langle r^4 \rangle$ and $\langle r^6 \rangle$ are the mean fourth and sixth powers of the radii of the 4f electrons of the impurity ion, β and γ are the Stevens's multiplicative constants [4]. The geometrical coordination factors A_4 and A_6 are given by the point charge crystal field model.

6.3 Fluorescence in SrS:Sm, SrS:Dy and SrS:Er phosphors

6.3.1. Introduction

In continuation of the work presented in the chapter 5, here the method of preparation and the results on SrS phosphors doped with Sm, Dy and Er are presented in this section. The rare earth element samarium is used as the luminescent activator to get the emission in the green and red region. Dysprosium is found to emit in the blue, green and red regions while Erbium is covering ultraviolet and the visible regions. Most emission bands of these three phosphor system show well resolved line structure. The probable level transitions giving rise to the various emissions are analysed on the basis of the crystal field theory.

6.3.2. Phosphor preparation and experimental set up

The details of the method are given in chapter 5. In these samples, the activators were added in the prefired mixture as their oxides. The preparation and the experimental

set up used for recording the fluorescence emission spectrum at room temperature are the same as described previously.

6.3.3. SrS:Sm Phosphors

The luminescence spectra of samarium activated sulphides usually include a contribution from Sm^{3+} ions, because these readily enter the lattice, where as the activation by Sm^{2+} is not complete even under reducing the synthesis conditions[5]. In [6], the emission from divalent samarium in SrS was not observed. In an earlier investigation of infrared stimuable phosphors, Keller et al [7] had studied the properties of SrS:Sm phosphors. These phosphors have great sensitivity, storageability and rapid time response. It is assumed that 4f electrons of rare earth ion are responsible for the optical properties of these phosphors and that while bound, they are substitutionally shielded from the dielectric effects of the SrS matrix [6]. The luminescence of Sm^{3+} has been investigated in various host lattices such as CaS:Sm (Pillai and Vallabhan [8]), SrS: Sm is the least studied except for some preliminary investigations reported by

Yamashita and Asano [9] and Allsalu et al.[10].

The Sm^{3+} emission in SrS consists of three groups of bands which are well resolved into discrete lines in the region 550–675 nm (Fig.6.1) [11–13]. The broad band at 520 nm is observed in the case of undoped sample also. (inset of Fig.6.1) and hence arises due to the host lattice vacancies. As the Sm concentration increases, we observed appreciable decrease in intensity of the 520 nm band due to the usual concentration quenching as well as the transfer of energy to samarium ions. There is no perceptible shift in peak wavelength of the 520 nm band with the change of activator concentrations.

The three groups of intense lines are attributed to the well known transitions ${}^4G_{5/2} \longrightarrow {}^6H_{5/2}$, ${}^4G_{5/2} \longrightarrow {}^6H_{7/2}$ and ${}^4G_{5/2} \longrightarrow {}^6H_{9/2}$ [9,14]. The occurrence of the sub levels is due to the splitting of the free ion term of Sm^{3+} under the influence of the ligands of the surrounding ions which has not been studied qualitatively by earlier workers in SrS:Sm. In the present case, since SrS crystallises in NaCl structure [15], an

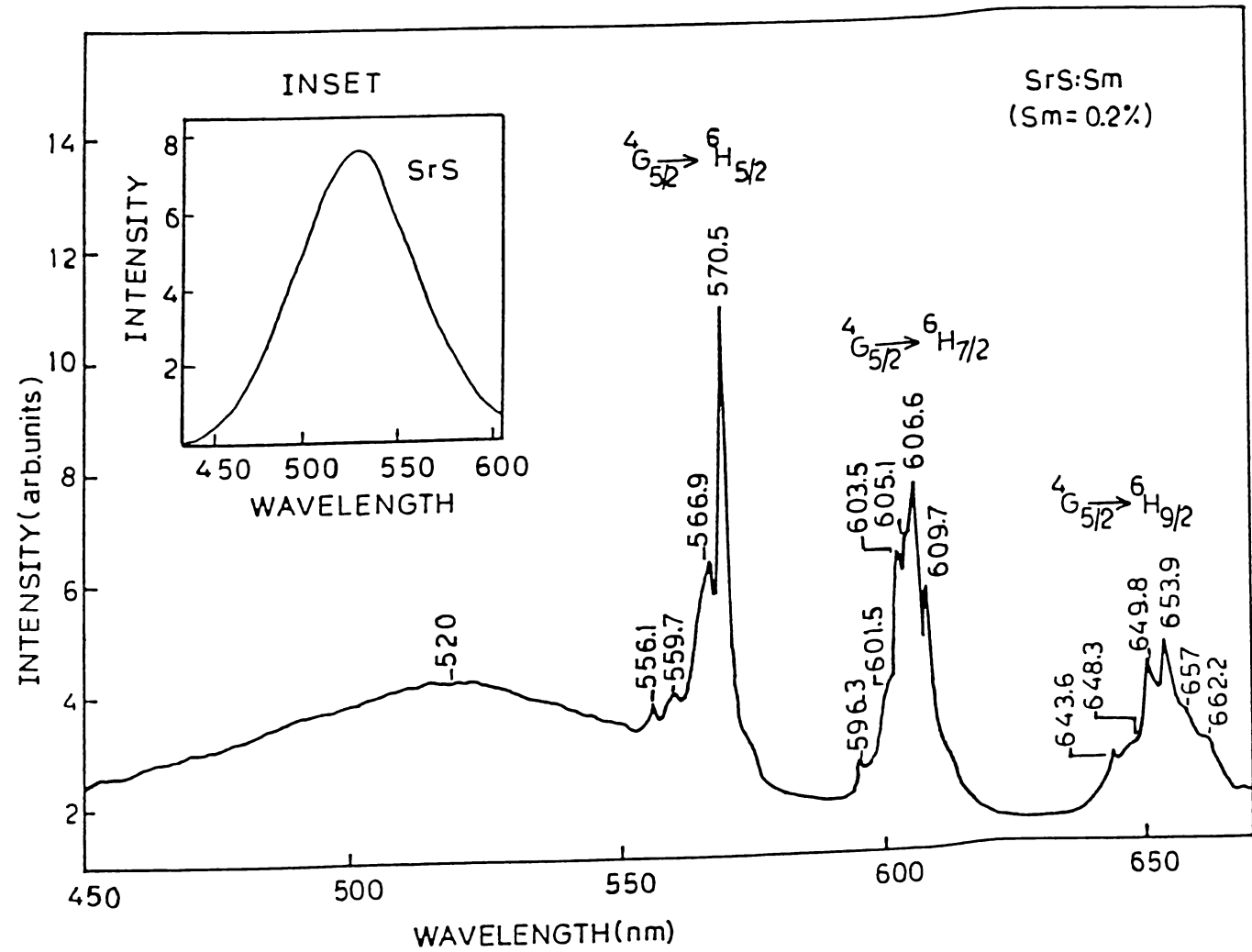


Fig.6.1 Fluorescence emission spectrum of SrS:Sm phosphor. Inset shows the fluorescence emission spectrum of undoped SrS.

Table. 6.4. Wavelength and assignments of fluorescence emission bands in SrS:Sm phosphor.

Group	Level transitions	Wavelength (nm)	Wavenumber (ν cm ⁻¹)	
			Observed	Calculated
${}^4G_{5/2} \longrightarrow {}^6H_{5/2}$	$\Gamma_8 \longrightarrow \Gamma_7$	556.1	17982	17982
	$\Gamma_7 \longrightarrow \Gamma_7$	559.7	17867	17867
	$\Gamma_8 \longrightarrow \Gamma_8$	566.9	17640	17643
	$\Gamma_7 \longrightarrow \Gamma_8$	570.5	17528	17528
${}^4G_{5/2} \longrightarrow {}^6H_{7/2}$	$\Gamma_8 \longrightarrow \Gamma_7$	596.3	16770	16740
	$\Gamma_7 \longrightarrow \Gamma_7$	601.5	16625	16625
	$\Gamma_8 \longrightarrow \Gamma_8$	603.5	16570	16600
	$\Gamma_7 \longrightarrow \Gamma_8$	606.6	16485	16485
	$\Gamma_8 \longrightarrow \Gamma_6$	605.1	16525	16525
	$\Gamma_7 \longrightarrow \Gamma_6$	609.7	16401	16410
${}^4G_{5/2} \longrightarrow {}^6H_{9/2}$	$\Gamma_8 \longrightarrow \Gamma_8^{(1)}$	643.6	15538	15538
	$\Gamma_7 \longrightarrow \Gamma_8^{(1)}$	648.3	15425	15423
	$\Gamma_8 \longrightarrow \Gamma_6$	649.8	15389	15389
	$\Gamma_7 \longrightarrow \Gamma_6$	653.9	15293	15274
	$\Gamma_8 \longrightarrow \Gamma_8^{(2)}$	657.0	15221	15267
	$\Gamma_7 \longrightarrow \Gamma_8^{(2)}$	662.2	15101	15152

Impurity ion (Sm^{3+}) occupying a Sr^{2+} site will experience a cubic field with octahedral co-ordination. In such an environment, the free ion term with $J = 5/2$ and $J = 7/2$ will split into two and three sub levels respectively [2]. Thus the emission due to ${}^4G_{5/2} \longrightarrow {}^6H_{5/2}$ transition will consist of four lines and those due to ${}^4G_{5/2} \longrightarrow {}^6H_{7/2}$ and ${}^4G_{5/2} \longrightarrow {}^6H_{9/2}$ will comprise of six lines each. The wavelengths and term assignments of the fluorescence emission bands were given in Table 6.4.

Considering the separations between the four lines observed due to ${}^4G_{5/2} \longrightarrow {}^6H_{5/2}$ transition in the wavelength region 550-575 nm, it can be seen that both the upper and lower levels are Stark-split into doublets of separations 115 cm^{-1} and 339 cm^{-1} respectively.

Fine structure analysis of fluorescence spectra corresponding to ${}^4G_{5/2} \longrightarrow {}^6H_{7/2}$ and ${}^4G_{5/2} \longrightarrow {}^6H_{9/2}$ transitions in the wavelength region 595-675 nm can be analysed by the method suggested by Zhong et al [16]. For Sm^{3+} , Steeven's multiplicative constants have the values as $\beta = 25.012 \times 10^{-4}$

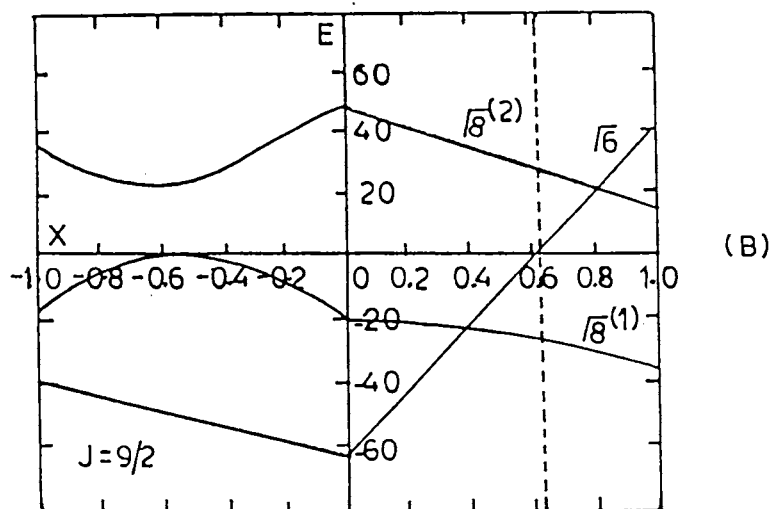
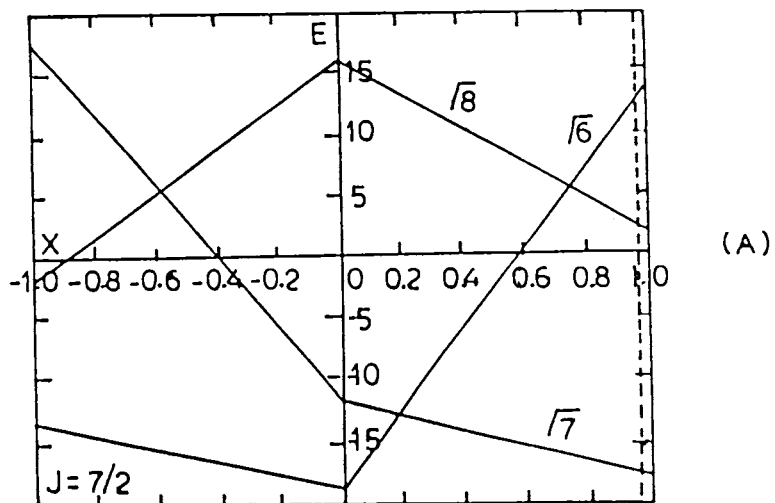


Fig.6.2 The splitting pattern of the ${}^6H_{7/2}$ and ${}^6H_{9/2}$ manifold of the Sm^{3+} ion in the SFS lattice. E is in cm^{-1} and x is a dimensionless parameter defined in the text. The broken lines indicate the values of x used to evaluate the scale factor W (in cm^{-1}) required for the experimental determination of crystal field parameters.

and $\gamma = 0$. The geometrical coordination factors A_4 and A_6 are given by the point charge crystal field model. Freeman et al [3] gave the respective values of $\langle r^4 \rangle$ and $\langle r^6 \rangle$ for Sm^{3+} ion as $1.897 a_H^4$ and $8.775 a_H^6$ (a_H is the Bohr radius) respectively.

In order to identify the various sub levels giving rise to the six lines occurring in the ${}^4G_{5/2} \longrightarrow {}^6H_{7/2}$ level, an analysis of the spectrum has been carried out. It is found that these six lines can be grouped into two sets corresponding to two Stark levels of ${}^4G_{5/2}$ with separation of 115 cm^{-1} . From the separations between the lines it has been found that ${}^6H_{7/2}$ split into three sublevels with intervals as 75 cm^{-1} and 140 cm^{-1} (Fig.6.3). The splitting pattern of the ${}^6H_{7/2}$ level of the Sm^{3+} ion in a cubic field is given by Lea et al. [2] and is shown in Fig.6.2A. An exact fit with the above pattern occurs for the scale factor $W = 6.08 \text{ cm}^{-1}$ and $x = 0.97$. Using the equations (6.3), (6.4) and (6.7), the crystal field parameters calculated are $B_4 = 0.098$; $B_6 = 2.38 \times 10^{-5}$; $A_4 \langle r^4 \rangle = 39.3 \text{ cm}^{-1}$.

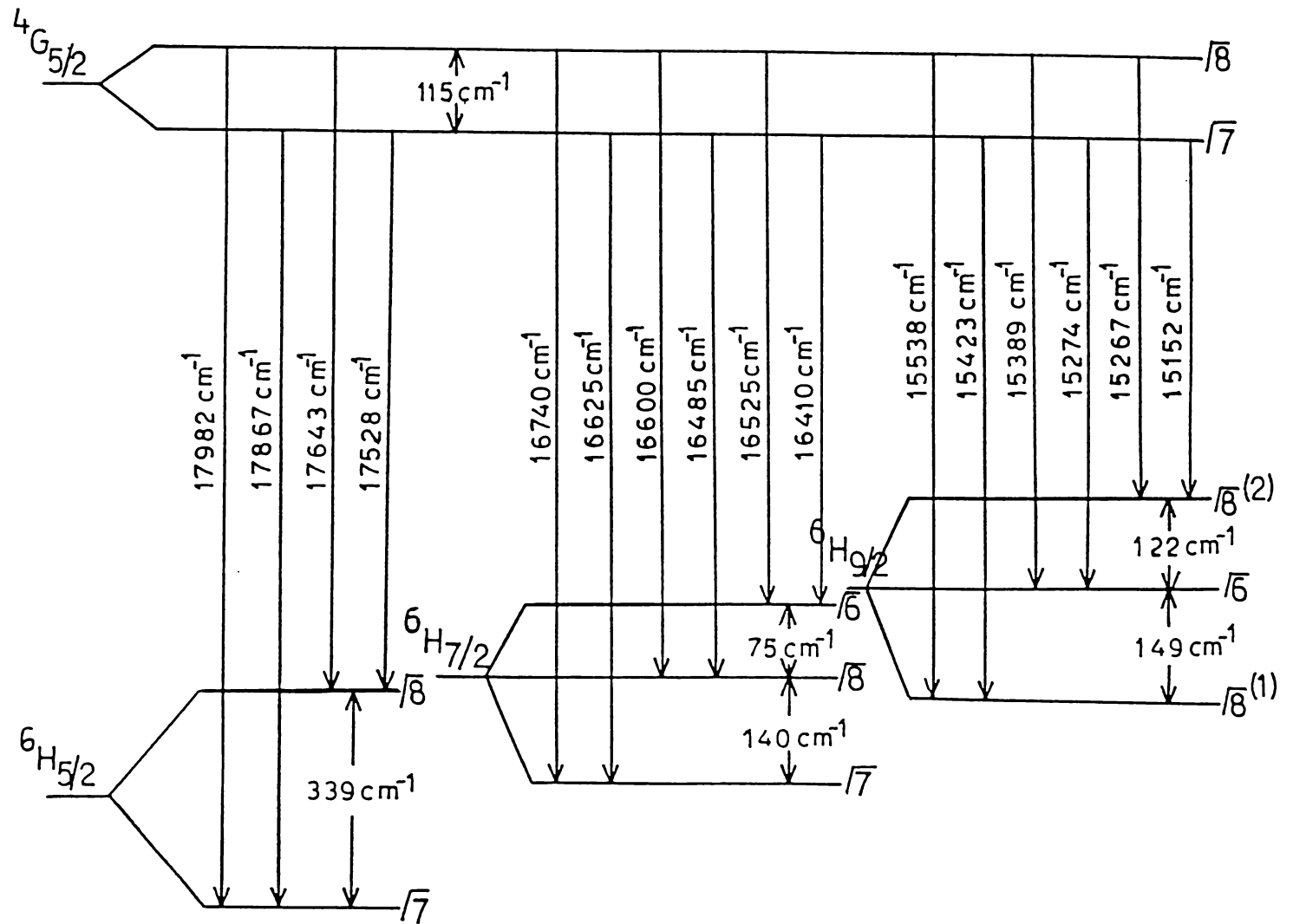


Fig.6.3 The energy level scheme showing the various sublevels and transitions which give rise to the fluorescence spectrum of SrS:Sm.

For the ${}^4G_{5/2} \longrightarrow {}^6H_{9/2}$ transition, the upper level Stark splitting is also found to be 115 cm^{-1} . Analysis shown that the ${}^6H_{9/2}$ level has been splitted into three sublevels with relative spacings of 122 cm^{-1} and 149 cm^{-1} (Fig.6.3). The splitting pattern of ${}^6H_{9/2}$ level of Sm^{3+} ion is shown in Fig.6.2B. For this group, the best fit is obtained when $W = 5.11 \text{ cm}^{-1}$ and $x = 0.62$ giving $B_4 = 0.053$; $B_6 = 1.51 \times 10^{-4}$ and $A_4 \langle r^4 \rangle = 21.12 \text{ cm}^{-1}$.

The charge compensation of Sm^{3+} in the lattice is accomplished by the creation of cation vacancies which may perturb the site symmetry. However, the agreement between theoretical calculations and observed values (Table 6.4) suggests that the site symmetry is cubic in character. The model suggests that Sm^{3+} occupies in SrS substitutionally. It is observed that the energy level splitting depends on the host lattices. For example, value of $A_4 \langle r^4 \rangle$ obtained by earlier report for the ${}^4G_{5/2} \longrightarrow {}^6H_{7/2}$ transition in CaS:Sm is 237.84 cm^{-1} [8].

6.3.4. SrS:Dy Phosphors

The fluorescence emission spectrum of SrS:Dy is

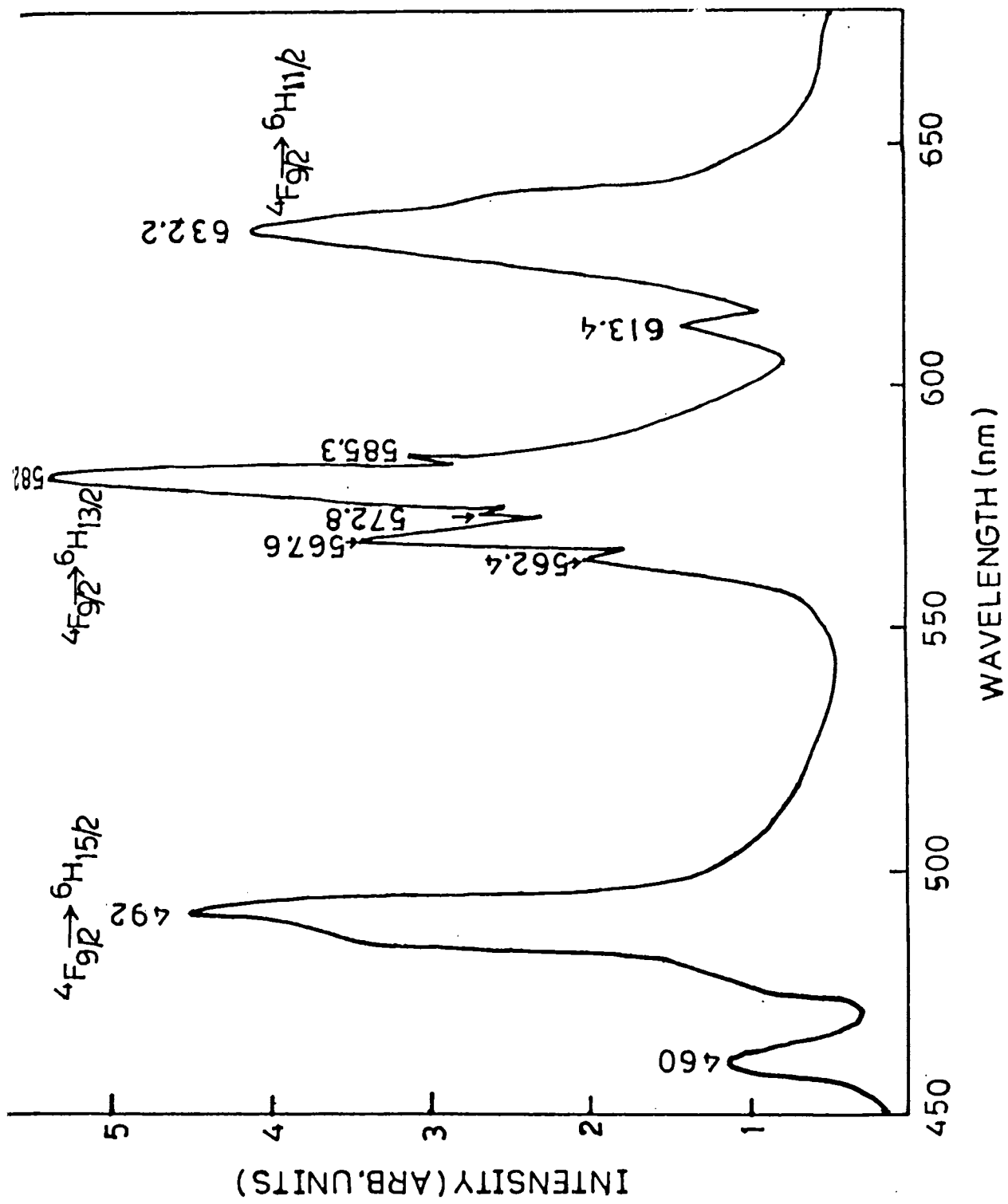
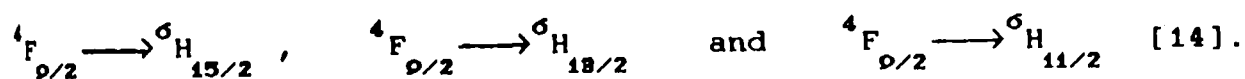


Fig.6.4 Fluorescence emission spectrum of SrS:Dy.

shown in Fig.6.4. It consists of three emission bands, viz;



The most intense band occurring at 582.2 nm band originates from



An important feature of the spectrum is that the maximum intensity occurs for a transition for which the lower level is not the ground state of the ion. Such effect has been observed for ${}^4G_{9/2} \longrightarrow {}^6H_{13/2}$ transition in the Dy^{3+} ion previously [17] and is explained as due to the hyper sensitive nature of this transition.

It is observed that one or two transitions of each lanthanide is extremely sensitive to the environment. They exhibit a normal intensity, for example, in aquo ions but have a marked increase in intensity relative to all other observed transitions in certain environment. These are termed as hypersensitive transitions. This has been explained as due to the effect of the polarization of the ligand by the f electrons of the Ln^{2+} which extends the sphere of influence of the f-electrons. So long as there is no centre of inversion,

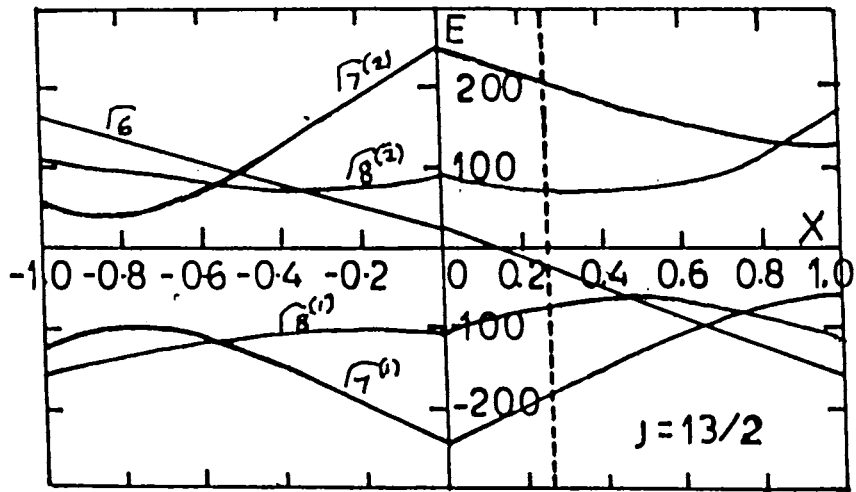


Fig.6.5 The splitting pattern of the ${}^6H_{13/2}$ manifold of the Dy^{3+} ion in SrS lattice.

the induced dipoles can interact and yield a non vanishing dipole moment. This, then interacts with the radiative field, and the result is that a normally forbidden electric dipole transition becomes allowed [17]. In the present case, it can be speculated that such an effect is taking place in the case of Dy^{3+} ion in SrS lattice also.

The emission due to ${}^4F_{9/2} \longrightarrow {}^6H_{13/2}$ transition consists of five lines. The wavelengths and term assignments

Table 6.5 The wavelength and assignments of ${}^4F_{9/2} \longrightarrow {}^6H_{13/2}$ transition in SrS:Dy³⁺.

Transition	Wavelength (nm)	Wavenumber (ν cm ⁻¹)	
		Observed	Calculated
${}^4F_{9/2} \longrightarrow \Gamma_7^{(1)}$	562.4	17781	17781
${}^4F_{9/2} \longrightarrow \Gamma_8^{(2)}$	567.6	17618	17555
${}^4F_{9/2} \longrightarrow \Gamma_6$	572.8	17458	17442
${}^4F_{9/2} \longrightarrow \Gamma_8^{(2)}$	582.2	17176	17216
${}^4F_{9/2} \longrightarrow \Gamma_7^{(2)}$	585.3	17085	17161

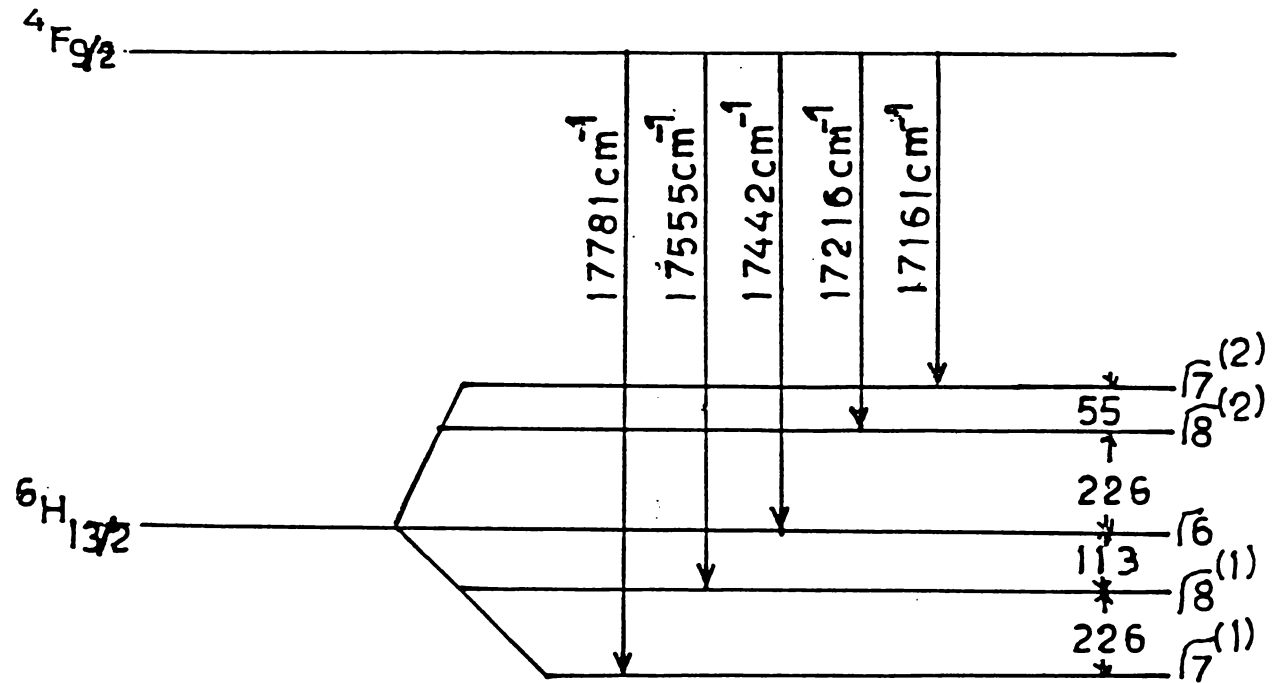


Fig.6.6 The energy level scheme showing the various sublevels and transitions which give rise to the fluorescence emission spectrum of SrS:Dy.

of the bands were given in Table 6.5. Analysis shown that ${}^6\text{H}_{13/2}$ level has been splitted into five sub levels with relative spacings as shown in Fig.6.6. The splitting pattern of ${}^6\text{H}_{13/2}$ level of Dy^{3+} ion is shown in Fig.6.5. For this group, the best fit is obtained when $W = 2.26 \text{ cm}^{-1}$ and $x = 0.25$ giving $B_4 = 9.4 \times 10^{-8}$; $B_6 = 9.9 \times 10^{-5}$; $A_4 \langle r^4 \rangle = 158.78 \text{ cm}^{-1}$ and $A_6 \langle r^6 \rangle = 95.65 \text{ cm}^{-1}$.

6.3.5. SrS:Er Phosphors

The fluorescence emission spectrum of SrS:Er phosphor is found to have essentially six emission bands covering the ultraviolet and visible regions (Fig.6.7). The wavelenghts and the probable energy level transitions giving rise to the emission bands are given in Table 6.6. The emission band occuring at 550 nm is found to have maximum intensity. A comparison of the experimentally observed emission line splitting of the 550 nm band with energy splitting calculated on the basis of the point charge crystal field model shows that Er^{3+} ion can occupy Sr^{2+} substitutional sites.

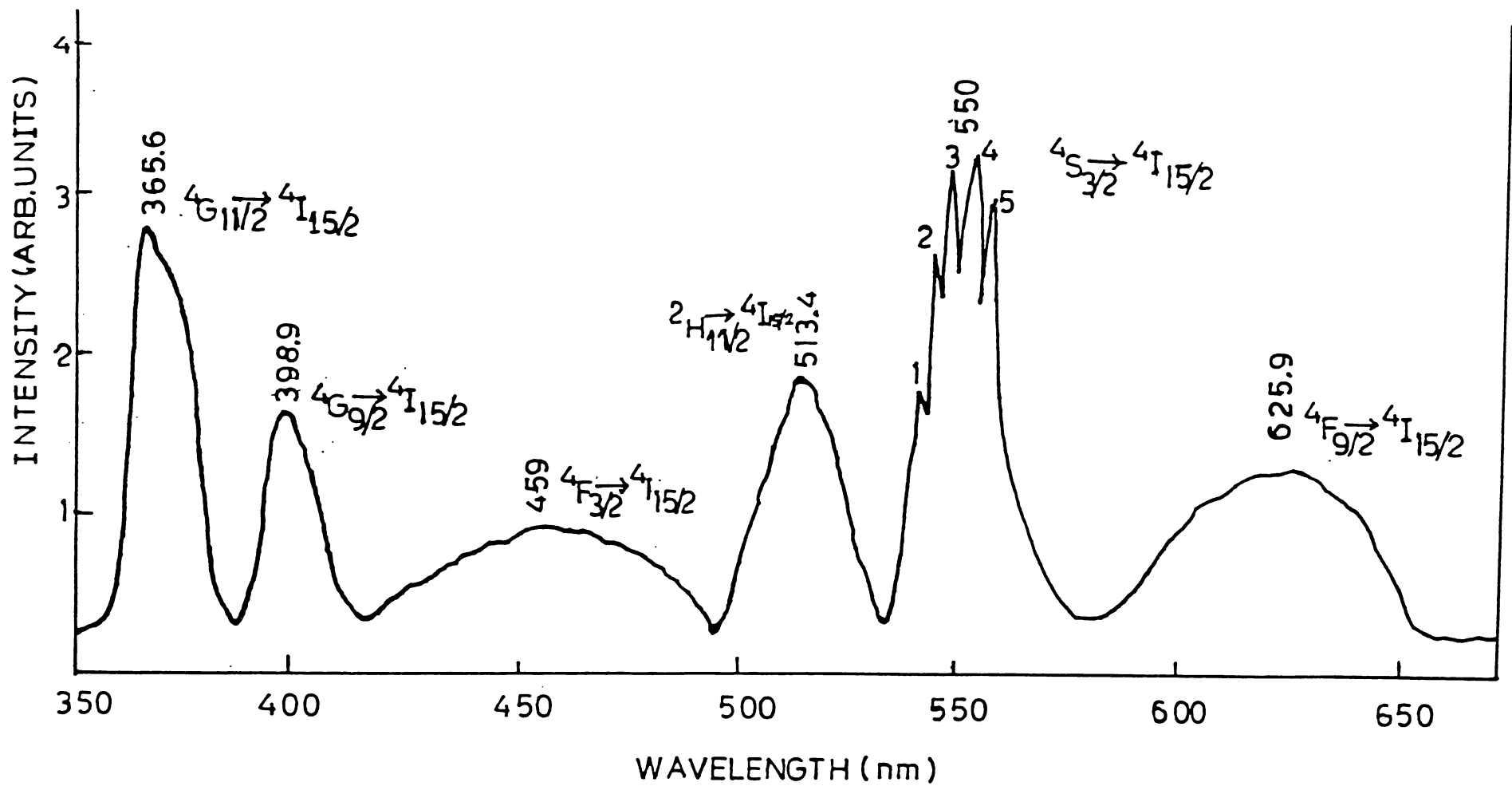


Fig.6.7 Fluorescence emission spectrum of SrS:Er.

Table 6.6. Wavelength and assignments of fluorescence emission bands in SrS:Er phosphors.

Band	Wavelength λ (nm)	Wavenumber ν (cm^{-1})	Level transition
1	365.6	27352	${}^4G_{11/2} \longrightarrow {}^4I_{15/2}$
2	398.9	25069	${}^4G_{9/2} \longrightarrow {}^4I_{15/2}$
3	459	21786	${}^4F_{3/2} \longrightarrow {}^4I_{15/2}$
4	513.4	19478	${}^2H_{11/2} \longrightarrow {}^4I_{15/2}$
5	550	18182	${}^4S_{3/2} \longrightarrow {}^4I_{15/2}$
6	625.9	15977	${}^4F_{9/2} \longrightarrow {}^4I_{15/2}$

In the present case, where an Er^{3+} ion is introduced into a SrS lattice, we are encountering a situation in which a lanthanide ion is placed in a cubic crystal field of octahedral co-ordination. A detailed study [2] reveals that in such a crystal field the ground state ${}^4I_{15/2}$ of the Er^{3+} ion will split into five sub levels, viz., Γ_6 , $\Gamma_8^{(1)}$, Γ_7 , $\Gamma_8^{(2)}$ and $\Gamma_8^{(3)}$. The upper level of this transition doesnot split since Er^{3+} ion is in a cubic crystal field [18].

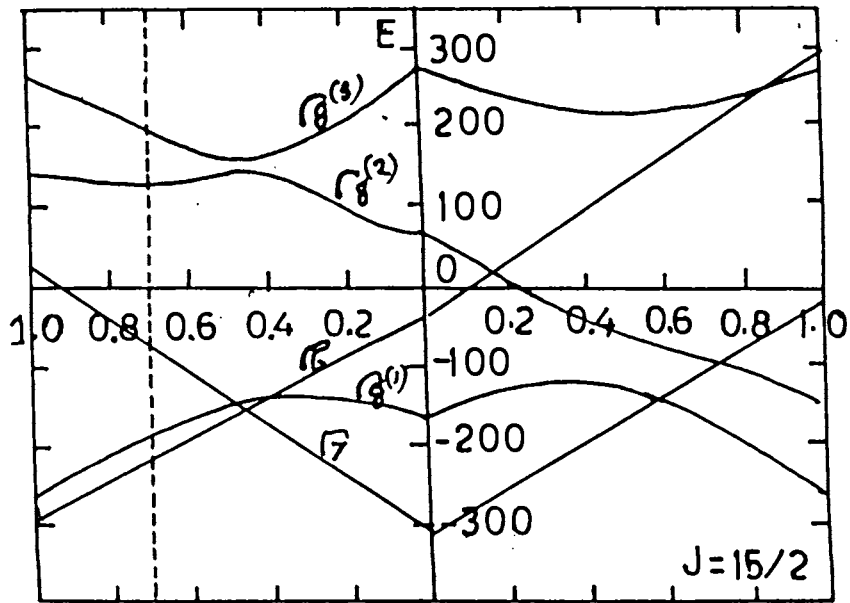


Fig.6.8 The splitting pattern of the $^4I_{15/2}$ manifold of the Er^{3+} ion in the SrS lattice.

Table 6.7. The transitions involved in ${}^4S_{3/2} \longrightarrow {}^4I_{15/2}$
 emission band of SrS:Er phosphor

Line No.	Transition	Wavelength λ (nm)	Wavenumber ν (cm^{-1})	Ground level splitting
1	${}^4S_{3/2} \longrightarrow \Gamma_6$	540.5	18501	18501
2	${}^4S_{3/2} \longrightarrow \Gamma_8^{(1)}$	543.6	18396	18411
3	${}^4S_{3/2} \longrightarrow \Gamma_7$	547.8	18255	18240
4	${}^4S_{3/2} \longrightarrow \Gamma_8^{(2)}$	553	18083	18129
5	${}^4S_{3/2} \longrightarrow \Gamma_8^{(3)}$	556.1	17982	18098

The groups of lines were analysed and from the

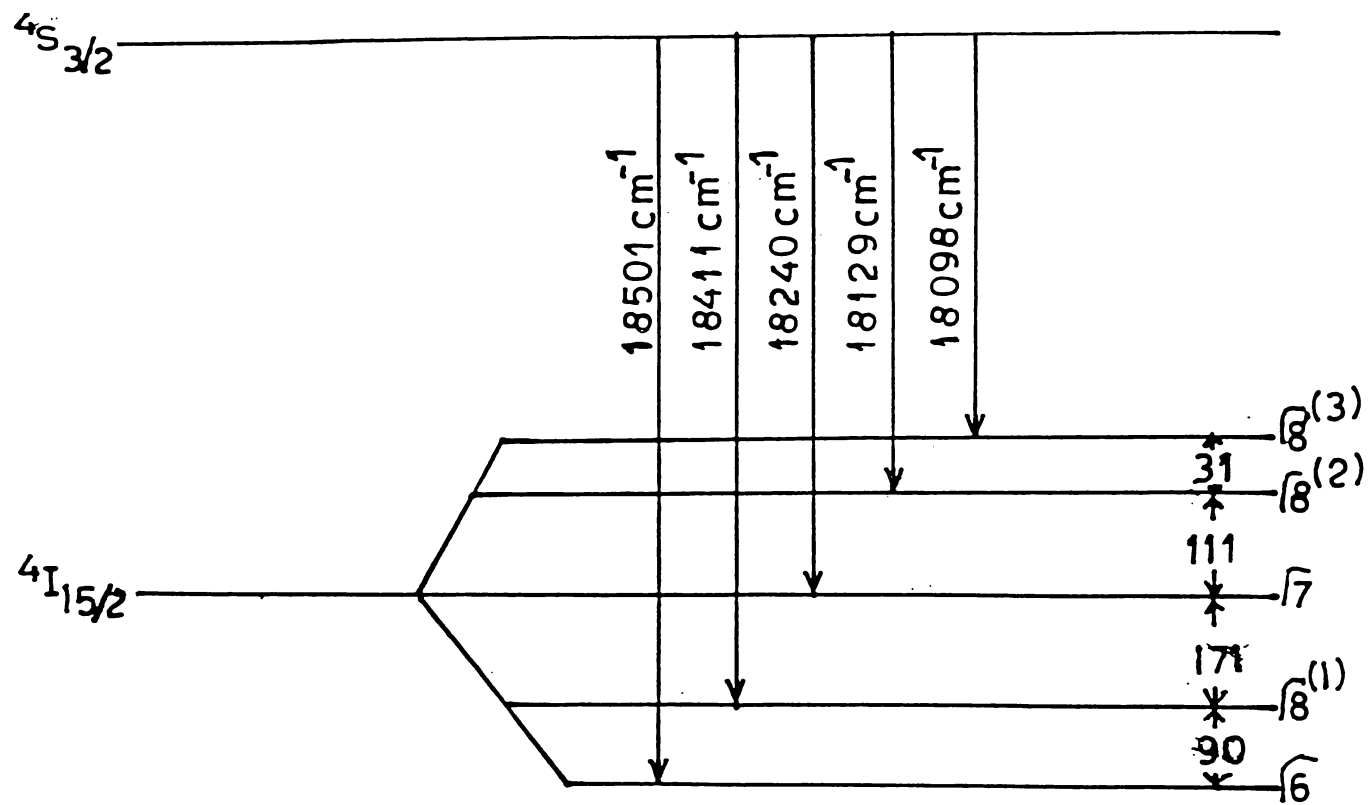


Fig.6.9 The energy level scheme showing the various sublevels and transitions which give rise to the fluorescence emission spectrum of SrS:Er.

energy level separations of the lines in the group, the crystal field parameters were calculated employing the method suggested by Lea et al.[2] and later used by Bryant et al.[13].

The splitting pattern of the ${}^4I_{15/2}$ manifold of the Er^{3+} ion in the SrS lattice is shown in Fig.6.8 . This corresponds to the ground level splitting pattern of Er^{3+} ion in a cubic crystal field and also shows that it splits into five sub levels. The values of β and γ for an Er^{3+} ion is 0.444×10^{-4} and 2.0699×10^{-6} respectively. Freeman and Watson [3] gave the value of $\langle r^4 \rangle$ and $\langle r^6 \rangle$ for the 4f electrons of Er^{3+} ion as $1.126 A_H^4$ and $3.978 A_H^4$ respectively where A_H is the Bohr radius. The probable energy level diagram is shown in Fig.6.9.

The energy level separation of the lines were compared with the splitting pattern shown in Fig. 6.8 . The best fit with the observed energy level splitting occur when $x = 0.7$ and $W = 1.8 \text{ cm}^{-1}$. Substituting the values of W and x and calculating $A_4 \langle r^4 \rangle$ and $A_6 \langle r^6 \rangle$ from the expression for B_4 and B_6 , the values obtained are:

$$A_4 \langle r^4 \rangle = 473 \text{ cm}^{-1} \quad \text{and}$$
$$A_6 \langle r^6 \rangle = 10.6 \text{ cm}^{-1}.$$

Thus the energy levels of RE^{3+} in SrS lattice has been discussed by taking into account of crystal field effect. Relevant parameters and splitting patterns of energy levels were also evaluated.

REFERENCES

- [1] H.Bethe, *Ann.Phys.Lpz.*, **3**, 133 (1929).
- [2] K.R.Lea, M.J.M.Leask, W.P.Wolf, *J.Phys.Chem.Solids.*,
23, 1381 (1962).
- [3] A.J.Freeman and R.E.Watson, *Phys.Rev.*,**127**, 2058 (1962).
- [4] K.W.H.Stevens, *Proc.Phys.Soc.Lond.*, **A65**, 209 (1952).
- [5] W.Kaiser, C.G.Garrett and D.L.Wood, *Phys.Rev.*,
123, 766 (1961).
- [6] S.P.Keller, *J.Chem.Phys.*, **29**, 180 (1958).
- [7] S.P.Keller, J.E.Mapes, G.Cheroff, *Phys.Rev.*,**108**,663(1957).
- [8] S.M.Pillai and C.P.G.Vallabhan,*Phys.Stat.Sol*,**134**,383(1986).
- [9] N.Yamashita and S.Asano, *J.Phys.Soc.Japan.*,**56**, 352 (1987).
- [10] M.L.Yu.Allsalu, O.V.Kondakov, V.V.Mikhailin, V.V.Nelipa
and E.Yu.Pedak, *Moscow Univ.Phys.Bull.*, **39**, 101 (1984).

- [11] Thomas Baby and V.P.N.Nampoori, (in press).
- [12] Thomas Baby and V.P.N.Nampoori, Proc. of 18th Optical Soc. of India Symp; Indian Institute of Astro Physics, Bangalore, OI-6, P.6 (1990). (to appear in Kodaikanal Observatory Bulletin).
- [13] Thomas Baby and V.P.N.Nampoori, Proc. of the Seminar on Photochemistry and Photobiology, Madras (1991).
- [14] A.S.Marfunin, Spectroscopy, Luminescence and Radiation Centres in Minerals (Springer-Verlag Publishers, New York), p.198,207,210 (1979).
- [15] S.P.Keller and G.D.Pettit, J.Chem.Phys., 30, 434 (1959).
- [16] C.Z.Zhong and F.J.Bryant, J.Phys.C: Solid State Phys., 13, 4797 (1980).
- [17] Shyama.P.Sinha, Systematics and the properties of the lanthanide, Ed.S.P.Sinha (D.Reidel Publishing Co; Dordrecht, Boslan, Lanchaster) (1983).
- [18] C.C.Yu and F.J.Bryant, J.Lumin., 18/19, 841 (1979).
- [19] Thomas Baby and V.P.N. Nampoori, Proc. of Second Indo-USSR

Symp.on Rare-earth Materials Research, Trivandrum; P.34,
(1980). (to appear in Bulletin of Materials Science).

CHAPTER 7

GENERAL CONCLUSIONS

The work presented in this thesis is the design, fabrication and parametric studies of a high power nitrogen laser system and its use to study the fluorescence characteristics of certain doped phosphors.

NITROGEN LASER : We observed significantly improved discharge uniformity and suppression of arcs over a wide pressure range, improved reproducibility of both spatial distribution and intensity of the laser output and increase in permissible operating pressures.

In general, the following conclusions were made from the present studies :

- (1) In order to obtain uniform and reproducible discharge, it is advisable to use the combination of cylindrical cathode and plane anode, as reported in the present work.
- (2) Sufficiently uniform gas flow is achieved with the holes distributed along each electrode and located in such a way that they do not face each other.
- (3) In order to achieve a shorter rise time, the inductance of

the cavity and spark gap are minimized by reducing their physical sizes.

- (4) For effective heat dissipation black painted fins are provided for cooling the laser cavity and spark gap.
- (5) The double-Blumlein circuit has been found to give higher output peak power and better efficiency than the single-Blumlein circuit.
- (6) The maximum peak power obtained for the double-Blumlein circuit was 700 kW at a charging voltage of 9.3 kV and the maximum efficiency obtained was 0.51%. The pulse width at FWHM was 3 ns.
- (7) For obtaining better stability in repetition rate, triggered spark gap switch may be used.
- (8) The additive gases $\text{CH}_2\text{Cl}-\text{CH}_2\text{Cl}$, CCl_4 and SOCl_2 enhances the emission intensity appreciably.

In conclusion, N_2 laser laser with transverse discharge geometry shows promise as a simple and ideal source for fluorescence analysis. It is compact, less divergent, and powerful. Its voltage requirements are comparable to those used with low pressure N_2 lasers. The N_2 laser described here

has been operating for several months in this laboratory giving satisfactory performance. With further parametric optimization, the performance can be improved.

FLUORESCENCE IN PHOSPHORS : The detailed preparation and fluorescence emission analysis of SrS phosphors doped with Ce, Eu, Sm, Dy and Er were discussed with accompanying energy level diagrams for each rare earth ions in SrS lattice. The fluorescence emission from Sm, Dy and Er were analysed in detail using a parametrized model. The crystal field parameters were calculated and the splitting pattern of the energy levels in SrS lattice were evaluated.

FUTURE SCOPE:

We believe on the basis of the parametric studies, that it should be possible by using preionization together with higher voltages and shaping the electrodes to achieve atmospheric or higher pressure operation with pure N_2 or possibly with a mixture of N_2 and a buffer gas suitable for collisional quenching of the lower levels. The recent trend to N_2 laser fabrication is towards making compact and reliable

lasers. Studies on the coherence properties of the laser radiation and the effects of additives enabled a better understanding of the laser action in N_2 . N_2 laser has varied applications which make this system equally popular among the scientists working in physical and life sciences.

The fluorescence measurements at low temperature is to be carried out, since UV excited fluorescence at low temperature will give more informations about the crystalline effects on the rare earth ions. It is certain that continued progress in the device field will yield major changes in the techniques of display devices necessitating the development and characterisation of different phosphor materials.

APPENDIX

APPLICATION OF PHOSPHORS IN OPTICAL DEVICES

A.1. Introduction

In recent years, there has been a growth of interest on luminescent materials based on the rare earths, either as host lattice constituents or activators [1]. Rare earth phosphors have found important commercial applications in such field as lasers, colour television and lighting. Rare earth phosphors have also been useful in theoretical studies of luminescence mechanisms. The red emitting europium-activated phosphors have been of particular commercial interest since the introduction of Yttrium Vanadate in 1964 as an efficient cathode-ray phosphor [2]. From 1964 to the present, europium activated phosphors have been adopted as the standard red primary in colour television picture tubes. These phosphors include : $(Y, Eu)VO_4$, $(Y, Eu, Bi)VO_4$, $(Y, Eu)_2O_3$, $(Y, Eu)_2O_3$, $(Gd, Eu)_2O_3$, and $(Gd, Y, Eu)_2O_3$. Certain primary colour phosphors which are suitable for TV screen are briefly discussed here.

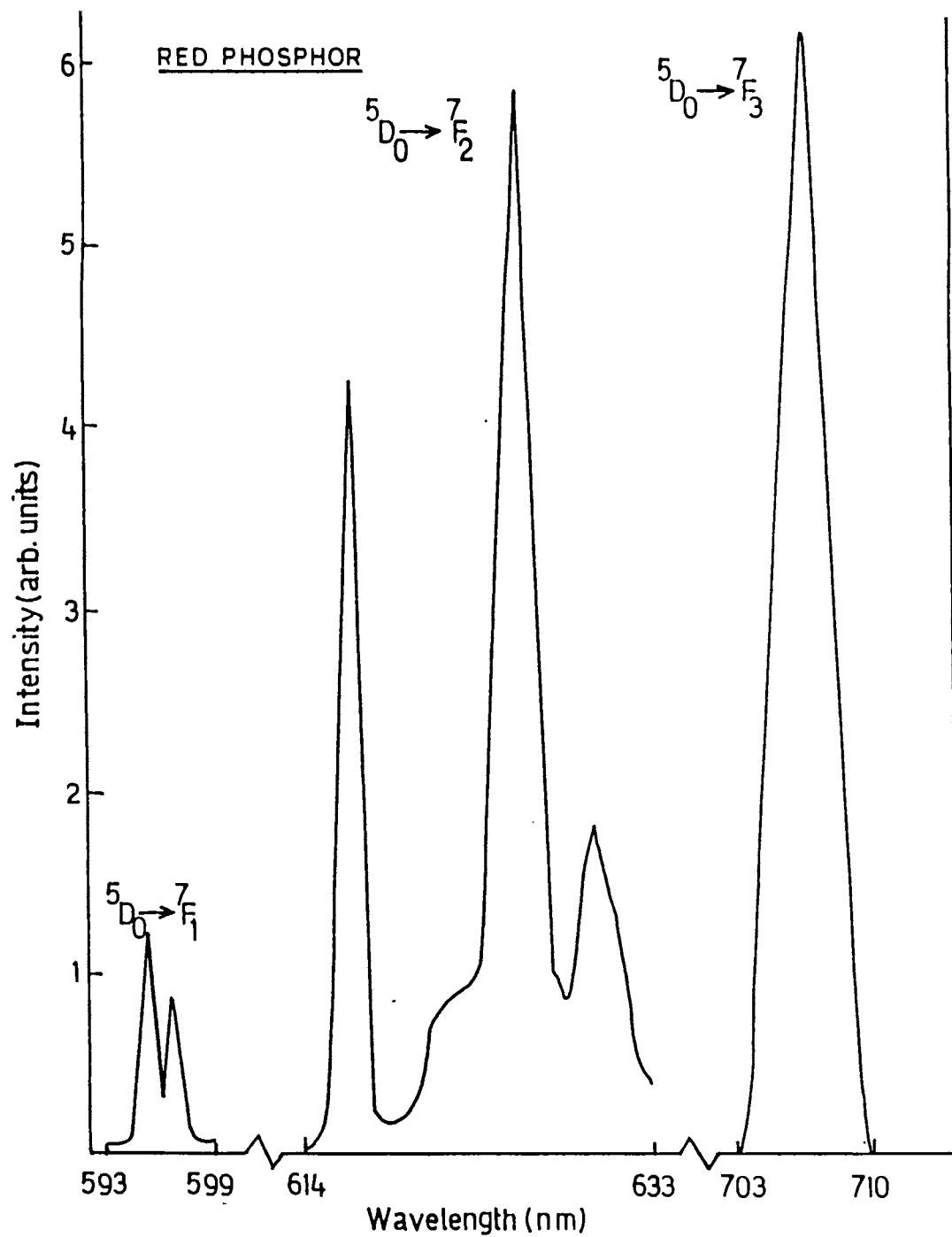
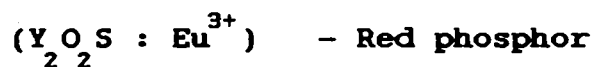


Fig. 1A. Fluorescence emission spectrum of $Y_2O_2S:Eu^{3+}$.

A.2. Trivalent Europium activated Yttrium Oxysulphide



Trivalent europium activated Yttrium Oxysulphide $(Y_2O_2S : Eu^{3+})$, one of the rare earth oxysulphide group of phosphors, is of great interest due to its potential application in colour television picture tubes as red component. It has better luminous efficiency and brightness and high resistance to acid treatment during the coating process when compared with other red phosphors for colour television picture tubes such as: $Zn_3(PO_4)_2 : Mn^{2+}$, $(Zn \ Cd)S : Ag$, $Y_2O_3 : Eu^{3+}$ and $Y_2O_3 : Eu^{3+}$.

Preparation of $Y_2O_2S : Eu^{3+}$ is carried out by flux method. This involves mixing of appropriate quantities of AR grade Yttrium Oxide, Europium Oxide, Sulfur, Sodium Carbonate and Potassium Phosphate and firing the temperature range of 1000–1100°C for 1–3 hours. Flux in this case will be sodium polysulphide. After the firing, excess flux was removed by washing with demineralised water and the traces of unreacted Y_2O_3 by dilute HCl. The powder thus obtained was converted into pellets of 10 mm radius and 3 mm thickness. The phosphors

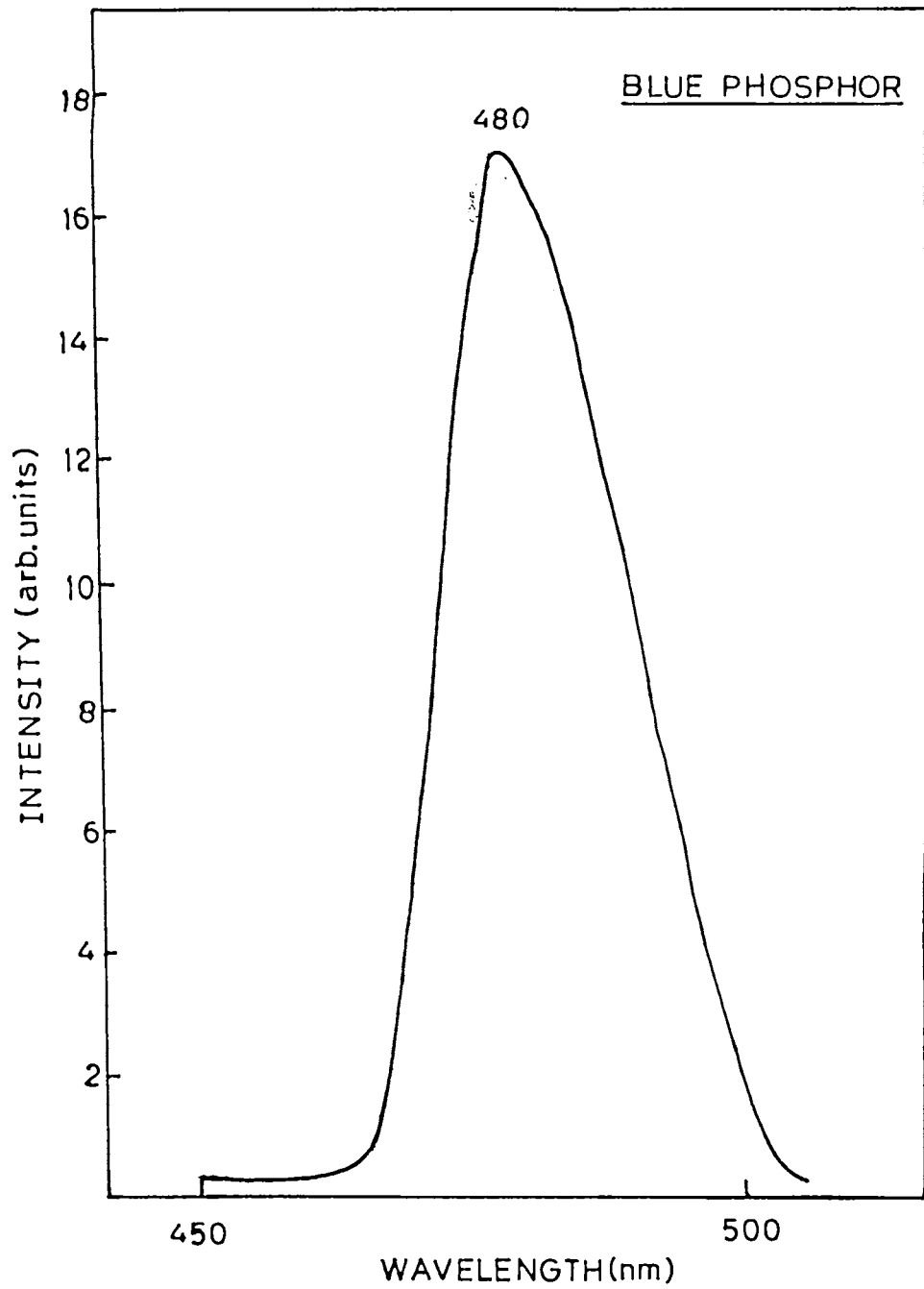


Fig. 2A Fluorescence emission spectrum of calcium tungstate.

were excited using the nitrogen laser as described previously. As shown in Fig.1A, line emission spectrum is obtained in the orange-red region which corresponds to the ${}^5D_0 \longrightarrow {}^7F_1$, ${}^5D_0 \longrightarrow {}^7F_2$ and ${}^5D_0 \longrightarrow {}^7F_3$ transitions.

A.3. Calcium Tungstate - Blue phosphor

In calcium tungstate crystal phosphor which has the structure and composition of the mineral 'scheelite', luminescence without external activators is due to the complex tungstate ions WO_4^{2-} in the lattice [3]. The tungstate ion is coordinated by four oxygen having predominantly a covalent bond. The calcium is coordinated by six oxygen ions having predominantly an ionic bond.

A mixture of calcium carbonate and tungstic acid in a suitable mole ratio is ground into a slurry with the addition of suitable quantity of water. The yellow slurry is ground thoroughly and dried, in an air oven at about $110^\circ C$ so that the resultant mass is nearly white as possible. This is due to the formation of tungsten dihydrate $H_2W_2O_4$ or $WO_3 \cdot 2H_2O$ which is white in colour. The powdered mass is subsequently

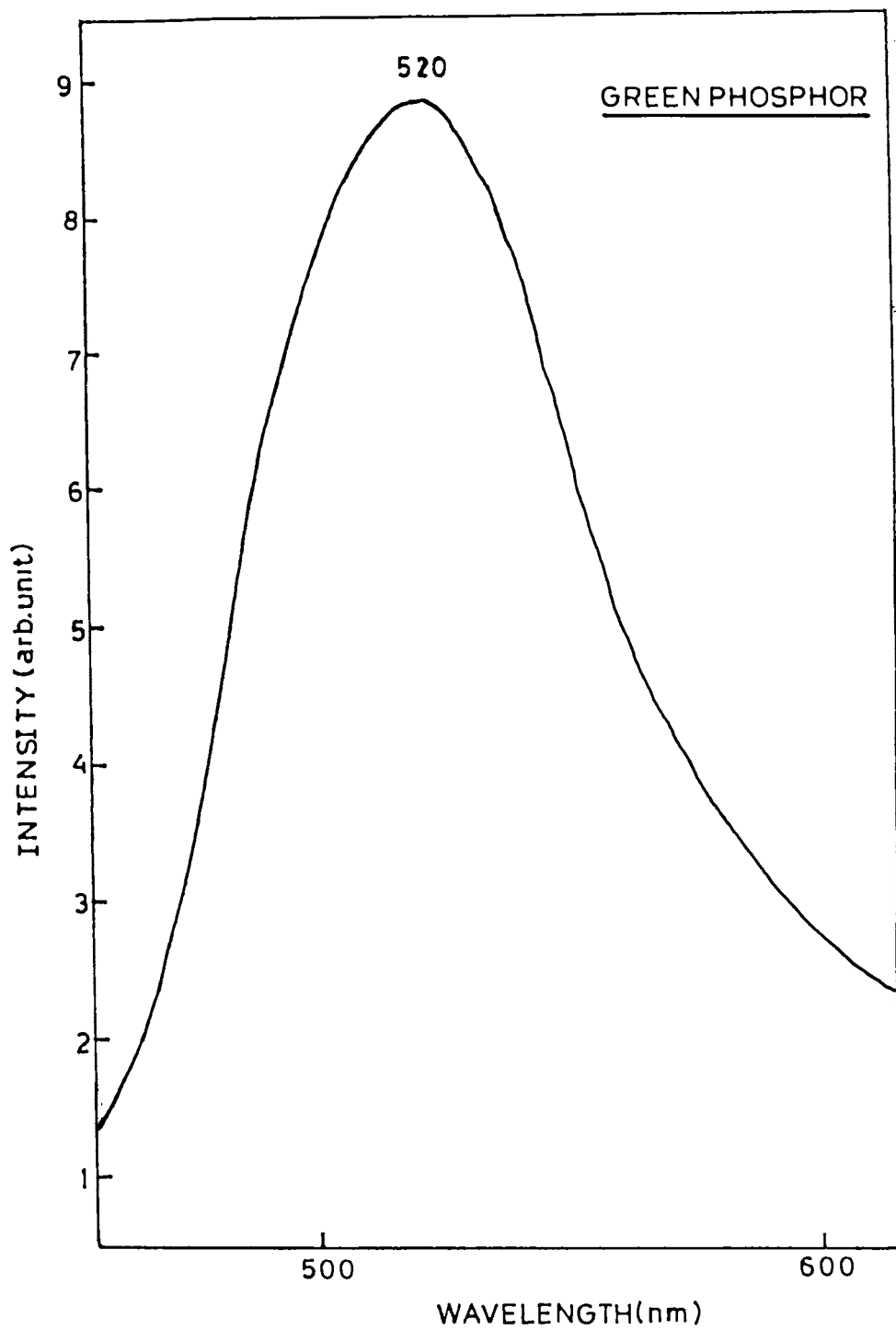


Fig.3A Fluorescence emission spectrum of zinc silicate.

heated in air at a temperature in the vicinity of 800-1000^oC for about 2 hours. The resulting mass is finally ground and pelletised. As shown in Fig.2A, a broad band peaking at 480 nm was observed.

A.4.Zinc Silicate - Green phosphor

Zinc Silicate matrix is known to be rhombohedral in its structure. The configurational coordinate diagram for Zn_2SO_4 : Mn has been worked out by various workers. The emission transition is attributed to a spin reversal of one of the 3d electrons of the Mn^{2+} ion. The mode of vibration is a radial one for the four oxygen ions surrounding the manganese ion. Depending on the interaction between the Mn^{2+} ion and the host lattice the luminescence peak centred at 520 nm (Fig.3A), the mechanism being explained by a configurational coordinate scheme.

REFERENCES

- [1] Analysis and Application of Rare Earth Materials; Odd.B. Michelsen (ed.), Universitets Forlaget, Norway (1973); P.241, "Production of rare earth red phosphors for color television and lighting applications", by J.E.Mathers.
- [2] A.K.Levine and F.C.Palilla, Appl.Phys.Lett., 5, 118 (1964).
- [3] On Luminescent Materials and Devices, Technical Note, CECRI (1986).